Structural and Biophysical Analysis of Netrin-1 with Heparan Sulfate Proteoglycans

by

Monika Gupta

A Thesis submitted to the Faculty of Graduate Studies of

The University of Manitoba

in partial fulfilment of the requirements of the degree of

DOCTOR OF PHILOSOPHY

Department of Chemistry

University of Manitoba

Winnipeg, Manitoba, Canada

Abstract

The development of the nervous system involves the migration of axons from their origin to destination and ultimately completing the synapse formation. This process involves guidance molecules, the expression of receptors on the cell surface, and ultimately complex cell signaling. This thesis focuses on the characterization of one of the guidance molecules, Netrin-1, in solution and the impact of heparan oligosaccharides on its dynamic behavior.

Netrin-1 is a chemotropic cue involved in the attraction and repulsion of axons, cell migration, adhesion, differentiation, angiogenesis, inflammation, and cancer. Overexpression of netrin-1 is found in different forms of cancer. It acts as a survival factor for cancer cells by preventing cell apoptosis mediated *via* dependence receptors, including Un coordinated 5 (Unc5) and Deleted in Colorectal cancer (DCC) families. Interference with netrin-1 and its receptors interactions is associated with tumor cell death in various preclinical models. Netrin-1 interacts with glycosaminoglycan (GAG) chains of diverse heparan sulfate proteoglycans (HSPG) such as glypican. DCC also binds with heparin. It has been suggested that DCC/heparin interaction is mediated by netrin-1. However, these GAG molecule's specific role with netrin-1 has not been demonstrated whether its interaction with netrin-1 concentrates it on the cell surface or it has some role in receptor binding. Therefore, a more detailed determination of the molecular interaction between netrin-1 and GAG molecules is of particular interest.

In this study, truncated netrin-1 containing domain V and domain VI was recombinantly produced, and further studied using a biophysical approach to investigate its behavior in solution and its crystal structure with a bound heparan sugar unit was determined. Size exclusion chromatography coupled with multi-angle light scattering (SEC-MALS), analytical ultracentrifugation (AUC), and small-angle X-ray scattering (SAXS) studies confirmed the monomer-dimer equilibrium of netrin-1 in solution. However, the addition of medium-length oligosaccharides promoted high molecular weight oligomer formation. AUC and SEC-MALS showed higher-order oligomers with calculated masses corresponding to 5-6 netrin-1 molecules. A solution structure determined *via* SAXS with octasaccharide showed the appearance of a trimer that might be a seed for higher-order oligomers. The crystal structure of the complex of netrin-1 and the smallest heparan sugar unit (Sucrose Octa Sulfate, SOS) revealed a dimer of netrin-1 with

one SOS per monomer unit. Distinct binding sites for two SOS suggest that GAG chains of different lengths could associate with netrin-1. Mutant studies also validated the observed netrin-1 GAG interface. Therefore, netrin-1 interaction studies with GAG molecules potentially promote new ideas for the development of small molecules targeting the GAG binding sites for the treatment of cancer.

To determine if there is a specific role of these GAG molecules on netrin-1 receptor interaction, ELISA-like binding experiments were performed. They showed that the short-chain GAGs do not act as a coreceptor. GAG and receptor bind independently to netrin-1 and have non-overlapping binding regions. From this information, we can begin to elucidate the interaction mechanism of netrin-1 with GAG and understand its biological relevance. The GAG molecules might concentrate netrin-1 on the cell surface and help netrin-1 in bringing receptors together to form receptor clustering and further cell signaling.

Acknowledgements

Foremost, I would like to express my sincere gratitude to my supervisor Dr. Jörg Stetefeld for his continuous support throughout my thesis. His patience, motivation, and immense knowledge not only helped to complete my thesis but also taught me how to become a better researcher. Thank you for showing confidence in me which helped to enhance my skills. I could not have asked for a better supervisor for my Ph.D. study. Thank you for all your support beyond academics also.

Beside my supervisor, I would like to thank other members of lab that make a Stetefeld Research Group with their immense knowledge and support. I would especially like to thank Drs. Aniel Moya Torres, Markus Meier, Mathew McDougall and George Orriss for their time and patience in teaching me new techniques and for helping me throughout the Ph.D. journey. I am grateful to Dr. Markus Meier for his patience and immense knowledge that helped us to continue our work remotely during the covid time. Many thanks to all past and present students, for their friendship, advice, and support. Altogether, these people have made my Ph.D. journey memorable and truly enjoyable.

My sincere thanks to my Ph.D. committee: Dr. Gregg Tomy, Dr. Joe O'Neil, and Dr. Francis Lin, for timely advice, encouragement, and insightful comments.

Last but not the least, I would like to thank my family, friends for their patience and understanding. My sincere thanks to my parents and in-laws for helping me continue my studies with my little one, Reyansh. Rahul and Reyansh, thank you for your patience and always being there for me with your enormous love.

My research was supported by the Faculty of Science, Manitoba Graduate fellowship, University of Manitoba Graduate fellowship and Graduate Enhancement of Tri-Council Stipends (GETS) fellowships provided by the University of Manitoba

Table of Contents

List of Figures

List of Tables

List of copyright material for which permission has been obtained

Figure 1.2 – Reproduced with permission from Development. License # 1205460

Lai Wing Sun K, Correia JP, Kennedy TE. Netrins: versatile extracellular cues with diverse functions. Development. 2011;138(11):2153–69.

Figure 1.3 – Reproduced from https://string-db.org.

Open Access with https://creativecommons.org/licenses/by/4.0/

Szklarczyk D, Gable AL, Lyon D, Junge A, Wyder S, Huerta-Cepas J, Simonovic M, Doncheva NT, Morris JH, Bork P, Jensen LJ, Von Mering C. STRING v11: Protein-protein association networks with increased coverage, supporting functional discovery in genome-wide experimental datasets. Nucleic Acids Res. 2019;47(D1):D607–13.

Figure 1.4, 1.5 and 1.8 – were reproduced with permission from Springer Nature. License # 5274181333190

Goldschneider D, Mehlen P. Dependence receptors: a new paradigm in cell signaling and cancer therapy. Oncogene. 2010;29(13):1865–82. http://dx.doi.org/10.1038/onc.2010.13

Figure 1.6 – was reproduced with permission from Elsevier. License # 5274180817160

Finci LI, Krüger N, Sun X, Zhang J, Chegkazi M, Wu Y, Schenk G, Mertens HDT, Svergun DI, Zhang Y, Wang J huai, Meijers R. The Crystal Structure of Netrin-1 in Complex with DCC Reveals the Bifunctionality of Netrin-1 As a Guidance Cue. Neuron. 2014;83(4):839–49.

Figure 1.7 – was reproduced from Cell http://creativecommons.org/licenses/by/4.0/

Robinson RA, Griffiths SC, van de Haar LL, Malinauskas T, van Battum EY, Zelina P, Schwab RA, Karia D, Malinauskaite L, Brignani S, van den Munkhof MH, Düdükcü Ö, De Ruiter AA, Van den Heuvel DMA, Bishop B, Elegheert J, Aricescu AR, Pasterkamp RJ, Siebold C. Simultaneous binding of Guidance Cues NET1 and RGM blocks extracellular NEO1 signaling. Cell. 2021 Apr 15;184(8):2103. https://doi.org/10.1016/j.cell.2021.02.045

Figure 1.9 – Reproduced with permission from Trends in Molecular Medicine. License # 5261291170000

Ko SY, Dass CR, Nurgali K. Netrin-1 in the developing enteric nervous system and colorectal cancer. Trends Mol Med. 2012;18(9):544–54. http://dx.doi.org/10.1016/j.molmed.2012.07.001

Figure 1.10 – was reproduced from International Journal of Molecular Sciences. open access with http://creativecommons.org/licenses/by/4.0/

Dun X-P, Parkinson D. Role of Netrin-1 Signaling in Nerve Regeneration. Int J Mol Sci. 2017;18(3):491. http://www.mdpi.com/1422-0067/18/3/491.

Chapter 2.1-2.4, 4.1 were reproduced with permission
http://creativecommons.org/licenses/by/4.0/

Moya-Torres, A., Gupta, M., Heide, F. Krahn N, Legare S, Nikodemus D, Imhof T, Meier M, Koch M, Stetefeld J. Homogenous overexpression of the extracellular matrix protein Netrin-1 in a hollow fiber bioreactor. *Appl Microbiol Biotechnol* **105,** 6047–6057 (2021). https://doi.org/10.1007/s00253-021-11438-0

https://link.springer.com/article/10.1007%2Fs00253-021-11438-0#rightslink

Figure 2.5 and 2.7 – were reproduced from Internationl Journal of Molecular Sciences, open access under https://creativecommons.org/licenses/by/4.0/

Kwan TOC, Reis R, Siligardi G, Hussain R, Cheruvara H, Moraes I. Selection of Biophysical Methods for Characterisation of Membrane Proteins. Int J Mol Sci. 2019;20(10).

Figure 2.11 – was reproduced from Elsevier. Open access under CC BY-NC-ND license https://creativecommons.org/licenses/by-nc-nd/3.0/

Seidel SAI, Dijkman PM, Lea WA, van den Bogaart G, Jerabek-Willemsen M, Lazic A, Joseph JS, Srinivasan P, Baaske P, Simeonov A, Katritch I, Melo FA, Ladbury JE, Schreiber G, Watts A, Braun D, Duhr S. Microscale Thermophoresis Quantifies Biomolecular Interactions under Previously Challenging Conditions. Methods. 2013 Mar 24;59(3):301–15. http://www.ncbi.nlm.nih.gov/pmc/articles/PMC3644557/

List of Abbreviations

$(NH_4)_2\,SO_4$	Ammonium sulfate
°C	Degree Celsius
µM	micromolar
2D	Two-dimensional
ACF	Auto correlation function
ADD	Addition dependence domain
Arg (R)	Arginine
BioID	Proximity dependent Biotin Identification
BLI	Biolayer Interferometry
$CaCl_2$	Calcium chloride
CDM-HD	Chemically Defined Medium for High Density cell culture
CHO	Chinese hamster ovary cells
CNS	Central Nervous System
CS	Chondroitin sulfate
CW	Cardin and Weintraub
DAPK	Death associated protein kinase
DB	DCC-P1 binding domain
DCC	Deleted in colorectal cancer
DD	Death domain
DENSS	DENsity from Solution scattering
DIP13α	DCC-interacting protein 13-α
DLS	Dynamic Light Scattering
D_{max}	maximal particle dimension
DMEM	Dulbecco's modified Eagle's medium
DMSO	Dimethyl sulfoxide
dp	Degree of polymerization
Draxin	Dorsal repulsive axon guidance protein
dRI	Refractive Index
DSCAM	Down syndrome cell adhesion molecule
ECM	extracellular matrix
ECS	Extra capillary space

EDTA	Ethylenediaminetetraacetic acid
EGF	Epidermal growth factor
ELISA	Enzyme-linked immunosorbent assay
ESI-MS	Electron spray ionization- mass spectrometry
FBS	Fetal bovine serum
FGF	Fibroblast growth factor
FL	Full length
FNIII	Fibronectin III
FPLC	Fast protein liquid chromatography
GAG	Glycosaminoglycan
GPI	Glycosylphosphatidylinositol
HEK293T	Human embryonic kidney 293 expressing mutant version of SV40 large T antigen
HeLa	Cervical cancer cells taken from Henrietta Lacks
HEPES	4-(2-hydroxyethyl)-1-piperazineethanesulfonic acid
HFBR	Hollow Fiber Bioreactor
HP	Heparin
HRP	Horseradish peroxidase
HS	Heparan sulfate
HSPGs	Heparan sulfate proteoglycans
HYPERFlask	High yielding performance flask
Ig	Immunoglobulin
ITC	Isothermal colorimetry
ITR	Terminal inverted repeat
kDa	kilodalton
KS	Keratan sulfate
LS	Light scattering
GPI	Glycosylphosphatidylinositol
MALS	Multi-Angle Static Light scattering
MAPK	Mitogen Activated protein kinase
MCAM	Melanoma cell adhesion molecule
MCS	Multiple cloning site
MES	2-(N-morpholino) ethanesulfonic acid

mL	milliliter
mM	millimolar
MS	Multiple sclerosis
MST	Microscale Thermophoresis
MW	Molecular Weight
MWCO	Molecular Weight Cutoff
NaCl	Sodium Chloride
nm	nanometer
nM	nanomolar
NMR	Nuclear magnetic resonance
NSD	Normalized spatial discrepancy
NTR	Netrin-terminal region
OD_{600}	Optical density at 600 nm
OPC	Oligodendrocyte precursor
OPCs	Oligodendrocyte's precursor cells
PBS	Phosphate buffer saline
PDB	Protein data bank
R_g	Radius of gyration
R_h	Hydrodynamic radius
rpm	revolutions per minute
RPTP	Receptor protein tyrosine phosphatase
RT-PCR	Real Time-Polymerase Chain Reaction
s	second
S	Svedberg
$s_{20,w}$	Svedberg constant at 20°C in water
SAXS	Small Angle X-ray Scattering
SDS PAGE	Sodium dodecyl sulfate polyacrylamide gel electrophoresis
SEC	Size exclusion chromatography
SOS	Sucrose OctaSulfate
SPR	Surface plasmon resonance
TRE	Tet response element

Tris	Tris(hydroxymethyl)aminomethane
TSP	Thrombospondin
Unc5	uncoordinated 5
UV	Ultraviolet
ZU5	Zona occuludens-5 domain
ΔG^0	Standard free energy
ΔH^0	Standard free enthalpy
ΔS^0	Standard free entropy
η_0	Viscosity

CHAPTER 1

Introduction

The nervous system development involves the migration of immature axons from their region of birth to their destination to complete the neural circuit (1,2). This is mediated by specialized projections from the neural cell body known as axons (3). A highly motile, cytoskeleton rich structure at the end of growing axon tips, the growth cone, helps guide them (4,5). The growth cone also detects and responds to the extracellular signals that direct pathfinding (6). These extracellular signals are also known as axon guidance molecules (7). The studies of guidance molecules have revealed the molecular basis of their activity and indicated that the axons expressing guidance receptors detect the guidance cues presented by the target cells. These guidance cues could be secreted or attached to the extracellular surface (7). Moreover, the different properties of each neuron arises because of the expression of different receptors on their surface and the interactions with different guidance molecules (8). There are four major families of guidance proteins: netrins, slits, semaphorins, and ephrins (9–13).

The name netrin came from the Sanskrit word "netr" which means "one who guides" (14). Netrins belong to the laminin-related proteins superfamily and were first described as chemical guidance cues for migrating motor and commissural axons (15). The first reported member of the netrin family was UNC-6 from *Caenorhabditis elegans*, identified in 1990 (16,17). The gradient of UNC-6 was present along the entire length of the nematode body wall and helped in guiding diverse migrations of axons through interactions with receptors (18). Gene mutation studies showed an uncoordinated phenotype in *C. elegans* due to disruptions of axon pathfinding and cell migration (19). The presence of netrins were confirmed in fruit flies (*Drosophila melanogaster*, (20)), chicken (*Gallus gallus*), mouse (*Mus musculus*) and humans (21), revealing high conservation in axon guidance and cell migration. The sequence alignment of Unc-6 shows 40-50% similarity to the netrins from mouse, chicken, or fruit fly (22).

In mammals, there are four secreted netrins named as netrin-1, 3, 4, 5 and two glycosylphosphatidylinositol (GPI) membrane bound netrins (netrin G1, netrin G2) (17,23,24). All netrins have a high sequence homology to the extracellular matrix protein laminin N-terminal (LN) domain and the laminin-type growth factor-like (LE) domains. The N-terminal sequences of netrin-1, 2, 3 and 5 are homologous to the domains in laminin γ1 chain with strong sequence

identity of about 50% (25,26), while the N-terminal domains of netrins 4, G1 and G2 are homologous to the domains in laminin β1 with sequence identity of about 43% (27). A positively charged domain C that is unique to netrin is known as Netrin-like region (NTR) (28).

1.1 Netrin-1 and its Expression

The best characterized member of the netrin family remains netrin-1, a secretory protein, composed of ~ 600 amino acids with a length of 150 Å. It has four glycosylation sites (17). N-terminal, LN domain also known as domain VI, followed by LE domains such as LE1, LE2, LE3, also known as domain V, and a positively charged domain towards the C-terminal known as netrin-like region (NTR) (13) **(Figure 1.1).** The domain VI has a conserved Ca^{2+} binding site and also three asparagine-linked glycosylation sites (28–30). The stalked domain V adopts the classical LE-fold consisting of irregular coil segments (31) and thus form a linear extended structure (24). It has 8 conserved cysteine residues that form intra-molecular disulfide bridges. Domain V-2 is highly positively charged with a cluster of arginine and lysine side chains and provides a recognition site for acidic ligands (28). The positively charged C-terminal domain is believed to interact with the heparan sulfate proteoglycans (HSPG) (28) and the domain VI and V of netrin-1 are proposed to be involved in the interactions with receptors (17,28).

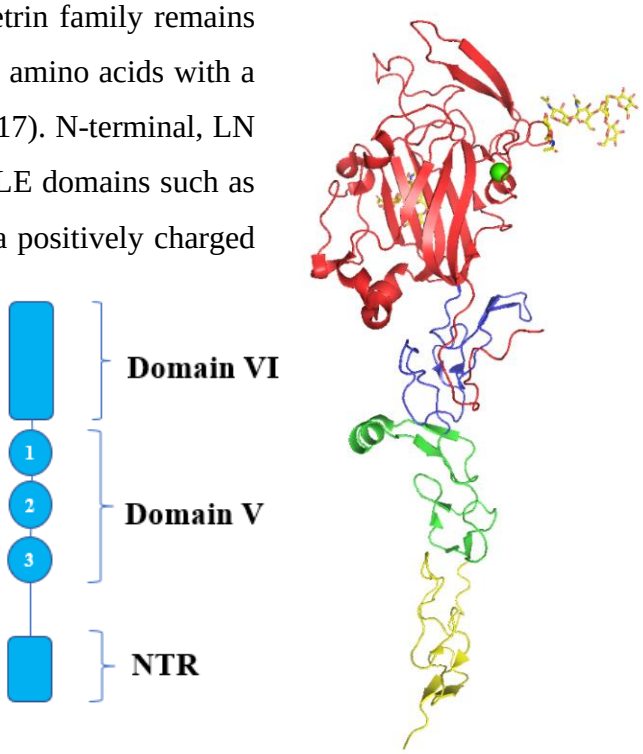

Figure 1.1 Structure of Netrin-1 and its domain organization.

Ribbon model structure of Netrin-1 (PDB: 4OVE). The N-terminal VI domain is shown in Red followed by three V domains: V1 (blue), V2 (green) and V3 (yellow). Ca^{2+} as green spheres.

In mammals, the expression of netrins is both in neuronal and non-neuronal tissues, during embryonic development and in adult stages. During spinal cord development, floor plate cells at the ventral midline of the embryonic neural tube secrete netrin-1 and create a gradient (17) **(Figure**

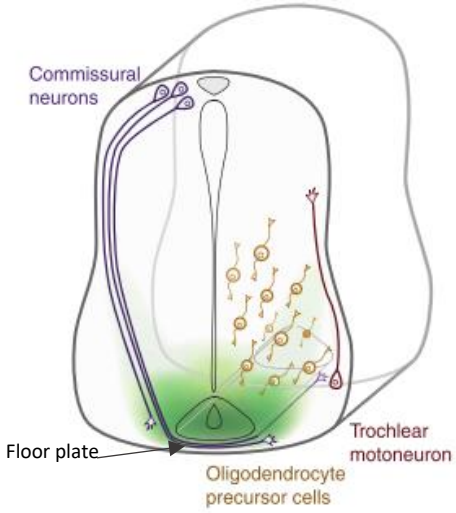

Figure 1.2 *Secretion of netrin-1 (green) by floor plate cells that forms the gradient and migration of different kind of cells from netrin-1 gradient. Figure with permission from* (17)*.*

1.2). The netrin-1 gradient helps in the migration of some cells, like commissural axons, oligodendrocytes precursor cells (OPCs) and the axons of trochlear motor neurons in the brainstem (23,32). Migration of these cells depends upon the presence of receptors on their surfaces (17,23). In addition, netrin-1 is expressed in the visual system (33), the developing and post olfactory system (34,35), the developing and adult forebrain and the cerebellum. Netrins are also expressed in other non-neural tissues such as ear epithelium, in the developing pancreas, lungs, mammary glands, heart, muscles and the intestine (25,34–37). Cell differentiation, proliferation, adhesion and migration, cell survival and synaptogenesis, are among the functions controlled by netrins (38,39).

The OPCs that mature into oligodendrocytes, the cells that form the myelin sheath of the central nervous system (CNS), express netrin-1 receptors in the adult mammalian CNS (40). The function of netrin-1 is not only restricted to the nervous system development during embryogenesis but it is also involved in other developing organs like mammary gland and lungs and is also involved in anti-inflammatory responses (41), angiogenesis, cell adhesion and cell survival in later stages of life (17,42). During embryogenesis, defective netrin signaling can cause developmental defects (31) whereas in adult life it is involved in cancer and neurodegenerative diseases (43,44).

Most of the netrin-1 is tightly associated with the cell membranes or extracellular matrix with the help of HSPG and guide axons (45). The presence of netrin-1 close to its cellular source is referred to as short-range guidance cue and it occurs in both the developing and mature central nervous system (23). Moreover netrin also functions at a distance from the area of its secretion, referred to as long-range guidance cue and mostly occurs in the embryonic nervous system (23).

Diffusion of netrin-1 creates a gradient to which commissural axons respond and shows chemotaxis (13) while substrate-bound netrin shows haptotaxis (7). Altogether, netrin-1, a guidance molecule, helps in guiding migrating neurons and can act as a chemotropic and haptotactic guidance molecule depending on the presence and distribution of receptors on the surface of migrating neurons during development of the CNS (7,17,25).

1.2 Receptors

In vertebrates, the first netrin-1 receptors to be identified belong to the Deleted in Colorectal Cancer family that includes DCC and Neogenin receptors (23,46). Other receptors for secreted netrin-1 include the Down's syndrome cell adhesion molecule (DSCAM), the uncoordinated 5 (Unc5) homolog family: Unc5 A-D in mammals (23), Draxin (47) and a more recent study has reported a new receptor CD146/ melanoma cell adhesion molecule (MCAM) (48). All of these receptors belong to the immunoglobulin (Ig) superfamily of proteins (17).

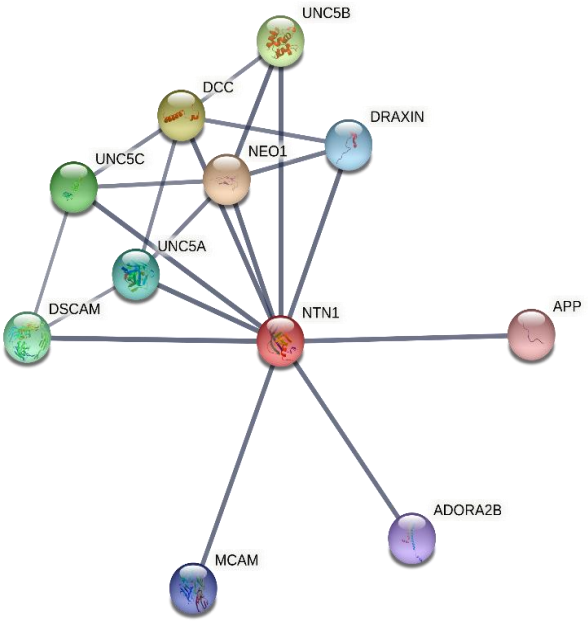

Figure 1.3 Interaction of netrin-1 with different receptors.

Minimum required Interaction Score=0.700 (High confidence). The receptors are represented with different colors with known structure. Interaction of netrin-1 with respective receptor is shown by a line and line connecting the receptors shows that these receptors also interact with each other. Figure with permission from https://string-db.org protein-protein interaction network (49).

DCC, Neogenin and Unc5 are also known as dependence receptors that trigger cell death through apoptosis in the absence of the ligand netrin-1 (17) but binding of ligand starts a different signaling pathway and acts like a survival factor for cells (17,50). Therefore, netrin-1 acts as a survival factor for tumor cells (51).

Proper neuronal wiring might require the change in direction of migrating axons. Different guidance cues along with their receptors play a very important role in changing the direction of the axons. Projecting axons are attracted towards the netrin-1 gradient source at the floor plate (chemo attraction) but repelled by this gradient after crossing the midline (chemo repulsion) (14).

Attraction and repulsion of these projecting axons could be related with the expression of the different receptor on the surface of growth cone. DCC and Neogenin, alone or with DSCAM show attraction towards the netrin-1 while Unc5 alone or with DCC/DSCAM show repulsion.

1.2.a. DCC

DCC is a single transmembrane receptor, vertebrate homologue of UNC40 in *C. elegans* (52). DCC shows deletion in many cancers such as colorectal cancer and is described as a candidate for the tumor suppression and thereby got its name Deleted in Colorectal Cancer (DCC). The extracellular region of DCC consists of four immunoglobulin (Ig) repeats that form a horseshoe-like conformation (53) and six fibronectin (FN) III repeats connected to a helical transmembrane domain and intracellular conserved cytosolic domains called P1, P2 and P3 (54) **(Figure 1.4)**.

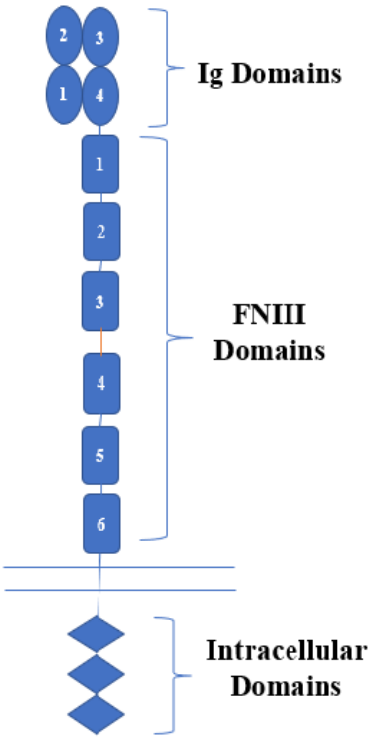

Figure 1.4 *Netrin-1 receptor Deleted in Colorectal Cancer (DCC) and its domain organization. Figure adapted and modified with permission from (50).*

Splicing is the post transcriptional process in which introns and sometimes exons are cut from the primary-ribonucleic acid (pre-RNA) to generate messenger RNA (mRNA). Alternate splicing creates several different mRNA that ultimately produce protein variants with different function or localization. Splicing factors play a very important role by producing the right protein for the appropriate activity (55). Many axon guidance molecules such as netrin (56) and its receptors (55), slit and its receptor (57), and semaphorin and its receptors, undergo alternate splicing that generates the complexity of neural development processes.

DCC/Neogenin undergoes alternate splicing to generate four isoforms and only two isoforms appear in embryonic and adult stage (58). Splicing occurs in the linker sequence between domain FNIII 4 and 5 and they are named DCC/Neo short if 20 amino acids are missing in the linker region and long form if those 20 amino acids are present (55,59). Knockout (KO) of spicing factor, NOVA1/2, shows severe neuronal and migration defects as DCC KO, result from the defective alternate splicing that changes the ratio of DCC variants (55). These two variants adopt different conformations in the ligand-receptor complex (30) but still the

downstream signaling of distinct conformation complexes need to be explained. It has been shown that DCC short forms the continuous netrin-1 DCC complex while netrin-1 DCC long complex has been suggested to form a 2:2 complex like the netrin-1 Neogenin short complex (30). DCC plays roles in apoptosis, dendritic growth and guidance, and in synapse formation and function but the effects of alternate splicing on these processes is still unknown.

Mutational studies showed that deletion of exon 29 or other mutations lead to the mirror movement and defective commissural development (60). Frameshift mutation results from the skipping of exon 6 that produces a truncated DCC that does not bind to netrin-1 (60). Interaction of netrin-1 with DCC, mainly studied in nervous system development, shows growth cone attraction, repulsion, and outgrowth. The absence of DCC has the same effect as of netrin-1 mutants, commissural path finding defects.

According to the published studies, FNIII repeats 4, 5 and 6 of DCC are involved in binding with netrin-1 (29,30,54,61). Interaction of a single netrin-1 molecule with two DCC receptors *via* two different binding sites (29) allows homodimerization of DCC intracellular domains and helps in signal transduction. According to Xu *et al*., 2014 (30), FNIII4 and FNIII5 domains of DCC have distinct binding sites on netrin-1 such as domain VI and V3 (site 0 and site 1) **(Figure 1.5)**. Finci *et al*., 2014 (29), reported a different binding site naming it as 'binding site 2' while using a

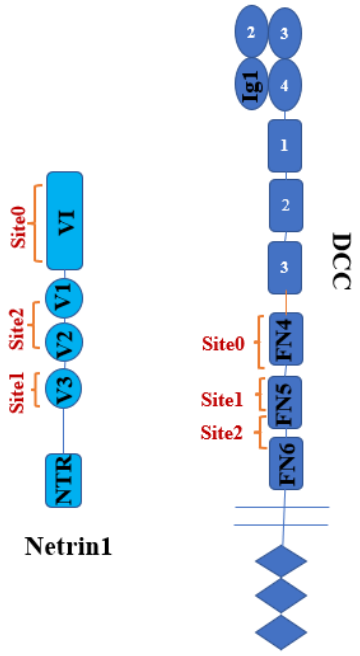

Figure 1.5 *Structure of netrin-1 and its receptor DCC with already proposed binding sites: site1, site2, site3. Figure adapted and modified with permission from (50).*

different construct of DCC containing domains FNIII5 and FNIII6. The regions on netrin-1 molecule that bind with DCCFN5-6, are also different such as V1 and V2 **(Figure 1.5)**. The crystal structure of netrin-1 DCC complex showed the involvement of negatively charged molecules in DCC FNIII5 domain interaction with netrin-1 (29) that could be heparan/ heparan sulfates (54,62). These two crystal structures agree with binding site 1 but not with binding site 2 and binding site 0, because the Xu *et al*., 2014 structure lacks the FN6 domain and the Finci *et al*., 2014 structure lacks the FN4 domain in their DCC construct (29,30). Based on the above findings, a complementary model was generated that shows the association of two DCC molecules with one netrin molecule *via* the V domain and forming a signaling unit (binding site 1, FN5 green and binding site 2, purple FN5-FN6) (29) **(Figure 1.6).** The DCC molecule that is attached to netrin-1 *via* the FN5 domain (binding site 1, green) also engages another netrin-1 *via* the FN4 domain (binding site 0, green) to join different netrin-1/DCC signaling units together (29) **(Figure 1.6)**.

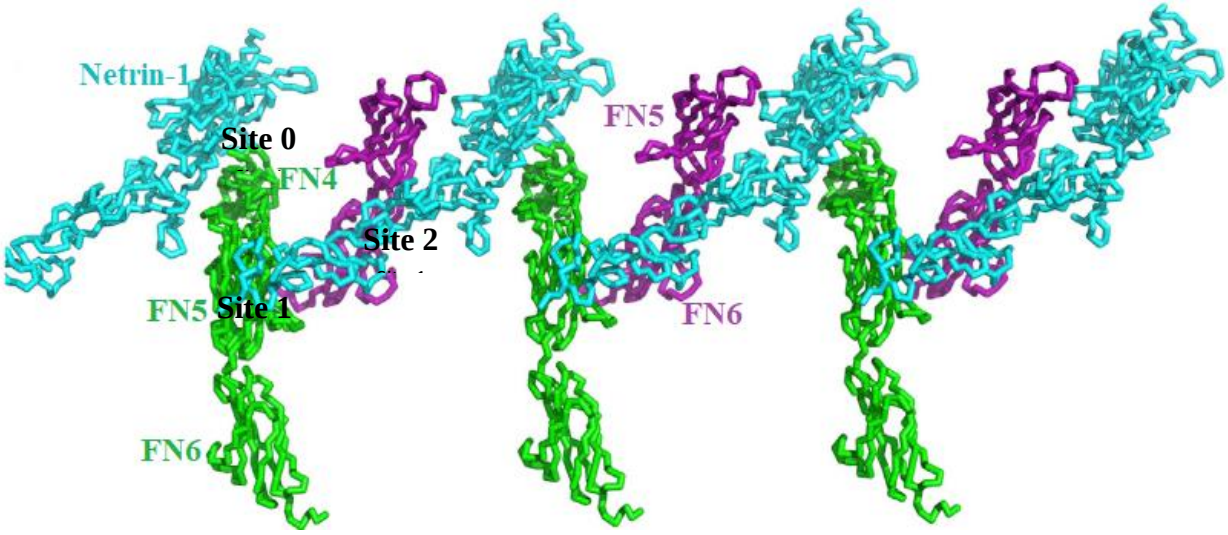

Figure 1.6 *Model of an extended netrin-1 DCC cluster based on the superposition of netrin-1 DCCFN4-5 complex by Xu et al., 2014 and netrin-1 DCC FN5-6 complex by Finci et al., 2014. The netrin-1 molecules are colored in cyan, the DCC molecules occupying sites 0 and 1 are colored green and the DCC molecules occupying binding site 2 are colored purple. Figure with permission from* (29).

Ross *et al*., 2021 showed that netrin-1 neogenin (NEO1) binding induces receptor clustering similar to that described by Xu *et al*., 2014 for netrin-1 DCC clustering (30,61) **(Figure 1.7A)** and also observed the receptor clustering that was mediated by netrin-1 *via* binding site 0 and site 1 and reported the concentration dependence on clustering (61).

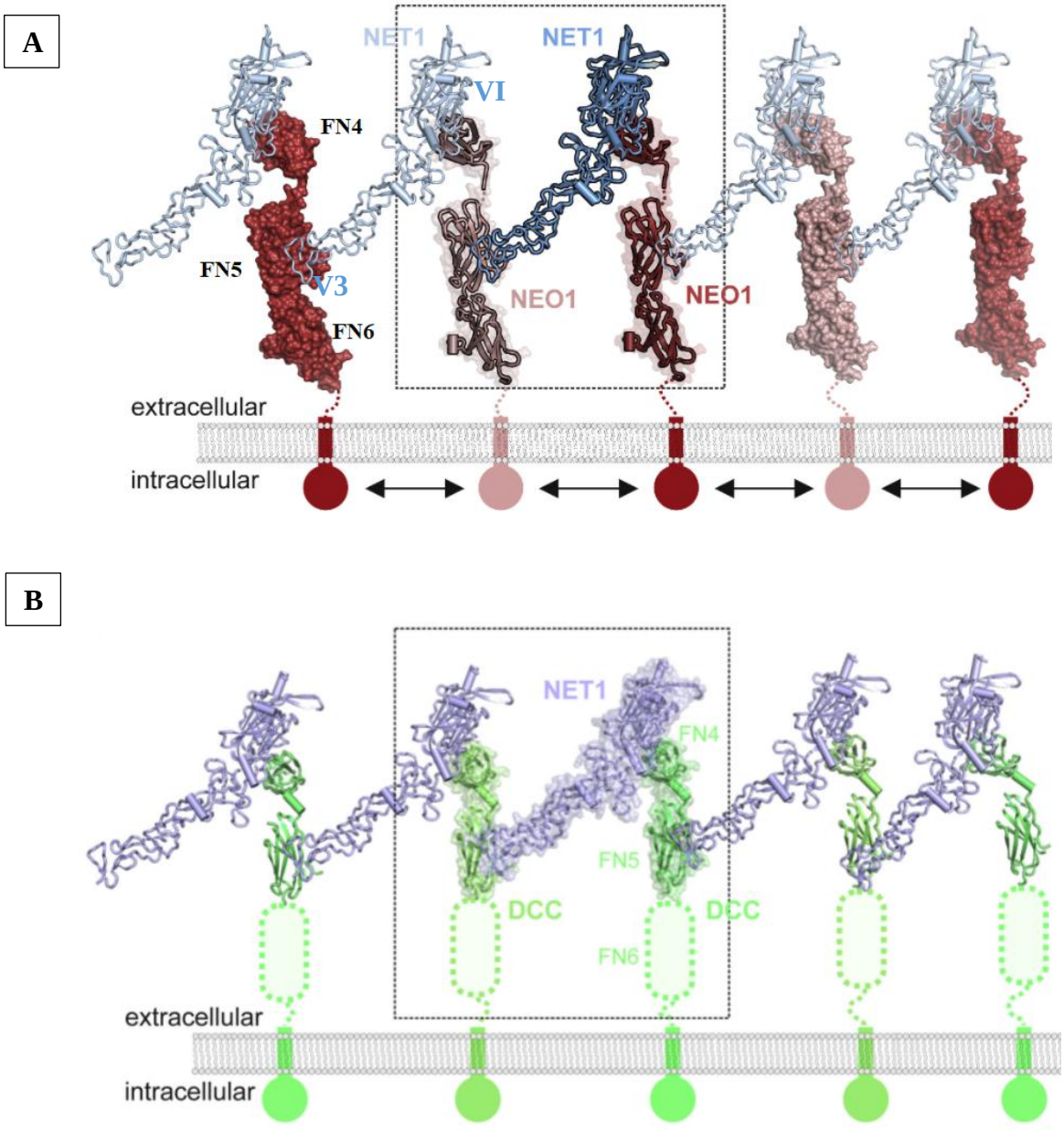

Figure 1.7 A) *An arrangement of netrin-1 (NET1) neogenin (NEO1), pdb id 7NE1.* ***B)*** *Cartoon representation of netrin-1 DCC complex by Xu et al., 2014, PDB id 4PLO. Both complexes form a continuous array in the crystal. The relative orientation of the plasma membrane and the DCC FN6 domain are depicted schematically. The netrin-1 molecules are represented in purple, the neogenin molecules are represented in red and the DCC molecules are in green. Figure with permission from (61).*

1.2.b. Unc5 A-D

Vertebrates Unc5 (A-D) are orthologs of *C. elegans* Unc5 (63). The ectodomain of Unc5 A-D consists of two N-terminal immunoglobulin-like (Ig1 and Ig2) domains and two thrombospondin-like (TSP1 and TSP2) domains **(Figure 1.8)**. The ectodomain is connected by a transmembrane helix to the intracellular region containing a zona occludens-5 domain (ZU5), a UPA domain (DCC-P1 binding domain, DB) and a death domain (DD) (63). Ig1 and Ig2 domains of Unc5 are involved in binding with netrin-1 V2 domain (28). Similar to DCC, Unc5 is also a dependence receptor of netrin-1 and its expression is downregulated in several cancers (64). Endothelial cells express Unc5b and mediate the repulsive effect to netrin-1 (65). In the presence of netrin-1, apoptotic activity of Unc5 is inhibited and helps in fine tuning of developmental angiogenesis (66,67).

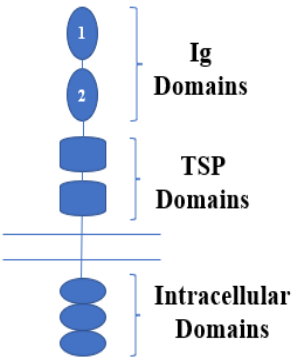

Figure 1.8 *Structure of netrin-1 receptor Unc5 and its domain organization. Figure adapted and modified with permission from (50).*

As mentioned before, Unc5-expressing axons are repelled by the netrin-1 gradient. Unc5 alone can mediate short range repulsion but it requires the expression of DCC protein along with Unc5 for long-range repulsive response (29,68). At low netrin-1 concentrations, Unc5/DCC heterodimers facilitate long-range repulsion (7).

Based on netrin-1 DCC structures explained above in section **1.2.a,** the molecular mechanism of netrin-1 bifunctionality could be envisioned. The distance between the two binding sites on the receptors is larger than the netrin-1 structure that allows one netrin-1 molecule to bind with two receptors. This enables netrin-1 interaction with different receptors *via* different binding sites (30). As Ig1 and Ig2 domains of Unc5 have positively charged residues (54) and binding site 2 of netrin-1 and DCC also have a large number of positively charged residues (29), this suggests some kind of switching between these receptors for binding to netrin-1. It also suggests that the presence of negatively charged heparin/heparan sulfates might act as a co-receptor or linker for netrin-1 interaction with receptor DCC or Unc5 or heparan sulfate may colocalize with netrin-1 on the cell surface (54).

The extracellular domains of these receptors are involved in binding with netrin-1 and the chemotropic properties are due to the intracellular domain's interactions (32,69). The interaction of netrin-1 with DCC results in the attraction of migrating axons towards the netrin gradient *via*

dimerization of intracellular domains that ultimately activate the Rho GTPases and thus organization of the cytoskeleton leads to the attraction of axons towards netrin-1 (17,70,71). However, co-expression of Unc5 with DCC results in the formation of a heterodimer of intracellular domains leading to the repulsion of axons from a netrin gradient (25,72).

Ligand-induced multimerization of receptors is very important for the positive signaling during axon guidance and blocking their proapoptotic activity (73). The cytoplasmic DD of Unc5 has some role in apoptosis by binding to the death-associated protein kinase (DAPk). The structural and structure-based functional analysis of the cytoplasmic domain of Unc5 revealed that a closed conformation of ZU5-UPA-DD with dephosphorylated DAPk leads to cell survival (74,75). On the other hand, an open conformation with the phosphorylated form of DAPk leads to cell death and blood vessel formation (74,75). Multimerization of Unc5b by netrin-1 leads to the closed conformation and inhibition of cell death (75). The cell biology studies (76) have investigated domains of receptors mainly DCC that are involved in interactions and the intracellular proteins involved in signaling cascades, however, information regarding the interactions at the molecular level is still missing.

Netrin-1, DCC/Unc5 and Cancer

Apoptosis, a programmed cell death, involves a series of caspase proteolytic activities to facilitate death. There is up-regulation of netrin-1 in a number of metastatic breast, lung, ovary and pancreatic cancers, in inflammatory-associated-colorectal cancer and in neuroblastoma (77) that blocks the apoptosis process induced by netrin-1 dependence receptors (78). It makes netrin-1 essential for the survival of cancer cells (51). DCC or Unc5 are caspase substrates and their intracellular domain DD recruits and activates caspase-9 which activates caspase-3 (25).

In the case of DCC, the cleavage allows exposure of a site known as the addition dependence domain (ADD) that is important for recruitment of the proteins such as DCC-interacting protein 13-α (DIP13α) and caspase-9. This process leads to the activation of caspase-9 which ultimately activates more caspase-3 **(Figure 1.9a)** (79).

In the case of Unc5, after cleavage of the DD by caspase-3, the serine/threonine DAPK interacts with the cleaved DD and initiates the apoptotic pathway through caspase-9, followed by more caspase-3 activation **(Figure 1.9c)** (80).

The inhibition of apoptosis is induced by the dimerization of receptors after netrin-1 binding **(Figure 1.9b)**. The change in conformation after dimerization does not allow caspase-3

cleavage and thus leads to the activation of the protein kinase B /AKT signaling pathway after dissociation of DIP3α from the receptor (79). AKT signaling blocks the release of pro-apoptotic proteins from the mitochondria and activates Nuclear factor kappa-light-chain-enhancer of activated B cells (NF-κB) mediated transcription of anti-apoptotic genes (79). Moreover, activation of Mitogen Activated protein kinase (MAPK) signaling pathway, involved in chemo attraction during neural outgrowth, is also involved in blocking apoptosis by inhibiting caspase-9 (79). However, downregulation of netrin-1 receptor expression could be another factor by downregulating apoptotic signaling. It is not clear whether targeting netrin-1 itself or netrin-1 receptor will be a suitable approach to finding a treatment for cancer.

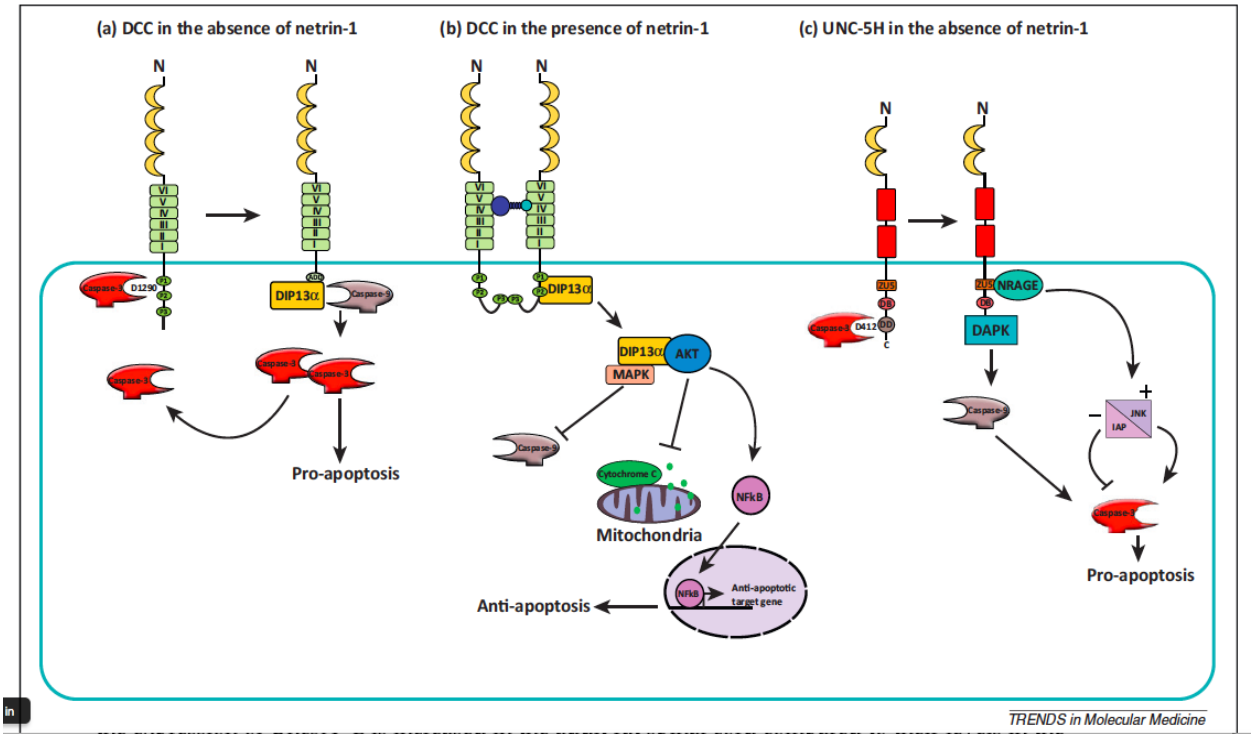

Figure 1.9 Netrin-1 dependence receptors signaling.

(a, c) when Netrin-1 is absent, both DCC and Unc5 are cleaved by caspase-3 (b) When Netrin-1 is present, DCC receptors dimerize that leads to blocking of caspase-3 cleavage site and dissociation of DIP12. Figure reproduced with permission from (79).

1.2.c. CD146

As mentioned before, netrin-1 interacts with different receptors and depending upon the expression of receptors, it can act in different ways. Netrin-1 acts like a pro- or anti-angiogenic factor depending upon its interaction with different receptors (81). CD 146 (melanoma cell adhesion molecule, MCAM) is a member of the immunoglobulin superfamily, has five extracellular Ig-like domains, a transmembrane domain, and a cytoplasmic tail **(Figure 1.10)**.

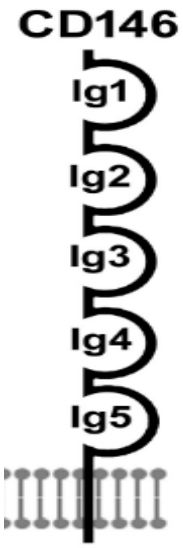

Figure 1.10 *Structure of CD146 and domain organization. Figure with permission from* (2).

CD146 express on endothelial cells and is involved in many biological processes such as angiogenesis, tumor metastasis, lymphocyte activation and tissue regeneration (48,82). Netrin-1 binds with the CD146 with high affinity and induces endothelial cell activation and downstream signal transduction by dimerization of the receptors (48). Many studies on zebrafish show that the netrin-1 and CD146 downregulation results in blocking vascular sprouting and branching (48). Therefore, netrin-1 in its interaction with CD146, acts like a pro-angiogenic factor during vertebrate development. The 4th Ig domain of CD146 is involved in the binding (48). Both CD146 and Unc5b are present on the endothelial cells and binding of netrin -1 is concentration dependent. At low concentration, CD146 binds to netrin-1 and at high concentration, Unc5b binds to it and changes the pro angiogenic effect to an anti-angiogenic effect (48,81)

1.2.d. DSCAM

Another receptor for netrin-1 is DSCAM, Down syndrome cell adhesion molecule, is a type I transmembrane receptor and is structurally similar to DCC. It acts as a coreceptor with Unc5c to mediate short-range repulsion and is found partially co-localized with Unc5 in primary neurons and brain tissues (7,83). It is involved in midline crossing of spinal commissural neurons independent of DCC (homophilic binding) and in collaboration with DCC (heterophilic binding) (84). Like other receptors, DSCAM has to coordinate with ligand and other receptors. Extracellular and intracellular receptors dimerization coordinates downstream signaling cascade for axonal repulsion (83). Interaction of DSCAM with Unc5 leads to the axonal growth cone collapse in mouse cerebellar granular cells by promoting many downstream signaling molecules involved in repulsive signaling like FAK, Fyn, and PAK1 (83). Ig domains seven to nine are sufficient for

netrin-1 binding to DSCAM (84). Any changes in the expression level of DSCAM is associated with altered neural wiring which causes changes in cognitive function and shows the phenotype associated with Down Syndrome mental retardation.

1.2.e. Draxin

Another binding partner for netrin-1 is draxin, dorsal repulsive axon guidance protein, known to show repulsive behavior of axons from misprojecting before midline crossing. Netrin-1 with its haptotaxis nature, guides axons *via* acting as an adhesive axon growth substrate and promotes axon fasciculation (47). Draxin interacts with the netrin-1 through the EGF-3 domain, in the same region where the DCC FN5 domain binds netrin-1 and it also shows interaction with DCC *via* the N-terminal Ig domains (47). Therefore, in this DCC-draxin-netrin-1 interaction, netrin-1 acts as a hub for receptors allowing adhesion and fasciculation between the axons either in cis or trans (47). Modulation of multivalent netrin-1 DCC complex by other receptors shows clearly the complexity of axon guidance and involvement of substrate-bound netrin-1 gradients for axon movement (85,86).

1.3 Heparan Sulfate Proteoglycan

HSPGs play an essential role in various axon guidance processes (87). They are composed of a core protein with covalently attached long glycosaminoglycan (GAG) chains that are highly acidic (88). Extracellular matrix (ECM) and basement membrane (BM) are specialized supermolecular networks of protein, glycoproteins, and proteoglycans underlying epithelial and endothelial cells. The GAGs are involved in many physiological and pathological processes such as cell growth, regulation of cell signaling *via* ECM assembly, infections, angiogenesis, cancer, and neurodegenerative diseases (89,90). There are different types of GAGs in mammals such as heparin (HP), heparan sulfate (HS), chondroitin sulfate (CS), keratan sulfate (KS) and other classes too but netrin-1 shows binding to mainly HS (90). All these GAGs are sulfated at various positions to different extent and finally attached to the protein to form proteoglycans (90). HSs are a heterogeneous family of macromolecules, composed of repeating disaccharide building blocks having alternating linked units of uronic acid (glucuronic acid or iduronic acid) and glucosamine (N-acetylated/N-sulfated glucosamine) (91,92). Structural complexity in HP and HS are either substitutions or modifications, that include O-sulfation and N-sulfation, N-acetylation and uronic acid C5 epimerization and HP, primarily produced in mast cells and heavily sulfated form of HS (89,91). The complex nature of these proteoglycans might be necessary in mediating interactions of netrin-1 to different receptors or the different nature of these molecules could be involved in switching between the receptors (2,29).

HSPG and Netrin-1

The HSPGs attach to the cell surface either with a transmembrane domain, for example, syndecans or with GPI like glypicans (88). Glypican, a HSPG secreted from the epidermal cells, modulates netrin-1 mediated both attractive and repulsive signaling *via* guiding cells and axons through its interaction with both netrin-1 and DCC (88). It is well known that HP- or HS-binding sites have the basic consensus sequences, X-B-B-X-B-X and X-B-B-B-X-X-B-X, where B is a basic amino acid and X is a hydrophobic amino acid, the Cardin and Weintraub (CW) motifs (90).

The C-terminal domain of netrin-1 is the major binding area for HP (9,93) and might mediate the binding of netrin-1 to the proteoglycans or glycolipids on the cell surface or in the ECM (9). A cluster of basic amino acids at the C-terminal of netrin-1 is responsible for their binding to heparin and forms a heparin-binding motif (9,93). Binding studies gave an average binding dissociation constant K_d of 15 nM for the binding of the C-terminal region of netrin-1 to

heparin (93). The addition of high salt in the binding buffer abolished the binding to heparin and indicated the electrostatic mode of interaction (93). A truncated version of netrin-1 containing domain V and VI has a CW motif for HS-binding and shows specific activity for outgrowth of commissural axons similar to the full length netrin-1 containing VI, V, and C-terminal domains (46). However, truncated netrin-1 interactions with HSPGs and regulation of the netrin-1 guided signaling during nervous system development remain elusive. To unravel the molecular mechanism underlying GAG-protein interaction and ultimately their biological function, binding interfaces knowledge is essential.

HSPG and Netrin-1 receptors

It is known that both netrin-1 and DCC bind to heparin and thus are involved in the commissural axon guidance (88,94). It has been suggested that HSPGs play very important roles in specific binding between netrin-1 and DCC (46) and any change in HS synthesis results in axon pathfinding defects (87). Netrin-1 triggers the multimeric complex formation involving DCC/Unc5 receptors, and receptor multimerization may result from the aggregation of netrin-1 by proteoglycans on the cell surface (46,69). Geisbrecht *et al*., 2003 proposed that the DCC/heparin interaction is mediated by netrin-1 which binds to heparin through its C-terminal (54). Further, netrin-1 interaction with heparin might concentrate the netrin-1 on the cell surface or spatially limit the netrin signal. They also suggested that this interaction does not seem essential for the netrin signaling (54) as netrin-1 full length (VI, V, and C domains) and truncated netrin-1 (VI and V domains) both show axon outgrowth (46). There is no information about the interaction of heparin and truncated netrin-1.

The crystal structure of netrin-1 and Neogenin/DCC FN4-FN5 shows a positively charged surface on the netrin-1 V2 domain and receptors FN5 domain (30). These surfaces are exposed to solvents in the crystal structure and are potentially available to interact with negatively charged molecules (30). Netrin-1 allows the interaction of two DCC/Neogenin *via* two different binding sites as the distance between two binding sites on netrin-1 is significantly larger than the binding sites on DCC and might form continuous netrin-1/DCC assembly (30,61) **(**discussed earlier in section 1.2.a **Figure 1.7).** This structure of netrin-1 with DCC does not show any interaction *via* negatively charged molecules. Another crystal structure of netrin-1 and DCC FN5-FN6 shows another binding site involving both V1 and V2 domains of netrin-1 and FN5 as well as the tip of FN6 of DCC (29). The positively charged patches of netrin-1 V2 and DCC FN5 are neutralized by

sulfates ions and are correlated with the presence of certain proteoglycans (29,54). It was proposed that this binding site is a switching point that allows the switch in the netrin-1 response from chemoattraction to chemo repulsion by replacing DCC with Unc5 (29). And also proposed is the involvement of different HS molecules in the interaction of netrin-1 with different receptors (29). However, there is not much known in the literature showing the involvement of heparin in the binding of netrin-1 with Unc5 (95) and the V-2 domain of netrin-1 interaction with DCC FN5 (54,61). There is no evidence in the literature showing Unc5 interaction with heparin.

Heparanase, the only known mammalian endoglycosidase cleaves HS of HSPG in mammals and disassembles the ECM and BM (96). This modification makes the ECM more susceptible to cellular invasion, metastasis, angiogenesis and inflammation (97). In normal conditions, heparanase activity is in the placenta, skin and blood cells, but, its activity is increased in many human cancers (97). Heparanase treatment of naturally occurring polysaccharides was used in the formation of a small oligosaccharides library that can be used for GAG-protein interactions (89).

However, the specific role of GAG molecules in the protein-protein network mediated by netrin-1 has not been demonstrated. Therefore, a detailed molecular understanding of netrin-1 and its interactions with GAG molecules will help to understand the involvement of GAG in the netrin-1 dependence receptor.

1.4 Netrin-1 and neurodegenerative diseases

Netrin-1 plays a very important role in neural development including cell migration, extension, and cell adhesion (98). Oligodendrocytes are the cells that help in the formation of myelin sheath around the axons to facilitate fast and efficient signal conduction. Netrin-1 plays a very important role in different stages of their development *via* signaling through their receptors DCC and Unc5 (43,99). OPC express the netrin-1 receptors DCC and Unc5 and they are guided by netrin-1 by its chemorepellent response (44). The loss of remyelination of damaged axons by oligodendrocytes is characteristic of multiple sclerosis (MS). MS lesions inhibit the differentiation of the OPCs to the oligodendrocytes and their recruitment (43). Expression of netrin-1 in the extracellular matrix and macrophages in MS lesions suggests its involvement in the migration of OPC and ultimately in remyelination (2,43). Detectable amounts of full length and truncated version (without C-terminal domain) are found in both the adult human white matter and MS lesions thus are involved in myelin formation and maintenance (43). In pathological circumstances, the loss of attraction but preserving the repellent activity of truncated versions of netrin-1, inhibits OPC migration to MS plaques and repair of the demyelinated plaques (43).

1.5 Aim of the Work

The present study concentrated on the characterization of a guidance cue, netrin-1 and its interaction with GAG molecules.

Netrin-1, an extracellular cue, shows chemotaxis and haptotaxis, is essential for the maturation of the CNS cells both in embryonic and adult life. Many studies have already shown the important functions of netrin-1 starting from axon guidance, branching, adhesion, cell migration, cell survival to axon regeneration (17,44,47,100). In addition, netrin-1 is overexpressed in metastatic tissues and MS lesions (43,73,101). Netrin-1 has glycosylation sites and cysteine-cysteine disulfide bonds and therefore a mammalian expression system, HEK293T cells, was chosen for stable expression.

The aim of this dissertation was to find the specific role of GAGs with netrin-1 (activator, selector, coreceptor, or concentrator) and to study molecular details of the netrin-1 and GAG.

There are still some inconsistencies in the literature regarding the binding behavior of netrin-1 with its dependence receptors (28–30). Netrin-1 showed multiple binding sites for DCC/Neogenin and switching of some of the sites with other receptors showed a change in the function of the netrin-1 DCC/Neogenin interacting hub (61). The focus of my work is to study netrin-1's dynamic behavior in detail and its interaction with GAG molecules attached to HSPGs that are present extracellularly. HSPGs might increase netrin-1 local concentration on the cell surface *via* GAG molecules interactions and are also proposed to be involved in the netrin-1 receptor interactions similar to cytokines-cytokines receptor complexes (102). A crystal structure of netrin-1 DCC by Finci *et al*., 2014, reported the involvement of negatively charged molecules in the binding between netrin-1 V-2 domain and DCC FN5-6 domains and suggested that HSPG might be involved in switching the netrin-1 mediated attraction *via* DCC to repulsion *via* Unc5 or vice versa (29). There is not much structural information of netrin-1 bound with the HSPG. Two models are possible where netrin-1 would bind to the GAGs on the HSPG **(Figure 1.11A)** and the first possibility is shown in **Figure 1.11B.** Here, heparanase cleaves the GAG chains resulting in the formation of high molecular weight clusters of netrin-1 in the ECS. These oligosaccharides bound netrin-1 might diffuse and create a concentration gradient for receptors. A second possibility

is that the GAG clustered netrin-1 localize near the receptors on the cell surface **(Figure 1.11C)** and could make receptor clustering that influences further downstream signaling.

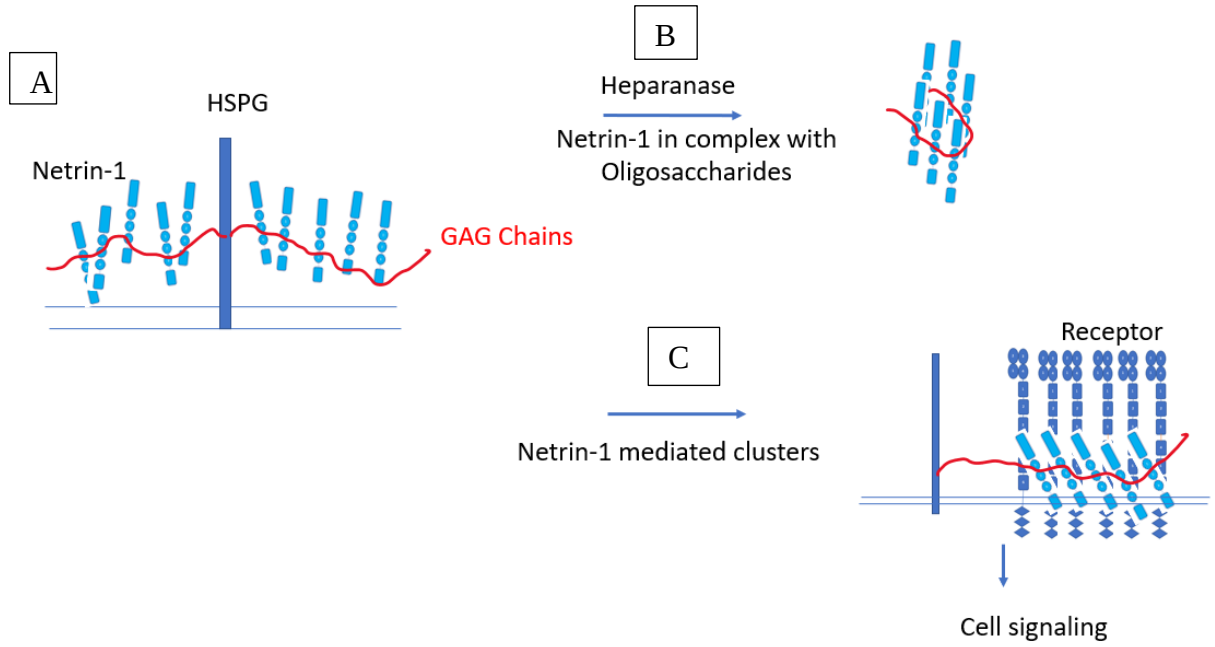

Figure 1.11 *Model of netrin-1 GAGs interactions. A) Netrin-1 binds to the GAGs molecules on the HSPG near the cell surface via C domain and V2 domain. B) Heparanase might cleave the GAG chains and form oligosaccharides with netrin-1 attached to it. C) Netrin-1 molecules interact with the receptors on the cell surface and allow receptor clustering (netrin-1 localize near the receptors with the help of HSPGs).*

To gain deeper insight into the binding, their structure was studied by X-ray crystallography with Sucrose OctaSulfate (SOS), a synthetic heparin mimic. Further biophysical studies were performed using different length oligosaccharides to see the effect of these shorter versions of HSs on the dynamic behavior of netrin-1. Binding studies were performed to verify the involvement of short-length oligosaccharides in netrin-1 dependence receptor complex formation. This work would potentially provide fundamental information about how netrin-1 could colocalize or concentrate on the cell surface and show signaling *via* specific receptors. The results obtained from this study could possibly contribute to a better understanding of netrin-1 dynamic behavior, including the involvement of GAG molecules. This could potentially promote new ideas for the development of small molecules targeting the GAG binding sites for the treatment of cancer.

References

1. Ahmed G, Shinmyo Y. Multiple Functions of Draxin/Netrin-1 Signaling in the Development of Neural Circuits in the Spinal Cord and the Brain. Front Neuroanat. 2021 Nov 25;15:93.
2. Dun XP, Parkinson D. Role of Netrin-1 Signaling in Nerve Regeneration. Int J Mol Sci . 2017;18(3):491. Available from: http://www.mdpi.com/1422-0067/18/3/491
3. Finci L, Zhang Y, Meijers R, Wang JH. Signaling mechanism of the netrin-1 receptor DCC in axon guidance. Prog Biophys Mol Biol . 2015 Sep 14;118(3):153–60. Available from: http://www.ncbi.nlm.nih.gov/pmc/articles/PMC4537816/
4. Dent EW, Gupton SL, Gertler FB. The Growth Cone Cytoskeleton in Axon Outgrowth and Guidance. Cold Spring Harb Perspect Biol . 2011 Mar;3(3):1–39. Available from: /pmc/articles/PMC3039926/
5. Hur EM, Saijilafu, Zhou FQ. Growing the growth cone: remodeling the cytoskeleton to promote axon regeneration. Trends Neurosci . 2012 Mar;35(3):164. Available from: /pmc/articles/PMC3294076/
6. Tessier-Lavigne M, Goodman CS. The Molecular Biology of Axon Guidance. Science (80) . 1996 Nov 15;274(5290):1123–33. Available from: https://www.science.org/doi/abs/10.1126/science.274.5290.1123
7. Boyer NP, Gupton SL. Revisiting netrin-1: One who guides (Axons). Front Cell Neurosci. 2018;12(July):1–18.
8. Dudanova I, Klein R. Integration of guidance cues: parallel signaling and crosstalk. Trends Neurosci . 2013 May 1;36(5):295–304. Available from: http://www.cell.com/article/S0166223613000192/fulltext
9. Serafini T, Kennedy TE, Galko MJ, Mirzayan C, Jessell TM, Tessler-Lavigne M. The Netrins Define a Family of Axon Outgrowth-Promoting Proteins Homologous to C. elegans UNC-6. Cell. 1994;79:409–24.
10. Kolodkin AL, Matthes DJ, Goodman CS. The semaphorin genes encode a family of transmembrane and secreted growth cone guidance molecules. Cell . 1993 Dec 31;75(7):1389–99. Available from: http://www.cell.com/article/009286749390625Z/fulltext
11. Brose K, Bland KS, Kuan HW, Arnott D, Henzel W, Goodman CS, Tessier-Lavigne M,

Kidd T. Slit Proteins Bind Robo Receptors and Have an Evolutionarily Conserved Role in Repulsive Axon Guidance. Cell . 1999 Mar 19;96(6):795–806. Available from: http://www.cell.com/article/S0092867400805905/fulltext

12. Rothberg JM, Jacobs JR, Goodman CS, Artavanis-Tsakonas S. slit: an extracellular protein necessary for development of midline glia and commissural axon pathways contains both EGF and LRR domains. Genes Dev . 1990 Dec 1;4(12a):2169–87. Available from: http://genesdev.cshlp.org/content/4/12a/2169
13. Kennedy TE, Serafini T, de la Torre J, Tessier-Lavigne M. Netrins are diffusible chemotropic factors for commissural axons in the embryonic spinal cord. Cell . 1994 Aug 12;78(3):425–35. Available from: http://dx.doi.org/10.1016/0092-8674(94)90421-9
14. Kennedy TE, Serafini T, de la Torre JR, Tessier-Lavigne M. Netrins are diffusible chemotropic factors for commissural axons in the embryonic spinal cord. Cell. 1994 Aug 12;78(3):425–35.
15. Hedgecock EM, Culotti JG, Hall DH. The unc-5, unc-6, and unc-40 genes guide circumferential migrations of pioneer axons and mesodermal cells on the epidermis in C. elegans. Neuron . 1990 Jan 1;4(1):61–85. Available from: http://www.cell.com/article/089662739090444K/fulltext
16. Ishii N, Wadsworth WG, Stern BD, Culotti JG, Hedgecock EM. UNC-6, a laminin-related protein, guides cell and pioneer axon migrations in C. elegans. Neuron . 1992;9(5):873–81. Available from: https://pubmed.ncbi.nlm.nih.gov/1329863/
17. Lai Wing Sun K, Correia JP, Kennedy TE. Netrins: versatile extracellular cues with diverse functions. Development . 2011;138(11):2153–69. Available from: http://www.ncbi.nlm.nih.gov/pubmed/21558366
18. Ishii N, Wadsworth WG, Stern BD, Culotti JG, Hedgecock EM. UNC-6, a laminin-related protein, guides cell and pioneer axon migrations in C. elegans. Neuron. 1992 Nov;9(5):873–81.
19. Hedgecock EM, Culotti JG, Hall DH. The unc-5, unc-6, and unc-40 genes guide circumferential migrations of pioneer axons and mesodermal cells on the epidermis in C. elegans. Neuron . 1990;4(1):61–85. Available from: https://pubmed.ncbi.nlm.nih.gov/2310575/
20. Harris R, Sabatelli LM, Seeger MA. Guidance Cues at the Drosophila CNS Midline:

Identification and Characterization of Two Drosophila Netrin/UNC-6 Homologs. Neuron . 1996 Aug 1;17(2):217–28. Available from: http://www.cell.com/article/S0896627300801543/fulltext

21. Serafini T, Colamarino SA, Leonardo ED, Wang H, Beddington R, Skarnes WC, Tessier-Lavigne M. Netrin-1 Is Required for Commissural Axon Guidance in the Developing Vertebrate Nervous System. Cell . 1996 Dec 13;87(6):1001–14. Available from: http://www.cell.com/article/S009286740081795X/fulltext
22. Krahn N, Meier M, Reuten R, Koch M, Stetefeld J, Patel TR, Ka Shing L. Solution Structure of C. elegans UNC-6: A Nematode Paralogue of the Axon Guidance Protein Netrin-1. Biophys Soc . 2019;116:2121–30. Available from: https://doi.org/10.1016/j.bpj.2019.04.033
23. Rajasekharan S, Kennedy TE. The netrin protein family. Genome Biol. 2009;10(9):239.
24. Reuten R, Patel TR, McDougall M, Rama N, Nikodemus D, Gibert B, Delcros JG, Prein C, Meier M, Metzger S, Zhou Z, Kaltenberg J, McKee KK, Bald T, Tüting T, Zigrino P, Djonov V, Bloch W, Clausen-Schaumann H, Poschl E, Yurchenco PD, Ehrbar M, Mehlen P, Stetefeld J, Koch M. Structural decoding of netrin-4 reveals a regulatory function towards mature basement membranes. Nat Commun . 2016;7:13515. Available from: http://www.nature.com/doifinder/10.1038/ncomms13515
25. Cirulli V, Yebra M. Netrins: beyond the brain. Nat Rev Mol Cell Biol . 2007;8(4):296–306. Available from: http://www.nature.com/doifinder/10.1038/nrm2142
26. Koch M, Murrell JR, Hunter DD, Olson PF, Jin W, Keene DR, Brunken WJ, Burgeson RE. A novel member of the netrin family, β-netrin, shares homology with the β chain of laminin: Identification, expression, and functional characterization. J Cell Biol. 2000;151(2):221–34.
27. Nakashiba T, Ikeda T, Nishimura S, Tashiro K, Honjo T, Culotti JG, Itohara S. Netrin-G1: A novel glycosyl phosphatidylinositol-linked mammalian netrin that is functionally divergent from classical netrins. J Neurosci. 2000;20(17):6540–50.
28. Grandin M, Meier M, Delcros JG, Nikodemus D, Reuten R, Patel TR, Goldschneider D, Orriss G, Krahn N, Boussouar A, Abes R, Dean Y, Neves D, Bernet A, Depil S, Schneiders F, Poole K, Dante R, Koch M, Mehlen P, Stetefeld J. Structural Decoding of the Netrin-1/UNC5 Interaction and its Therapeutical Implications in Cancers. Cancer Cell.

2016;29(2):173–85.

29. Finci LI, Krüger N, Sun X, Zhang J, Chegkazi M, Wu Y, Schenk G, Mertens HDT, Svergun DI, Zhang Y, Wang J huai, Meijers R. The Crystal Structure of Netrin-1 in Complex with DCC Reveals the Bifunctionality of Netrin-1 As a Guidance Cue. Neuron. 2014;83(4):839–49.
30. Xu K, Wu Z, Renier N, Antipenko A, Tzvetkova- D, Xu Y, Minchenko M, Nardi-dei V, Kanagalaghatta R, Himanen J, Tessier-lavigne M, Nikolov DB. Structure of Netrin1 bound to two receptors provide insight into its Axon Guidance Mechanism. Science (80). 2014;344(6189):1275–9.
31. Serafini T, Colamarino SA, Leonardo ED, Beddington R, Skarnes WC, Tessier-lavigne M, Wang H. Netrin-1 Is Required for Commissural Axon Guidance in the Developing Vertebrate Nervous System. Cell. 1996;87(6):1001–14.
32. Bradford D, Cole SJ, Cooper HM. Netrin-1: Diversity in development. Int J Biochem Cell Biol . 2009;41(3):487–93. Available from: http://www.sciencedirect.com/science/article/pii/S1357272508001271
33. Livesey FJ, Hunt SP. Netrin and netrin receptor expression in the embryonic mammalian nervous system suggests roles in retinal, striatal, nigral, and cerebellar development. Mol Cell Neurosci. 1997;8(6):417–29.
34. Salminen M, Meyer BI, Bober E, Gruss P. Netrin 1 Is Required for Semicircular Canal Formation in the Mouse Inner Ear. Development. 2000;127(1):13–22.
35. Madison RD, Zomorodi A, Robinson GA. Netrin-1 and peripheral nerve regeneration in the adult rat. Exp Neurol. 2000;161(2):563–70.
36. Dalvin S, Anselmo MA, Prodhan P, Komatsuzaki K, Schnitzer JJ, Kinane TB. Expression of Netrin-1 and its two receptors DCC and UNC5H2 in the developing mouse lung. Gene Expr Patterns. 2003;3:279–83.
37. Srinivasan K, Strickland P, Valdes A, Shin GC, Hinck L. Netrin-1/neogenin interaction stabilizes multipotent progenitor cap cells during mammary gland morphogenesis. Dev Cell. 2003;4(3):371–82.
38. Ekblom P, Vestweber D, Kemler R. Cell-matrix interactions and cell adhesion during development. Cell Biol. 1986;2:27–47.
39. Yebra M, Montgomery AMP, Diaferia GR, Kaido T, Silletti S, Perez B, Just ML,

Hildbrand S, Hurford R, Florkiewicz E, Tessier-Lavigne M, Cirulli V. Recognition of the neural chemoattractant netrin-1 by integrins α6β4 and α3β1 regulates epithelial cell adhesion and migration. Dev Cell. 2003;5:695–707.

40. Manitt C, Colicos MA, Thompson KM, Rousselle E, Peterson AC, Kennedy TE. Widespread Expression of Netrin-1 by Neurons and Oligodendrocytes in the Adult Mammalian Spinal Cord. J Neurosci . 2001 Jun 1;21(11):3911 LP – 3922. Available from: http://www.jneurosci.org/content/21/11/3911.abstract
41. Ranganathan P, Mohamed R, Jayakumar C, Ramesh G. Guidance cue netrin-1 and the regulation of inflammation in acute and chronic kidney disease. Mediators Inflamm. 2014;2014.
42. Mehlen P, Furne C. Netrin-1 : when a neuronal guidance cue turns out to be a regulator of tumorigenesis. 2005;62:2599–616.
43. Bin JM, Rajasekharan S, Kuhlmann T, Hanes I, Marcal N, Han D, Rodrigues SP, Leong SY, Newcombe J, Antel JP, Kennedy TE. Full-length and fragmented netrin-1 in multiple sclerosis plaques are inhibitors of oligodendrocyte precursor cell migration. Am J Pathol . 2013;183(3):673–80. Available from: http://dx.doi.org/10.1016/j.ajpath.2013.06.004
44. Jarjour A a., Manitt C, Moore SW, Thompson KM, Yuh SJ, Kennedy TE. Netrin-1 Is a Chemorepellent for Oligodendrocyte Precursor Cells in the Embryonic Spinal Cord. J Neurosci. 2003;23(9):3735–44.
45. Serafini T, Kennedy TE, Galko MJ, Mirzayan C, Jessell TM, Tessier-Lavigne M. The netrins define a family of axon outgrowth-promoting proteins homologous to C. elegans UNC-6. Cell . 1994 Aug 12;78(3):409–24. Available from: https://pubmed.ncbi.nlm.nih.gov/8062384/
46. Keino-Masu K, Masu M, Hinck L, Leonardo ED, Chan SSY, Culotti JG, Tessier-Lavigne M. Deleted in Colorectal Cancer (DCC) Encodes a Netrin Receptor. Cell . 1996 May 23;87(2):175–85. Available from: http://dx.doi.org/10.1016/S0092-8674(00)81336-7
47. Liu Y, Bhowmick T, Liu Y, Gao X, Mertens HDT, Svergun DI, Xiao J, Zhang Y, Wang J huai, Meijers R. Structural Basis for Draxin-Modulated Axon Guidance and Fasciculation by Netrin-1 through DCC. Neuron . 2018;1–7. Available from: http://linkinghub.elsevier.com/retrieve/pii/S0896627318301090
48. Tu T, Zhang C, Yan H, Luo Y, Kong R, Wen P, Ye Z, Chen J, Feng J, Liu F, Wu JY, Yan

X. CD146 acts as a novel receptor for netrin-1 in promoting angiogenesis and vascular development. Cell Res . 2015 Mar 6;25(3):275–87. Available from: http://www.ncbi.nlm.nih.gov/pmc/articles/PMC4349246/

49. Szklarczyk D, Gable AL, Lyon D, Junge A, Wyder S, Huerta-Cepas J, Simonovic M, Doncheva NT, Morris JH, Bork P, Jensen LJ, Von Mering C. STRING v11: Protein-protein association networks with increased coverage, supporting functional discovery in genome-wide experimental datasets. Nucleic Acids Res. 2019;47(D1):D607–13.
50. Goldschneider D, Mehlen P. Dependence receptors: a new paradigm in cell signaling and cancer therapy. Oncogene . 2010;29(13):1865–82. Available from: http://www.nature.com/doifinder/10.1038/onc.2010.13%5Cnhttp://dx.doi.org/10.1038/onc.2010.13
51. Llambi F, Causeret F, Bloch-Gallego E, Mehlen P. Netrin-1 acts as a survival factor via its receptors UNC5H and DCC. EMBO J. 2001;20(11):2715–22.
52. Hedgecock EM, Culotti JG, Hall DH. The unc-5, unc-6, and unc-40 genes guide circumferential migrations of pioneer axons and mesodermal cells on the epidermis in C. elegans. Neuron. 1990;4(1):61–85.
53. Chen Q, Sun X, Zhou X hong, Liu J huan, Wu J, Zhang Y, Wang J huai. N-terminal horseshoe conformation of DCC is functionally required for axon guidance and might be shared by other neural receptors. J Cell Sci . 2013 Jan 1;126(1):186–95. Available from: http://www.ncbi.nlm.nih.gov/pmc/articles/PMC3603515/
54. Geisbrecht B V., Dowd KA, Barfield RW, Longo PA, Leahy DJ. Netrin binds discrete subdomains of DCC and UNC5 and mediates interactions between DCC and heparin. J Biol Chem. 2003;278(35):32561–8.
55. Leggere JC, Saito Y, Darnell RB, Tessier-Lavigne M, Junge HJ, Chen Z. NOVA regulates Dcc alternative splicing during neuronal migration and axon guidance in the spinal cord. Elife. 2016;5(MAY2016):1–25.
56. Bruikman CS, Zhang H, Kemper AM, Van Gils JM, Majerciak V. Netrin Family: Role for Protein Isoforms in Cancer. J Nucleic Acids; 2019. Available from: /pmc/articles/PMC6408995/
57. Chen Z, Gore BB, Long H, Ma L, Tessier-Lavigne M. Alternative Splicing of the Robo3 Axon Guidance Receptor Governs the Midline Switch from Attraction to Repulsion.

Neuron . 2008 May 8;58(3):325–32. Available from: http://www.cell.com/article/S0896627308001694/fulltext

58. Keeling SL, Gad JM, Cooper HM. Mouse Neogenin, a DCC-like molecule, has four splice variants and is expressed widely in the adult mouse and during embryogenesis. Oncogene. 1997;15(6):691–700.
59. Reale MA, Hu G, Zafar AI, Getzenberg RH, Levine SM, Fearon ER. Expression and Alternative Splicing of the Deleted in Colorectal Cancer (DCC) Gene in Normal and Malignant Tissues. Cancer Res. 1994;54(16):4493–501.
60. Srour M, Rivière JB, Pham JMT, Dubé MP, Girard S, Morin S, Dion PA, Asselin G, Rochefort D, Hince P, Diab S, Sharafaddinzadeh N, Chouinard S, Théoret H, Charron F, Rouleau GA. Mutations in DCC cause congenital mirror movements. Science (80). 2010;328(5978):592.
61. Robinson RA, Griffiths SC, van de Haar LL, Malinauskas T, van Battum EY, Zelina P, Schwab RA, Karia D, Malinauskaite L, Brignani S, van den Munkhof MH, Düdükcü Ö, De Ruiter AA, Van den Heuvel DMA, Bishop B, Elegheert J, Aricescu AR, Pasterkamp RJ, Siebold C. Simultaneous binding of Guidance Cues NET1 and RGM blocks extracellular NEO1 signaling. Cell . 2021 Apr 15;184(8):2103. Available from: /pmc/articles/PMC8063088/
62. Bennett KL, Bradshaw J, Youngman T, Rodgers J, Greenfield B, Aruffo A, Linsley PS. Deleted in colorectal carcinoma (DCC) binds heparin via its fifth fibronectin type III domain. J Biol Chem. 1997;272(43):26940–6.
63. Leonardo ED, Hinck L, Masu M, Keino-Masu K, Ackerman SL, Tessier-Lavigne M. Vertebrate homologues of C. elegans UNC-5 are candidate netrin receptors. Nature . 1997 Apr 24;386(6627):833–8. Available from: http://dx.doi.org/10.1038/386833a0
64. He K, Jang SW, Joshi J, Yoo MH, Ye K. Akt-phosphorylated PIKE-A inhibits UNC5B-induced apoptosis in cancer cell lines in a p53-dependent manner. Mol Biol Cell . 2011 Jun 1;22(11):1943. Available from: /pmc/articles/PMC3103409/
65. Lu X, Le Noble F, Yuan L, Jiang Q, De Lafarge B, Sugiyama D, Bréant C, Claes F, De Smet F, Thomas JL, Autiero M, Carmeliet P, Tessier-Lavigne M, Eichmann A. The netrin receptor UNC5B mediates guidance events controlling morphogenesis of the vascular system. Nature . 2004 Nov 11;432(7014):179–86. Available from:

https://pubmed.ncbi.nlm.nih.gov/15510105/

66. Pradella D, Deflorian G, Pezzotta A, Di Matteo A, Belloni E, Campolungo D, Paradisi A, Bugatti M, Vermi W, Campioni M, Chiapparino A, Scietti L, Forneris F, Giampietro C, Volf N, Rehman M, Zacchigna S, Paronetto MP, Pistocchi A, Eichmann A, Mehlen P, Ghigna C. A ligand-insensitive UNC5B splicing isoform regulates angiogenesis by promoting apoptosis. Nat Commun. 2021;12(1).
67. Larrivée B, Freitas C, Trombe M, Lv X, DeLafarge B, Yuan L, Bouvrée K, Bréant C, Del Toro R, Bréchot N, Germain S, Bono F, Dol F, Claes F, Fischer C, Autiero M, Thomas JL, Carmeliet P, Tessier-Lavigne M, Eichmann A. Activation of the UNC5B receptor by Netrin-1 inhibits sprouting angiogenesis. Genes Dev . 2007 Oct 1;21(19):2433–47. Available from: https://pubmed.ncbi.nlm.nih.gov/17908930/
68. Keleman K, Dickson BJ. Short- and Long-Range Repulsion by the Drosophila Unc5 Netrin Receptor. Neuron . 2001 Nov 20;32(4):605–17. Available from: http://www.cell.com/article/S0896627301005050/fulltext
69. Hong K, Hinck L, Nishiyama M, Poo M ming, Tessier-Lavigne M, Stein E. A Ligand-Gated Association between Cytoplasmic Domains of UNC5 and DCC Family Receptors Converts Netrin-Induced Growth Cone Attraction to Repulsion. Cell . 1999 Jun 25;97(7):927–41. Available from: http://dx.doi.org/10.1016/S0092-8674(00)80804-1
70. Cooper HM, Gad JM, Keeling SL, M H. The Deleted In Colorectal Cancer Netrin Guidance System: A Molecular Strategy For Neuronal Navigation. Clin Exp Pharmacol Physiol . 1999 Sep;26(9):749–51. Available from: http://10.0.4.22/j.1440-1681.1999.03106.x
71. Stein E, Zou Y, Poo M, Tessier-Lavigne M. Binding of DCC by netrin-1 to mediate axon guidance independent of adenosine A2B receptor activation. Science . 2001;291(5510):1976–82. Available from: http://www.ncbi.nlm.nih.gov/pubmed/11239160
72. Hong K, Hinck L, Nishiyama M, Poo MM, Tessier-Lavigne M, Stein E. A ligand-gated association between cytoplasmic domains of UNC5 and DCC family receptors converts netrin-induced growth cone attraction to repulsion. Cell. 1999;97(7):927–41.
73. Mille F, Llambi F, Guix C, Delloye-Bourgeois C, Guenebeaud C, Castro-Obregon S, Bredesen DE, Thibert C, Mehlen P. Interfering with multimerization of netrin-1 receptors

triggers tumor cell death. Cell Death Differ. 2009;16(10):1344–51.

74. Wang R, Wei Z, Jin H, Wu H, Yu C, Wen W, Chan LN, Wen Z, Zhang M. Autoinhibition of UNC5b Revealed by the Cytoplasmic Domain Structure of the Receptor. Mol Cell . 2009;33(6):692–703. Available from: http://dx.doi.org/10.1016/j.molcel.2009.02.016
75. Guenebeaud C, Goldschneider D, Castets M, Guix C, Chazot G, Delloye-Bourgeois C, Eisenberg-Lerner A, Shohat G, Zhang M, Laudet V, Kimchi A, Bernet A, Mehlen P. The Dependence Receptor UNC5H2/B Triggers Apoptosis via PP2A-Mediated Dephosphorylation of DAP Kinase. Mol Cell. 2010;40(6):863–76.
76. Bashaw GJ. Signaling from Axon Guidance Receptors. 2010;1–16.
77. Delloye-Bourgeois C, Brambilla E, Coissieux MM, Guenebeaud C, Pedeux R, Firlej V, Cabon F, Brambilla C, Mehlen P, Bernet A. Interference With Netrin-1 and Tumor Cell Death in Non–Small Cell Lung Cancer. JNCI J Natl Cancer Inst . 2009;101(4):237.
78. Mehlen P, Guenebeaud C. Netrin-1 and its dependence receptors as original targets for cancer therapy. Curr Opin Oncol. 2010;22(1):46–54.
79. Ko SY, Dass CR, Nurgali K. Netrin-1 in the developing enteric nervous system and colorectal cancer. Trends Mol Med . 2012;18(9):544–54. Available from: http://dx.doi.org/10.1016/j.molmed.2012.07.001
80. Williams ME, Strickland P, Watanabe K, Hinck L. UNC5H1 induces apoptosis via its juxtamembrane region through an interaction with NRAGE. J Biol Chem. 2003;278(19):17483–90.
81. Yang Y, Zou L, Wang Y, Xu KS, Zhang JX, Zhang JH. Axon guidance cue netrin-1 has dual function in angiogenesis. Cancer Biol Ther. 2007;6(5):743–8.
82. Wang Z, Yan X. CD146, a multi-functional molecule beyond adhesion. Cancer Lett . 2013 Apr 28;330(2):150–62. Available from: https://pubmed.ncbi.nlm.nih.gov/23266426/
83. Purohit AA, Li W, Qu C, Dwyer T, Shao Q, Guan KL, Liu G. Down syndrome cell adhesion molecule (DSCAM) associates with uncoordinated-5C (UNC5C) in netrin-1-mediated growth cone collapse. J Biol Chem. 2012;287(32):27126–38.
84. Ly Alice, Nikolaev Anatoli, Suresh Geetha, Zheng Yufang, Tessier-Lavigne Marc, Stein Elke. DSCAM is a netrin receptor that collaborates with DCC in mediating turning responses to netrin-1. Cell . 2008;133(7):1241–54. Available from: https://www.researchgate.net/publication/5269352_DSCAM_is_a_netrin_receptor_that_c

ollaborates_with_DCC_in_mediating_turning_responses_to_netrin-1

85. Dominici C, Moreno-Bravo JA, Puiggros SR, Rappeneau Q, Rama N, Vieugue P, Bernet A, Mehlen P, Chédotal A. Floor-plate-derived netrin-1 is dispensable for commissural axon guidance. Nature. 2017;545(7654):350–4. Available from: https://doi.org/10.1038/nature22331
86. Varadarajan SG, Kong JH, Phan KD, Kao TJ, Panaitof SC, Cardin J, Eltzschig H, Kania A, Novitch BG, Butler SJ. Netrin1 Produced by Neural Progenitors, Not Floor Plate Cells, Is Required for Axon Guidance in the Spinal Cord. Neuron . 2017;94(4):790-799.e3. Available from: http://dx.doi.org/10.1016/j.neuron.2017.03.007
87. Matsumoto Y, Irie F, Inatani M, Tessier-Lavigne M, Yamaguchi Y. Netrin-1/DCC Signaling in Commissural Axon Guidance Requires Cell-Autonomous Expression of Heparan Sulfate. J Neurosci . 2007;27(16):4342–50. Available from: http://www.jneurosci.org/cgi/doi/10.1523/JNEUROSCI.0700-07.2007
88. Blanchette CR, Perrat PN, Thackeray A, Bénard CY. Glypican Is a Modulator of Netrin-Mediated Axon Guidance. PLoS Biol . 2015;13(7):e1002183. Available from: http://journals.plos.org/plosbiology/article?id=10.1371/journal.pbio.1002183
89. Shipp EL, Hsieh-Wilson LC. Profiling the Sulfation Specificities of Glycosaminoglycan Interactions with Growth Factors and Chemotactic Proteins Using Microarrays. Chem Biol. 2007;14(2):195–208.
90. Vallet SD, Clerc O, Ricard-Blum S. Glycosaminoglycan–Protein Interactions: The First Draft of the Glycosaminoglycan Interactome. J Histochem Cytochem. 2021;69(2):93–104.
91. Pomin VH, Mulloy B. Current structural biology of the heparin interactome. Curr Opin Struct Biol . 2015;34:17–25. Available from: http://dx.doi.org/10.1016/j.sbi.2015.05.007
92. Gallagher JT, Lyon M, Steward WP. Structure and function of heparan sulphate proteoglycans. Biochem J. 1986;236(2):313–25.
93. Kappler J, Franken S, Junghans U, Hoffmann R, Linke T, Mü HW, Koch KW. Glycosaminoglycan-Binding Properties and Secondary Structure of the C-Terminus of Netrin-1. 2000; Available from: www.ibc.wustl.edu/
94. Matsumoto Y, Irie F, Inatani M, Tessier-Lavigne M, Yamaguchi Y. Netrin-1/DCC signaling in commissural axon guidance requires cell-autonomous expression of heparan sulfate. J Neurosci. 2007;27(16):4342–50.

95. Leonardo E, Hinck L, Masu M, Keino-Masu K, Ackerman SL, Tessier-Lavigne M. Vertebrate homologues of C. e/egans UNC-5 are candidate netrin receptors. Nature. 1997;386:833–8.
96. Hermano E, Goldberg R, Rubinstein AM, Sonnenblick A, Maly B, Nahmias D, Li JP, Bakker MAH, Van Der Vlag J, Vlodavsky I, Peretz T, Elkin M. Heparanase accelerates obesity-associated breast cancer progression. Cancer Res. 2019;79(20):5342–54.
97. Arvatz G, Shafat I, Levy-Adam F, Ilan N, Vlodavsky I. The heparanase system and tumor metastasis: Is heparanase the seed and soil? Cancer Metastasis Rev. 2011;30(2):253–68.
98. Bradford DK, Cole SJ, Cooper HM. Netrin-1: Diversity in development. Vol. 41, International Journal of Biochemistry and Cell Biology. 2009. p. 487–93.
99. Tsai HH, Tessier-Lavigne M, Miller RH. Netrin 1 mediates spinal cord oligodendrocyte precursor dispersal. Development. 2003;130(10):2095–105.
100. Kefeli U, Ucuncu Kefeli A, Cabuk D, Isik U, Sonkaya A, Acikgoz O, Ozden E, Uygun K. Netrin-1 in cancer: Potential biomarker and therapeutic target?. Tumour Biol . 2017;39(4):1010428317698388.
101. Delloye-Bourgeois C, Fitamant J, Paradisi A, Cappellen D, Douc-Rasy S, Raquin MA, Stupack D, Nakagawara A, Rousseau R, Combaret V, Puisieux A, Valteau-Couanet D, Bénard J, Bernet A, Mehlen P. Netrin-1 acts as a survival factor for aggressive neuroblastoma. J Exp Med . 2009;206(4):833–47. Available from: http://www.jem.org/lookup/doi/10.1084/jem.20082299
102. Mellor P, Harvey JR, Murphy KJ, Pye D, O'Boyle G, Lennard TWJ, Kirby JA, Ali S. Modulatory effects of heparin and short-length oligosaccharides of heparin on the metastasis and growth of LMD MDA-MB 231 breast cancer cells in vivo. Br J Cancer. 2007;97(6):761–8.

CHAPTER 2: Instrumentation and methods

2.1 Transfection and clonal selection

The C-terminal domain of netrin-1 is known to bind heparan sulfate (1) and is prone to aggregation *in vitro* (2,3). This domain is attached *via* a flexible linker and is not required for the receptor binding (4–6). Netrin-1 lacking domain C (V and VI domain Fc-fusion construct) induces similar axonal out-growth as full length netrin-1 (2). HEK293T cells, containing transfected netrin-1 lacking the C-terminus domain (netrin-1ΔC) *via* sleeping beauty transposon system (7,8), were a gift from Dr. Manuel Koch, University of Cologne, Köln, Germany. The purpose of using the sleeping beauty transposon system was to obtain stably transfected cells (7–10). Codon optimized netrin-1 from Gallus gallus (NP_990750, aa: 26 – 458) was synthesized (Thermo Fisher Scientific) and cloned *via* the two restriction sites NheI/BamHI into the vector for mammalian expression **(Figure 2.1 A)** (11). It also had a sequence for the Tet response element (TRE) (12,13), the BM-40 signal peptide (MRAWIFFLLCLAGRALAAPLE), a multiple cloning site (MCS) for different enzymes MCS like NheI, XhoI, NotI, and BamHI (11), and the thrombin cleavage sequence (LVPRGS) **(Figure 2.1 B).** The thrombin cleavage site is followed by

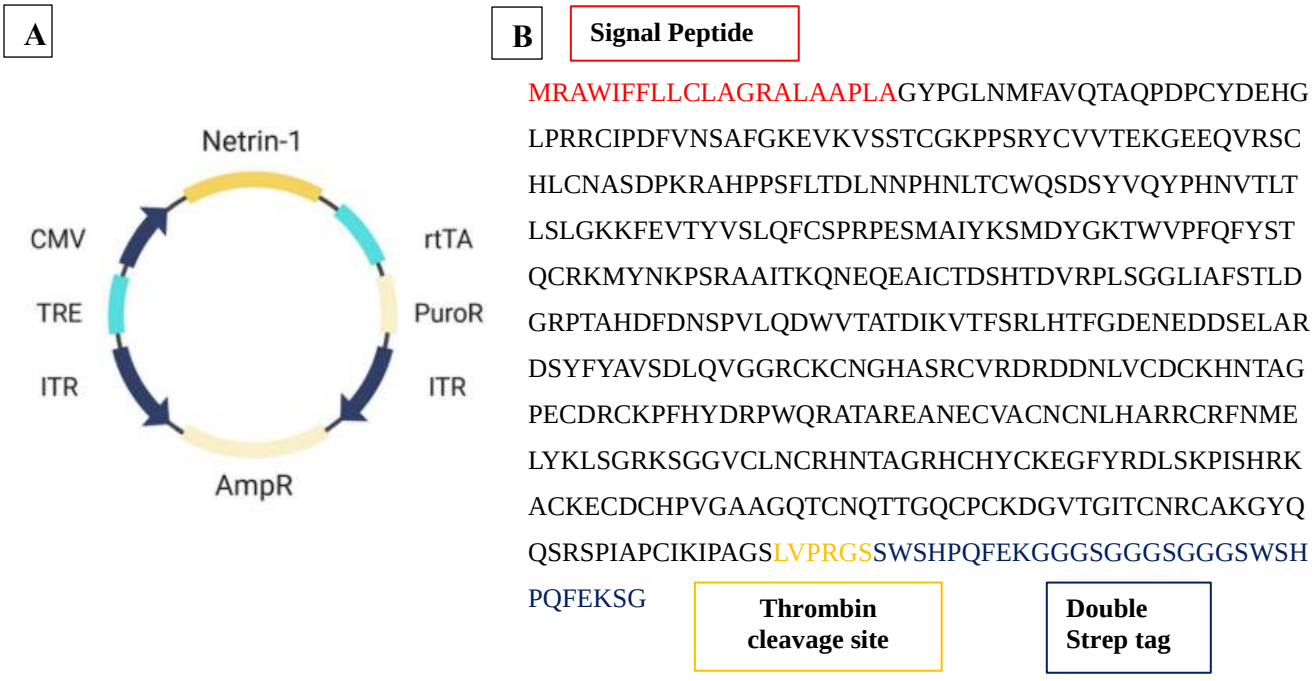

Figure 2.1 A. Representation of a sleeping beauty vector with inserted netrin-1. *The sleeping beauty vector contains the terminal-inverted sequence (ITR) – recognition sequence for the transposase, PuroR-antibiotic resistance genes for cell selection processes. The sleeping beauty vector along with the plasmid containing transposase are used to transfect the cells. Figure with permission from "Homogeneous overexpression of the extracellular matrix protein Netrin-1 in a hollow fibre bioreactor" (5). B. Sequence of netrin-1(black) without C domain, containing a sequence for the signal peptide (red), thrombin cleavage (yellow), and double strep-tag (blue).*

Strep-tag II sequences (SWSHPQFEKGGGSGGGSGGGSWSHPQFEKSG). The Strep-tag II contains a double strep-tag that was very useful during downstream purification to confer strong adhesion to the Strep-Tactin (11).

Clonal selection of the cell pool is a process to select a high-producing clone that also helps to reduce the glycan heterogeneity (11), that is very useful for crystallography. Stably transfected HEK293T cell pool was thawed quickly at 37 ºC and transferred to a T-75 cm^2 flask containing 10 ml of Dulbecco's Modified Eagle's Medium (DMEM) supplemented with 10% Fetal Bovine Serum (FBS). Cells were cultured at 37 ºC in a humidified incubator with 5% CO_2. Next day, the media was replaced by fresh media to remove any dead cells, and dimethyl sulfoxide (DMSO) traces from the cryo-media. Once cells were 90% confluent, cells were removed with Trypsin EDTA (TrypLE, Gibco) from the T-75 cm^2 flask followed by centrifugation at 200 rpm for 3 min. The cell pellet was then resuspended in DMEM supplemented with 10% FBS. Cell count and viability were assessed in a Countess II-FL (Thermo Fisher Scientific) using the trypan blue exclusion method by using Trypan Blue stain 0.4% (Life Technologies Corporation Oregon, USA). Cells were transferred to a 96-well culture plate (Corning Costar®), ensuring a one-cell inoculum per well for proper clonal selection. The selection of clones was based on high resistance to puromycin and faster growth with a high level of protein expression. Cells were allowed to adhere, and it took 5-10 days to cover more than 50% of the bottom of the well (5-10 days). Culture media was replaced in each well by expression media (DMEM containing 2.5% FBS and 1 µg/mL doxycycline) to check the protein production. The next day, supernatant in each well was transferred to a nitrocellulose membrane (GE Healthcare Life Sciences) in a Dot-Blot apparatus (BIO-RAD). Wells in the 96 well plate were replaced with DMEM containing 2.5% FBS. The microfiltration Dot-Blot apparatus allows the rapid immobilization of proteins onto the nitrocellulose membrane as a vacuum is applied (11). The Dot-Blot apparatus was washed with PBS to remove any non-bound proteins before taking out the nitrocellulose membrane to avoid cross-contamination between the wells. The nitrocellulose membrane was transferred to an iBind™ Western-Blot system (Thermo Fisher Scientific) and followed the manufacturer's instructions. The protein was detected using strep tag® II-specific monoclonal antibody conjugated to horseradish peroxidase (HRP) (IBA) diluted 1:10000. The membrane was washed and incubated with 2 ml of LuminataTM Forte Western HRP substrate (Millipore). The chemiluminescence generated by the HRP acting on the substrate was visualized using the FluorChemQ System (ProteinSimple, Inc.). Three clones were selected and inoculated in T-75 cm^2 flasks for further protein purification and storage. Clones were stored in cryoprotecting media containing FBS supplemented with 10% DMSO in liquid nitrogen, and only one was used for further studies.

2.2 Protein expression in a HYPERFlask

Corning ® HYPER*Flask*® cell culture vessels (14,15) were used according to the manufacturer instructions for protein expression. This high-yielding performance flask (HYPERFlask) contains 19 gas-permeable growing surfaces for enhanced cell attachment and growth. It provides greater surface area leading to 10 times the cell yield compared to a standard T-175 cm^2 flask. An initial inoculum of 5.0 x 10^6 to 1.72 x 10^7 cells is required per flask. For HEK293T sleeping beauty transposon system, two ~90% confluent T-75 cm^2 flasks were enough for the initial inoculum containing approximately 1 x 10^7 cells. The cells were resuspended in 50 ml DMEM and inoculated in the flask according to the specification (Corning HYPERFlask). The additional 200 ml of media helped distribute cells evenly in the HYPER-Flask. Cells were grown in the media containing 10% FBS initially and decreased to 5% FBS level for expression media. Once the top few layers in the HYPERFlask were more than 50% covered with the cells (mostly took two days), media was replaced with DMEM + 1 µg/ml doxycycline, and FBS reduced to 2.5%. Media was collected every two days, replaced with fresh media, and sterile filtered and stored at -20 ºC until use. A maximum of 5-6 collections were done initially, but it was found that after collection 4, there was less protein production in the collecting media. Cells started to die once cells cover the layers completely. Thus, more metabolism with an increase in by-products level in the media might lead to nutrient-deficient media and ultimately less protein production. We tried to detach all the cells and reinoculate the flask again, but the chances for contamination increased with this approach and made HYPERFlask a discontinuous way of producing netrin-1.

2.3 Protein expression in a Hollow Fiber Bioreactor (11)

The hollow fiber Bioreactor system has useful features such as *in vivo*-like environment, a 3-D cell culture environment along with a high surface area to grow cells at high densities of greater than $1*10^8$ per mL (FiberCell System Inc), for proper protein assembly and folding with little maintenance. Constant monitoring for any by-products like lactose, ammonia, and their removal allow continuous protein production by keeping cells in nutrient-rich media for proper glycosylation and good protein stability. The chemically defined media-high density (CDM-HD) by FiberCell system Inc., is a protein free medium designed to replace FBS which supports high density cell cultures. The use of CDM-HD and *in vivo*-like cell densities also simplify the downstream processing. FiberCell Systems Inc. has a lot of cartridges with assorted sizes, surface area, fiber type, and molecular weight cut-off. The Hollow Fiber Bioreactor (HFBR) cartridge C2008 (FiberCell Systems Inc.) was used to produce netrin-

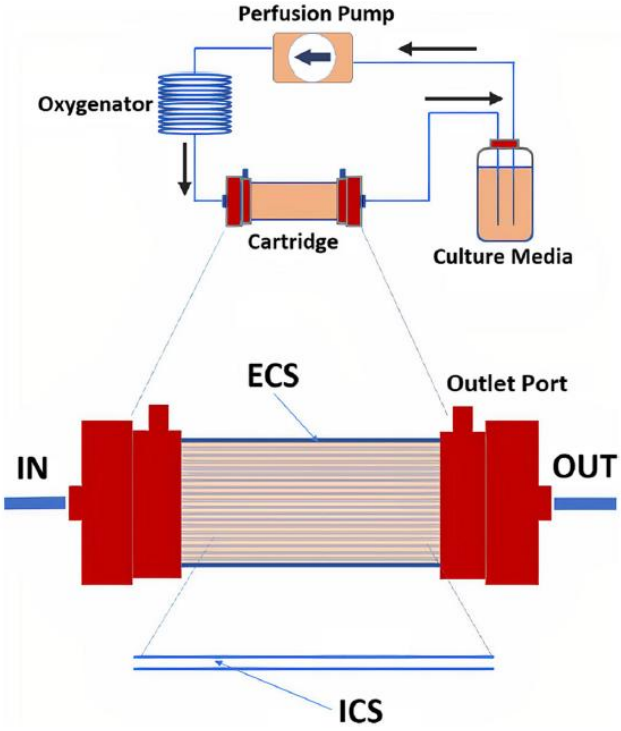

Figure 2.2 Diagram of a Hollow Fiber Bioreactor (16)***.*** *The HFBR unit consist of a reservoir bottle with the culture media, pump along with oxygenator, and a cartridge. The cartridge contains intra-capillary space (ICS), space inside the fibers for media transport and extra-capillary space (ECS), space outside the fibers where cells secrete proteins. Continuous exchange of media and waste occur through capillary walls. Outlet port is used for the extraction of expressed media and always replaced with fresh syringe to minimize any contamination Figure reproduced with permission from* (11).

1ΔC. C2008 cartridge is medium in size with a surface area of 4000 cm^2 with low flux polysulfone fiber for excellent cell culture performance. Extra-capillary space (ECS) is 20 ml with 5 kDa molecular weight cut-off (MWCO) fibers. This cartridge is suggested for recombinant proteins between 25 kDa and 100 kDa. It can support any cell line, for example CHO, HeLa, and HEK293, and cells up to 10^9 and produce

100 µg/ml or more protein in 20 ml ECS. A Hollow Fiber Bioreactor working unit is shown in **Figure 2.2.**

Before inoculating the cartridge with the cells, the HFBR system was pre-equilibrated by circulating phosphate buffer saline (PBS) followed by 250 ml of media DMEM and media supplemented with 10% FBS. A clonally selected HEK293T clone for netrin-1ΔC was thawed quickly in a 37 °C water bath and mixed with 10 mL pre-warmed DMEM media. The mixture was centrifuged at 200 g for 3 min to remove the DMSO from the cryoprotectant, and the cell pellet was resuspended in fresh media supplemented with 10% FBS. The cells were transferred to a T-75 cm^2 flask (Corning) and grew in a 37 °C humidified incubator until 90% of cell confluency. The cells were detached with Trypsin-EDTA as mentioned before and resuspended in 10 mL of DMEM. Cell viability was again measured in a Countess II FL automated cell counter (Thermo Fisher Scientific). A total of $1x10^7$ cells with >90% viability from four confluent flasks were used for further inoculation. Cells were resuspended in 20 mL of DMEM and further used to seed the pre-equilibrated ECS. This unit was placed inside a humidified 37ºC incubator with 5% CO_2. An attached peristaltic pump to the unit recirculated the media from the reservoir bottle into the cartridge.

According to manufacturer instructions, glucose levels were checked every day. There is a need to change the media once the glucose level decreases to 50% of fresh media to maintain proper cell viability. After reaching 50% of the initial glucose concentration, the volume of media in the reservoir bottle was increased to 500 ml. The media volume was further increased to 1 L as the glucose level decreased to 50%. Once the reservoir volume reached 1 L, it was replaced with fresh DMEM supplemented with CDM-HD. For the whole process, the replacement of media was the same as before, which depends on maintaining glucose in the system > 50%. Doxycycline was added to the culture media in the reservoir bottle for protein expression. Different concentrations of inducer doxycycline were used to check protein production and determine the final concentration used in the system for continuous production. Doxycycline concentrations were varied from 0.0625 to 2.0 µg/mL and finally 1.0 µg/mL concentration was used, for long-term running of the bioreactor and optimal protein production (11). During protein expression, a volume of 20 mL was collected from one of the ECS outlet ports with a sterile syringe every time to avoid any contamination and replaced with the new sterile syringe. To remove any dead cells, the alternate collection was done by mixing the media inside the ECS multiple times before collection with the help of another side of the ECS outlet connected with a sterile syringe.

Collected media was clarified by centrifugation at 22,000 g for 50 min and stored at 20 °C until further downstream processing.

Glucose and L-lactate measurement

By-products such as lactate and ammonia, accumulate during the cell growth and inhibit cell growth, protein expression, and may modify protein glycosylation patterns (17,18). Therefore, media was replaced once the glucose level decreases to 50% of fresh media. The carbohydrate level was checked daily from the reservoir bottle and after each ECS collection on an automatic glucose analyzer YSI 2700 SELECTTM biochemistry analyzer (YSI Inc.). Dextran and lactose were used for calibration. According to the manufacturer's protocol, glucose and lactate were measured on a calibrated analyzer.

2.4 Protein purification of Netrin-1

Netrin-1ΔC had a double Strep-tag II, thus it was purified by affinity chromatography using a 5 mL Strep-tactin Superflow Plus cartridge (Qiagen). Each collection (HFBR and HYPERflask) was loaded onto the column equilibrated with 50 mM tris, pH 8, 500 mM NaCl and washed with 15 ml of 50 mM tris, pH 8, 500 mM NaCl followed by 25 ml of 50 mM tris, pH 8, 1 M NaCl (11). The high salt washing step was to eliminate any non-specific binding as protein is highly charged. Protein elution was performed with 2.5 mM of d-Desthiobiotin (MilliporeSigma) in 50 mM tris, pH 8, 0.5 M NaCl. The strep tag was removed with one unit of thrombin (MilliporeSigma) per mg of protein in a dialysis bag with 10-25 kDa molecular weight cut-off (Repligen, Spectra/Por) in 50 mM tris, pH 8, 1 M NaCl, 2.5 mM $CaCl_2$ and incubated overnight or for 24 hr at room temperature. The sample was passed through the strep-tactin column on the next day to separate tagged and untagged proteins following the same protocol. Finally, thrombin was removed using a Benzamidine column (HiTrap® Benzamidine FF, Cytiva) following the manufacturer protocol. Protein sample before and after thrombin cleavage was mixed with reduced 2X Laemmli buffer (Bio-Rad Laboratories Inc. CA, USA) in 1:1 ratio and heated at 95°C for 5 minutes followed by a quick spin at high speed before being loaded onto an 8% Tricine SDS PAGE with molecular weight standard ladder (Precision plus protein ladder, Bio-Rad, CA, USA). The gel was run at 7 W for 1.5 hours in PowerPac HC (Bio-Rad Laboratories Inc. CA, USA) using running buffer (25 mM tris base, 200 mM glycine, 0.1% w/v sodium dodecyl sulfate, SDS). Gel Electrophoresis was followed by staining with Coomassie Brilliant Blue G250 dye and after a few hours, it was de-stained with a gel de-staining solution. The gel was visualized using the Alpha Imager HP system (Alpha Innotech, CA, USA).

Tag-free protein was further purified using an ÄKTA FPLC system with a Superdex 200 10/300 GL column (Cytiva, Healthcare), pre-equilibrated with 50 mM tris, pH 7.5, 1 M NaCl. Purified netrin-1ΔC was concentrated to 1 mg/mL (using a molecular mass of 49.5 kDa and extinction coefficient of 49455 M^{-1} cm^{-1} obtained from ProtParam (19) (ExPASy Server) and stored at 4 °C until further use.

The protein was further dialyzed in 50 mM tris pH 7.5, 500 mM NaCl and 500 mM $(NH_4)_2$ SO_4 in a 25 kDa molecular weight cut-off membrane overnight. The protein sample was passed through the Superdex 200 10/300 GL Increase column equilibrated with the same buffer. For further studies, collected peak fractions were dialyzed in 50 mM tris pH 7.5 200 mM NaCl.

2.5 Size Exclusion Chromatography

Size-exclusion chromatography (SEC) is an analytical technique to analyze proteins polymers. It is based on gel exclusion, allowing the transport of biomolecules in an aqueous mobile phase through a stationary phase of porous spherical beads **(Figure 2.3)**. The larger molecules pass through the column and elute earlier, while smaller molecules can penetrate to the pores and elute later. Any change in the pore size changes the separation capacity, and various SEC columns with different separation capacities to suit different molecular sizes have been manufactured. The stationary phase should be stable over a wide range of pH, chemical and denaturant providing flexibility in the buffer composition (20).

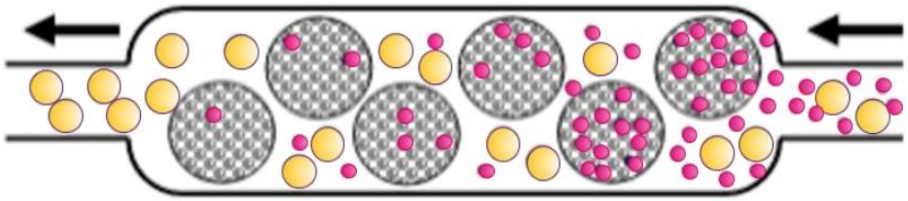

Figure 2.3 Schematic representation of size exclusion chromatography (SEC).

SEC separates based on hydrodynamic size. Figure with permission from "SEC-MALS for absolute biophysical characterization" (83).

In chromatography, the free energy change of a chromatographic process can be described:

$$\Delta G^0 = \Delta H^0 - T\Delta S^0 = RT\ ln\ k \qquad \text{(Equation 2.1)}$$

Where ΔG^0, ΔH^0, and ΔS^0 are the standard free energy, enthalpy, and entropy differences respectively; R is the gas constant, T is the absolute temperature and k is the partition coefficient (21). Typically, SEC is an entropic process if there is no protein adsorption to the column and therefore the Gibbs free energy equation

$$ln\,(K_D) = -\frac{\Delta S^0}{R} \qquad \text{(Equation 2.2)}$$

where K_D is the thermodynamic retention factor, with the implication that temperature should have no effect on the retention of the protein (21), ΔH=0.

So, SEC is very fast, simple, and widely used to separate the proteins based on their molecular weight. A SEC standard calibration curve is used to calculate the molecular weight of the unknown if it shares the same conformation as the standard (22). Non-adsorbing globular proteins are best for SEC calibration curves. Adsorbing protein alters the retention time and would not correlate with the protein size (23). A calibration curve based on size can be generated from a set of known molecular weight (M_w) proteins to estimate the M_w of an unknown **(Figure 2.4)**. Plotting the log molecular weight vs. the retention time of the known proteins can be fit to a third order polynomial with a linear region that describes the highest resolution and M_w accuracy of the selected column (21). The linear region can be modelled by the relationship:

$$log\,M_w = mK_D + b \qquad \text{(Equation 2.3)}$$

where m and b are the slope and intercept of the line respectively.

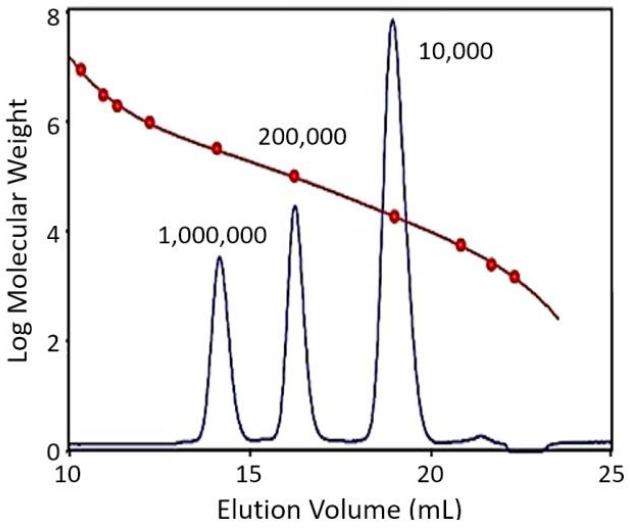

Figure 2.4 Size-exclusion chromatography calibration curve.

Log molecular weight is plotted as a function of retention time/elution volume. Figure with permission from (22,83).

SEC columns are typically composed of 3-20 µm silica particles (with and without modification) or crosslinked polymer beads with different pore sizes and possess different characteristics like hydrophobic, hydrophilic, or ionic (24). The Superdex 75 10/300 GL column is useful for separating

smaller proteins with M_w range 3,000 -70,000 Da, and the Superdex 200 10/300 column has a larger range from 10,000 to 600,000 Da.

2.6 Dynamic Light Scattering

In a typical light scattering experiment, a single frequency polarized light beam (laser light) is used to detect light scattering from macromolecules. Dynamic Light Scattering (DLS) is a non-destructive method that measures the Brownian motion of a macromolecule in solution over time and relates it to the particle size. Small molecules will move fast, and larger particles will move slow **(Figure 2.5)** (25).

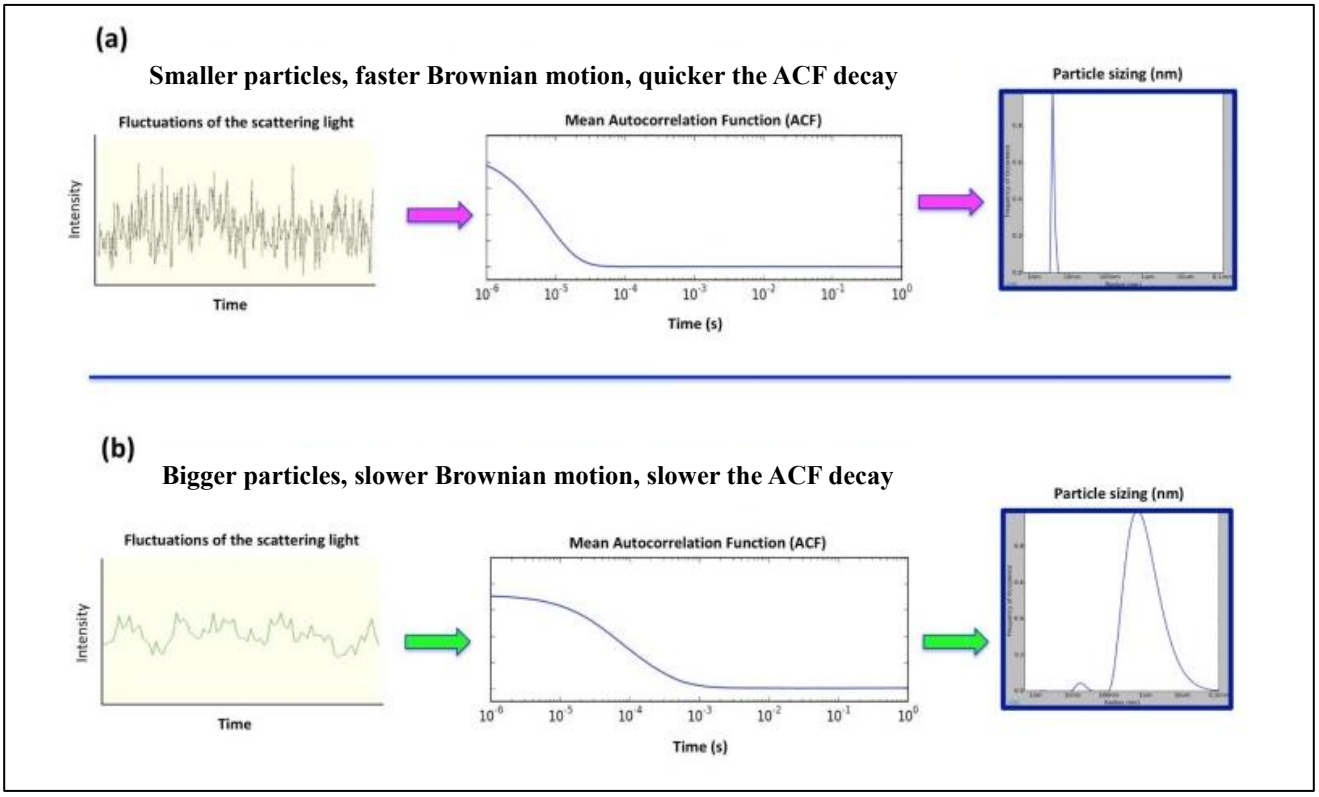

Figure 2.5 *Graphical representation of the intensity fluctuations for (a) smaller and (b) larger particles and its auto correlation function (ACF) decay. Figure reproduced with permission from (20).*

The larger molecules maintain the same position for a longer period while smaller ones constantly change position (26). The diffusion coefficient (D_τ), the hydrodynamic radii (R_h), and polydispersity of the particles can be obtained as the macromolecules undergo random bombardment by the solvent molecules and cause fluctuations in the intensity of scattered light. DLS is also known as photon correlation spectroscopy or quasi-elastic light scattering (27). The Brownian motion is affected by many factors, such as temperature and solvent viscosity. Since solvent viscosity changes with temperature,

therefore to get less error in the data, the measurements must be performed in a temperature-controlled environment (27,28).

Changes in constructive or destructive interference of the scattered light with time are collected and fitted with the autocorrelation function (25,27). To assess the sample homogeneity that is key for structural biology and hydrodynamic radius, the Zetasizer Nano-S instrument (Malvern Instruments Canada, Montreal, QC, Canada), equipped with a λ_0 = 633 nm (red), 4 mW He-Ne Laser and a 173° backscatter detection system was used. D_τ could be measured at multiple concentrations and extrapolated to infinite dilution as the backscatter system allows detection at a higher concentration by avoiding the multiple scattering phenomena.

The D_τ is related to the R_h using the following equation:

$$D_\tau = \frac{k_B T}{6\pi\eta R_h} \qquad \text{(Equation 2.4)}$$

Where κ_B is the Boltzmann coefficient (1.380 x 10^{-23} kg.m^2.s^{-2}.K^{-1}), T is absolute temperature and η is the solvent viscosity (29).

Additionally, the translational frictional coefficient, f, can be calculated from the

$$f = \frac{RT}{N_A D_\tau} \qquad \text{(Equation 2.5)}$$

Where R is the gas constant (8.314 x 10^{-7} erg/mol.K), T is the absolute temperature, N_A is Avogadro's number (6.022137 x 10^{23} mol). The f can be further used to determine the frictional ratio (f/f_0, where $f_0 = 6\pi\eta R_0$ and R_0 is the radius of a sphere). The f/f_0 relates the R_h to the radius of a sphere with the volume of a non-solvated molecule, and therefore can provide information on the solution conformation of the macromolecules (f/f_0 =1 for a compact sphere) (30).

The Zetasizer nano S® is equipped with software that analyzes the scattering data and gives us information about the size and homogeneity of the sample. For analysis, the refractive index of the macromolecules and solvent viscosity are needed for accurate calculation. The intensity-weighted distribution results give us z-average R_h.

$$\%I_a = \frac{a^6 N_a .100}{N_a a^6 + N_b b^6} \qquad \text{(Equation 2.6)}$$

where $\%I_a$ represents the intensity-weighted distribution for a particle with size a (31). N_a and N_b are the molecules in solution with sizes a and b, respectively. The Rayleigh approximation can be used to convert the intensity-weighted distribution to a volume-weighted distribution (32). The mass of a spherical molecule is proportional to its (size)^3; therefore, mass can be correlated to the volume, providing the uniform density of a system (27).

So, the volume-weighted distribution for a solution containing N_a and N_b molecules of size a and b, respectively, can be characterized as

$$\%V_a = \frac{a^3 N_a .100}{N_a a^3 + N_b b^3} \quad \text{(Equation 2.7)}$$

$\%V_a$ represents volume-weighted distribution for molecules with size a, based on the volume of molecules with size *a*. Volume weighted distribution provides the distribution of size based on the volume/mass of the molecules and used mostly to represent the R_h value (31).

The intensity distribution can be converted to a number-weighted distribution which represents the number of molecules present at a given size and is represented as

$$\%N_a = \frac{N_a .100}{N_a + N_b} \quad \text{(Equation 2.8)}$$

Where N_a and N_b are the number of particles of size *a* and *b*, respectively (31).

DLS Method

SEC-purified protein was dialyzed in 50 mM tris pH 7.5, 200 mM NaCl and concentrated using an Amicon® concentrator with 30,000 Da molecular weight cut-off. The sample was centrifuged at 13,000 rpm for 5 minutes in an Eppendorf™ MiniSpin™ centrifuge and filtered through a 0.1 μm Millipore Ultrafree®-MC filter immediately before transfer to the 3 × 3 mm quartz cell (Hellma Canada Ltd., Markham, ON, Canada) (33). The concentrated sample was diluted to the desired final concentrations with the same buffer for multiple concentration measurements. Before starting the measurements, samples were equilibrated at 20° C for 5 minutes. The R_h was plotted at multiple concentrations ranging from 0.2-9 mg/ml for netrin-1ΔC.

2.7 Multi-Angle Static Light scattering

The behavior of proteins in solution with respect to their molecular weight, oligomerization, or homogeneity is very important for biomolecular research. All this information helps the scientist to determine if the protein of interest is suitable for further experiments. Crystallography, nuclear magnetic resonance (NMR), or small-angle x-ray scattering (SAXS) all these techniques require homogeneous samples without any aggregation to provide a structural determination. Even unstable products like aggregated proteins/ fragments can also lead to artifacts in the functional assays. Researchers also use many other methods to analyze a protein molecular mass like sodium dodecyl sulfate-polyacrylamide gel electrophoresis (SDS-PAGE), Native PAGE, Mass Spectrometry (MS), SEC, and Analytical Ultracentrifugation (AUC).

As mentioned, analytical SEC relies on the same conformation of standard, and reference and reference protein should not interact with the column to give reliable information about molecular mass (22). There are many factors that can lead to errors in molecular mass determination like glycosylation, detergent, pH, and salt conditions because all these things can change the elution volumes of the proteins.

Combining ultraviolet (UV) spectroscopy, multiangle light scattering (MALS) **(Figure 2.6)**, and differential refractive index (dRI) detectors to the SEC **(Figure 2.7)** makes it a more versatile and reliable method to determine apparent molecular weight. A UV detector determines the concentration based on the absorbance at 280 nm. A MALS detector measures the proportion of light scattered by the analyte into multiple angles (34), while a dRI detector determines the concentration based on the refractive index (35). Refractive index of the solution changes after the addition of the analyte (36,37).

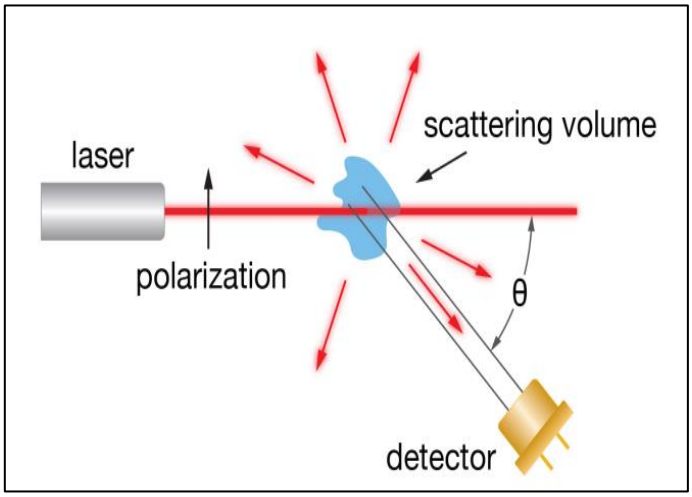

Figure 2.6 Schematic representation of Multiangle light scattering (MALS).
MALS measure the light scattered by the solute into several angles relative to the laser beam. Figure with permission from "SEC-MALS for absolute biophysical characterization" (83)

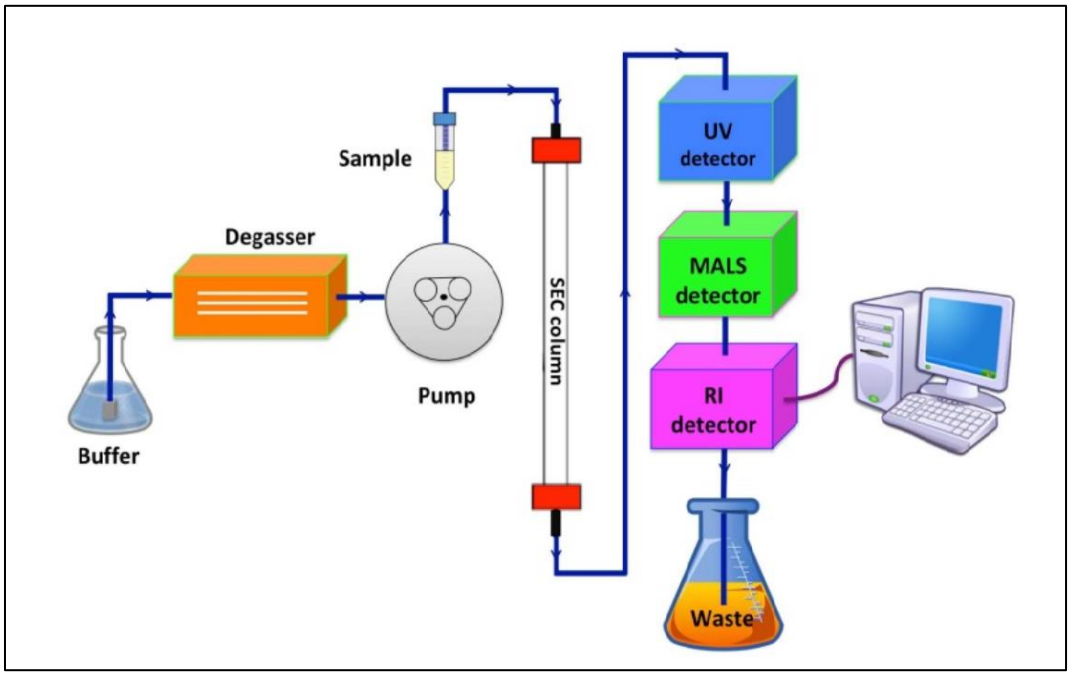

Figure 2.7 Schematic representation of a size-exclusion chromatography coupled with multiangle light scattering (SEC-MALS) system.
The de-gassed buffer is pumped into the system. The sample is loaded, and analytes separated with respect to their size through SEC column before it passes through the different detectors. The output signals from the detectors are combined and analyzed by the software. Figure with permission from (26).

The intensity of scattered light relies on the size of the macromolecules, wavelength of light and the Form factor (P_θ), that is associated with molecular size and the angle at which macromolecules scatter light, and is defined in equation (34).

$$\frac{1}{P_\theta} = 1 + \frac{16\pi^2 n_0^2 R_g^2}{3\lambda_0^2} sin^2\left(\frac{\theta}{2}\right) \qquad \text{(Equation 2.9)}$$

Where n_o is the refractive index of the solvent, R_g is the radius of gyration, λ is the laser wavelength and θ is the measurement angle, $1/P_\theta$ relies on several factors including the measurement angle (angular dependence).

A MALS detector measures scattered light at many angles, but most instruments measure at a minimum of two different angles relative to the incident beam. There are two kinds of scattering, right-angle light scattering (RALS) and low angle light scattering (LALS). Small macromolecules are detected at 90˚ RALS, and the large ones are detected by both RALS and LALS at 7˚relative to the incident light. Thus, a molecular weight calculation is independent of the elution time since molecular weight can be calculated from first principles using the following equation (34)

$$M = \frac{R(0)}{Kc(\frac{dn}{dc})^2} \qquad \text{(Equation 2.10)}$$

Where M is the molecular weight of the analyte, R (0) the reduced Rayleigh ratio (i.e., the amount of the light scattered by the analyte relative to the laser intensity) determined by the MALS detector and extrapolated to angle zero, c the weight concentration determined by the UV or dRI detector, dn/dc the refractive index increment of the analyte (difference between the refractive index of the analyte and the buffer), and K is an optical constant (34,35). dRI is a universal concentration calculator because it can analyze the sugar/polysaccharides that do not contain a UV chromophore (35).

Bovine serum albumin is a standard protein (monomer and dimer) to determine the system constants that is very helpful for further SEC-MALS analysis, including molecular complexes, glycoprotein, and detergent bound membrane proteins. SEC-MALS provides absolute molar mass determination of the protein in the solution and does not count on the reference standards **(Figure 2.8)**.

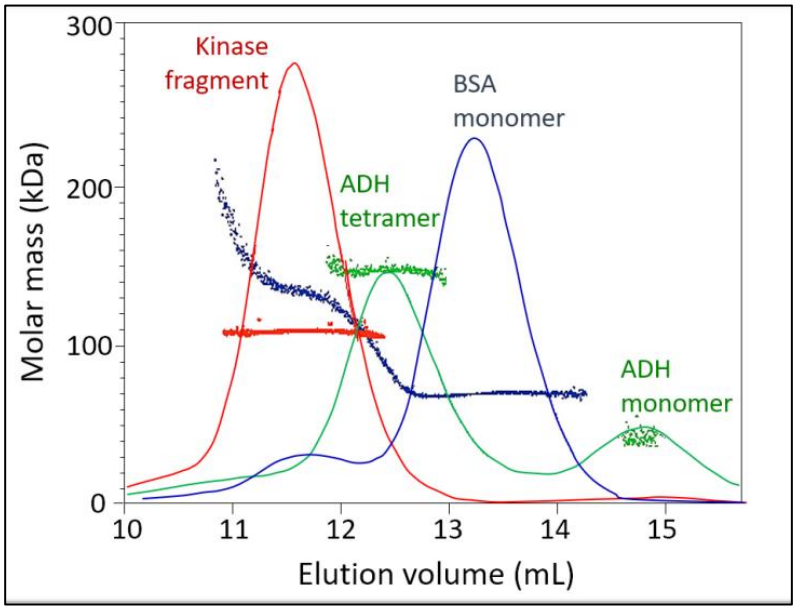

Figure 2.8 Elution profile of known protein.
Elution volume of different known proteins and molar mass determined by MALS. Dotted lines represent the molar mass in kDa. Alcohol dehydrogenase (ADH) tetramer has larger molar mass but elutes later than (Bovine serum albumin) BSA dimer, while kinase has a lower molar mass than BSA but elutes at the same position as BSA dimer. Figure with permission from "SEC-MALS for absolute biophysical characterization" (83).

The ASTRA method, developed by Wyatt technologies (34), is a commercial software package and does data processing and analysis based on the readings collected from three detectors (34,38,39).

SEC-MALS Method

An in-line Dawn® Heleos® II 18-angle static light scattering (MALS) detector (Wyatt Technology, Santa Barbara, CA, USA) was used in conjunction with an SEC column driven by an ÄKTA pure FPLC system (GE Healthcare, Toronto, ON, Canada) to determine the molecular mass of netrin-1.

Sample concentration was monitored by a 2 mm multi-wavelength UV flow cell (GE Healthcare) and an in-line Optilab T-rEX differential refractometer (Wyatt Technology) (33). Two different columns were used to study netrin-1ΔC (Table 2.1).

Table 2.1 Columns used for netrin-1ΔC.

Column	Volume injected (µl)	Sample concentration (mg/ml)	Flow rate (ml/min)
Superose ^{TM} 6 Increase 24 ml	300	3-4	0.3
Shodex (KW403 column) 10/300GE	150	More than 4	0.4

BSA at a concentration of 6 mg/ml was used for detector alignment in the same buffer used for the sample. Approximately 2 ml of netrin-1ΔC (concentration 1mg/ml) were concentrated to 300 µl (6 mg/ml) using an Amicon 4 concentrator (Millipore sigma, Oakville, Canada) with a 30 kDa MWCO. Netrin-1ΔC (6 mg/ml) with different HS oligosaccharides (10 times) were incubated for 1 hour. The sample was centrifuged for 5 minutes at 12100*g in a MiniSpin tabletop centrifuge (Eppendorf, Mississauga, ON, Canada) immediately before injection to remove aggregates. The ASTRA 6 (Wyatt) package was used for data analysis.

2.8 X-ray diffraction

Biomolecular interactions can be studied with many different techniques. Structural information is very important for determining the chemical composition/interaction residues involved in a binding event. Changes in a 3-D structure after binding can be studied *via* Nuclear Magnetic Resonance (NMR), Cryo-Electron microscopy (Cryo-EM), and X-ray diffraction. X-ray diffraction requires the crystalline material and is the ultimate method to determine the crystalline structure. Most of the proteins can be crystallized except dynamic systems and intrinsically disordered proteins. Some crystallize within minutes, and some may take months.

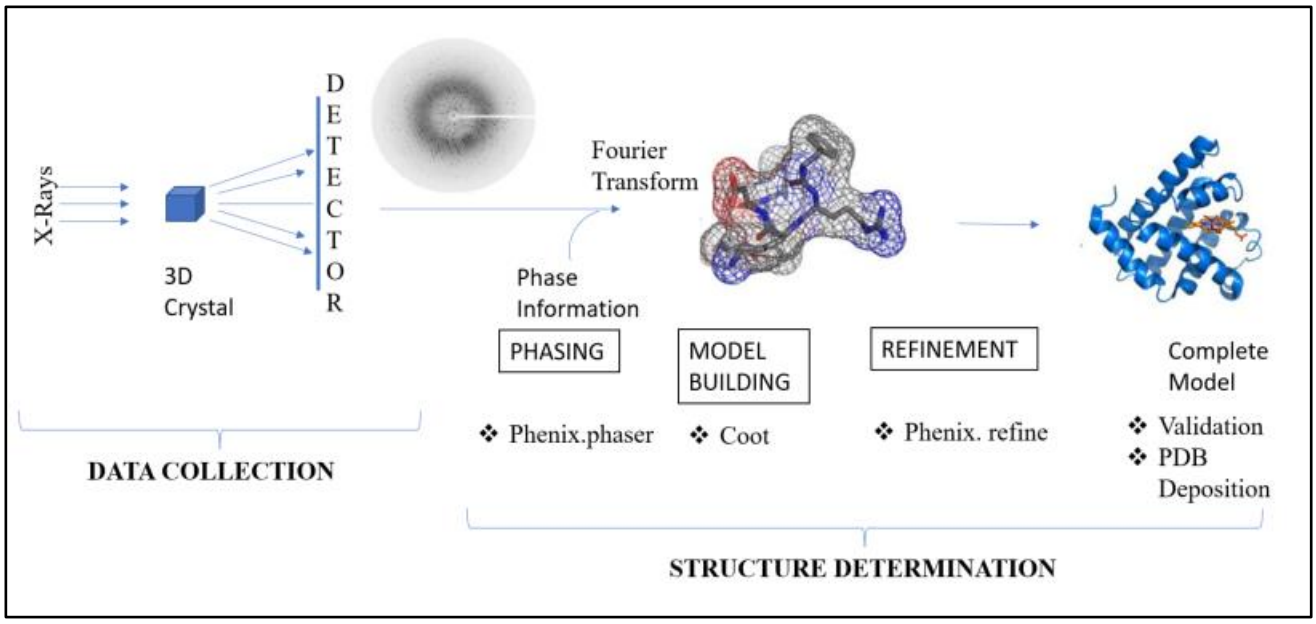

Figure 2.9 *Flow chart of X-ray crystallography*

An X-ray dataset is collected followed by phasing and ultimately yielding an electron density map. Refinement is performed using phenix.refine against the data and model building using coot. Completion of the structure building is followed by validation and deposition in the Protein Data Bank. Figure adapted and modified with permission from (84).

The diffracted x-rays are recorded by the charged coupled device detector, and the diffraction intensity data is collected (40). Different modern software packages are used to calculate the electron density maps. There are many methods available to solve the phase problem, including molecular replacement (MR), single/multiple isomorphous replacements (SIR/MIR), and single-wavelength anomalous dispersion/multiwavelength anomalous dispersion (SAD/MAD) (40). Once the model of the structure is predicted, further model building, and refinements are done using different computer programs. A flow chart of X-ray crystallography is shown in **Figure 2.9**.

Method

Purified netrin-1 was concentrated to 9 mg/ml. Netrin-1ΔC crystals were grown using the sitting-drop vapor diffusion technique at 293 K by mixing an equal volume of protein and reservoir solutions. The crystallization trials were conducted using commercial crystallization kits: Index, Natrix 1+2, JBS Classic 1-8, JCSG ++1 to ++4 (Jena Science), and HR2-117-112 from Hampton Research (CA, USA). The plates were covered with clear film and incubated at 20 ˚C. Crystals appeared in 20% w/v Polyethylene glycol (PEG) 8,000, 100 mM 2-(Cyclohexyl amino) ethane sulfonic acid (CHES) pH 9.5 (Jena Bioscience JBScreen JCSG++1).

For data collection, a single crystal of netrin-1ΔC was harvested directly from the initial screen, soaked in 20% w/v PEG 8,000, 100 mM CHES, pH 9.5 supplemented with a final concentration of

cryoprotectant 15% ethylene glycol and 1 mM SOS/ 1 mM decasaccharide (10 monomeric sugar units or dp10) for one week at 293 K before flash-cooling in liquid nitrogen.

X-ray diffraction data were collected from both crystals on a Rigaku Micromax-007 HF (λ=1.5418 Å) at 100 K in-house. X-rays images were integrated and scaled using X-ray Detector Software (XDS) (41) and merged using aimless, the Collaborative Computational Project No.4 (ccp4) software suite (42). Initial phases estimates were obtained from a molecular replacement experiment using the crystal structure of mouse netrin1 (PDB-4OVE) as a search model with phenix.phaser (43,44). An initial model was built using phenix.autobuild (45,46). A further model was built in coot (47)**,** and refinements were carried out in phenix.refine (46).

To refine the structure, different refinement strategies were included like bulk solvent correction and anisotropic scaling of the data, individual coordinate refinement, and translational-libration-screw-rotation (TLS) parameterization. Further refinements involved the inclusion of native amino acid residues, water molecules, ions, and N-glycan attachments. This led to the R_{value}/R_{free} falling to 26.8/33.1. At this stage, both SOS molecules had been fitted into a 3D contoured Sigma-A weighted Fo-Fc difference Fourier map using the coordinates of SOS. The final R_{value}/R_{free} factors for the SOS (PDB code: 7LRF) were refined to 22.7/28.1. The final model comprises amino acid residues P40-P357 and contains two calcium ions, one sodium ion, and one chloride ion, four 1,2-Ethanediol (EDO) molecules, 2 Polyethylene Glycol (PEG) molecules, one CHES (2-[N-Cyclohexylamino] ethane sulfonic Acid) (NHE) molecule and 44 water molecules. The side chains of N97, N118, N133, and N419 are N-glycosylated. The molecular illustrations were made with the molecular visualization system, PyMOL (Molecular Graphics System, Schrödinger, LLC, www.pymol.org). The structural model of netrin-1ΔC interacting with GAG molecules was prepared using PyMOL by taking a monomer unit of netrin-1 SOS structure with both SOS on the same netrin-1 monomer.

2.9 Analytical Ultracentrifugation

Analytical ultracentrifugation (AUC) is a versatile technique used to characterize macromolecules in their native state in solution. It can determine a macromolecules molecular mass, hydrodynamics, and thermodynamic properties. It works with a wide variety of particles with different ranges of concentration and solvent conditions. AUC involves the spinning of the macromolecule under the centrifugal field in an ultracentrifuge at high speed. The tracking of macromolecule sedimentation rate in real-time gives information about the size, anisotropy, polydispersity, and conformational changes of a molecule in solution (48). The AUC principle is that “mass will redistribute in a gravitational field

until the gravitational potential energy matches exactly the chemical potential energy at each radial position" (49). Optical systems used for AUC include Absorbance spectrophotometer and Rayleigh Interferometer (Absorbance and Interference Optics). There are two main approaches to study macromolecules: sedimentation velocity and sedimentation equilibrium (50)

In a typical sedimentation velocity (SV) experiment, the concentration gradient is formed as the sample sediments under centrifugal force. During sedimentation, the protein/buffer boundary moves from the meniscus towards the outer wall of the sample cell. The shape of the boundary and rate at which proteins sediment provide hydrodynamic characteristics such as sedimentation coefficient (s), frictional coefficient (f) , and diffusion coefficients (D) (49,51). These characteristics ultimately give us information about the size and the shape of the protein molecule (52) and are related by the Svedberg equation (48)

$$\frac{s}{D} = \frac{\left(\frac{M_b}{f}\right)}{\left(\frac{RT}{f}\right)} = \frac{M_b}{RT} = \frac{M(1-\nu\rho)}{RT} \qquad \text{(Equation 2.11)}$$

Where, M is the molar mass, M_b is the buoyant mass, ν is the partial specific volume of the macromolecule, ρ is the solvent density, R is the gas constant, and T is the absolute temperature. If s and f or s and D are known, the molar mass of the sedimenting macromolecule can be determined after considering the partial specific volume and buffer density.

Sedimentation of macromolecules in the centrifugal field is described by the Lamm equation (53)

$$\frac{dc}{dt} = \frac{1}{r}\frac{d}{dr}\left[rD\frac{dc}{d_r} - s\omega^2 r^2 c\right] \qquad \text{(Equation 2.12)}$$

Where c is the concentration of macromolecule, ω is the rotor speed, s is the sedimentation coefficient, and r is the distance from the center of rotation (54). According to the equation the concentration distribution of protein molecules depends on the strength of the centrifugal field, s of the sedimenting species and D. The sedimentation coefficient depends on both particle size and shape.

Absorbance optics

The most frequently and easiest to use detector for AUC is absorbance optics. Increased sensitivity allows us to measure diluted samples too. A double beam spectrophotometer with a high-intensity xenon flash lamp forms a wavelength range of 190 to 800 nm. Consequently, where the Beer-Lambert law holds, the absorbance is proportional to the concentration of the sample, c ($A=\varepsilon cl$, where A is the absorbance, ε is the molar extinction coefficient, c is the mass concentration, and l is the sample pathlength) with a precision of ± 0.10 OD (49). The noise associated with absorbance measurements scan is primarily stochastic and a little systematic. Stochastic noise appears as a high-frequency "fuzz" around

the signal, and systematic noise is either radially independent (means the entire scan is shifted up or down) or time-independent (means a feature, like a scratch, that does not move from scan to scan) (49).

Interference optics

As the name implies, this optics works on the principle that light velocity decreases as it passes through a region of a higher refractive index. An AUC cell is a double-sector cell, one side for the sample and another for the buffer, with a slit below each sector. Monochromatic light passes through these slits and undergoes interference to yield a band of alternate light and dark fringes. Any material with a difference in refractive index from the reference will contribute to an interference signal. Interference optics are little more sensitive than absorbance optics; any stress on the optical components can lead to refractive index changes (55,56). Careful alignment and focusing must be done for sapphire windows to obtain an accurate result.

Data analysis

There are many methods for analyzing the SV-AUC data that use different approaches and software. Sedfit (54) and Sedphat are programs that implement the c(s) method to obtain the sedimentation coefficient distribution function from a direct fit to the data (57) and were used for netrin-1 data analysis. Firstly, a grid of sedimentation coefficients is generated, which covers the expected range of interest. With an assumption that all species have a constant shape and an equal frictional ratio, the program creates a scaling relationship between s and D. The program then uses a numerical solution of the Lamm equation to simulate the sedimentation boundaries for each point.

Further data processing uses fitting of data to a sum of Lamm equations using a least-squares fitting procedure to define the concentration of each species in the grid (49). During this process, the systematic noise of the baseline and vertical displacements from the data are removed by considering them as additional linear fitting parameters. In the end, the program provides the result as a smooth distribution of data (49).

The c(s) method has advantages like excellent resolution and sensitivity, no limit on the number of scans that can be analyzed, characterizing homogeneity, quantifying impurities, and aggregation. The main requirement is that all associating species reach equilibrium before sedimentation begins. It assumes that the mixture is non-interacting or associates and dissociates rapidly such that the distribution appears similar to those expected for limiting models (34). Another approach, the van Holde-Weischet, is used for the initial, quantitative analysis of SV data. Furthermore, a new advancement allows the analysis of highly heterogeneous systems, too (49).

Another data analysis method, Ultrascan 3 developed by Demeler and colleagues (58,59), is a free software suite that provides high-quality, comprehensive data analysis and modeling of hydrodynamic data. US3 uses an online database with a web-based interface, named as UltraScan Laboratory Information Management System (USLIMS) (58). After initial refinement of the data, all further analyses can be performed without any additional noise processing or optimization of boundary conditions. Like Sedfit, it also uses the Lamm equation to model SV data by the finite element method (60,61). There are different analysis methods available in US3. For example, to obtain molecular weight and anisotropy distribution of a heterogeneous sample, two-dimensional spectrum analysis - Monte Carlo analysis (2DSA-MC) (62,63) is used. Another method to eliminate non-essential species from the solution without degrading the quality of the fit is the generic algorithm (GA) (64).

AUC Method

In my work, Sedimentation Velocity (SV) experiments on netrin-1 were performed using a ProteomeLab^{TM} XL-I analytical ultracentrifuge (Beckman Coulter Canada, Mississauga, ON, Canada) using an An50Ti 8-cell rotor, a rotor speed of 30,000 rpm, and a temperature T of 20 °C. Rotor speed depends on the size of the particle; for example, a size between 40-50 kDa mostly requires a rotor speed range from 20,000 to 40,000 to observe full sedimentation (65). Samples were dialyzed in 50 mM tris, pH 7.5, and 200 mM NaCl buffer for at least 8 hrs in Float-A-Lyzer G2 dialysis device (Repligen, Waltham, USA) with a 20 kDa MWCO membrane and then diluted to the desired concentration. A standard 12 mm Epon double sector centerpiece was filled with 400 µl of netrin-1 and buffer (in which sample was dialyzed) into the respective channel. The 8-place An-50 Ti rotor with samples was equilibrated to the pre-set temperature for at least 2 hrs. Data were analyzed using the SEDFIT program to determine the sedimentation coefficients of netrin-1 and then converted to standard solvent conditions (water) using buffer density and viscosity calculated from SEDNTERP.

2.10 Small Angle X-ray Scattering

In Small-angle X-ray scattering (SAXS), the sample is placed in a collimated monochromatic X-ray beam and an X-ray detector records the intensity of the scattered X-rays. The X-ray diffraction and SAXS have some differences, such as the angle at which these samples are exposed, the resolution limit, the crystalline/solvated nature of the sample, and the radial symmetry. In SAXS, there is no need to rotate the sample while collecting the data, as needed for crystalline samples in crystallography. Advancement in instrumentation, computational methods, and bright synchrotron X-ray sources have made SAXS a very powerful technique to study macromolecules in solution. SAXS is a complementary technique to NMR and x-ray diffraction that gives low-resolution structure information about protein size, shape, conformation, and flexibility. It requires modest sample preparation and is a very powerful technique to understand flexible systems. Combining low-resolution information from SAXS with a high-resolution crystal structure can provide us with much other information and thus provide an accurate and complete 3-D model of the macromolecule (conformational change, interactions, and assemblies in the solution) (66). A workflow of SAXS is shown in **Figure 2.10**.

The scattering curve, I(q), is a function of the momentum transfer of the photons $q= (4\pi\sin\theta)/\lambda$, where 2θ is the scattering angle, and λ is the wavelength of the incident X-ray beam (67). The scattering curve for a homogeneous, monodispersed sample can be derived from the electron distribution of the particle known as the pair-distance distribution function, P(r):

$$I(q) = 4\pi \int_0^{D_{max}} P(r) \frac{\sin(qr)}{qr} dr \qquad \text{(Equation 2.13)}$$

Where D_{max} is the maximal particle dimension and r is the interatomic distance (68).

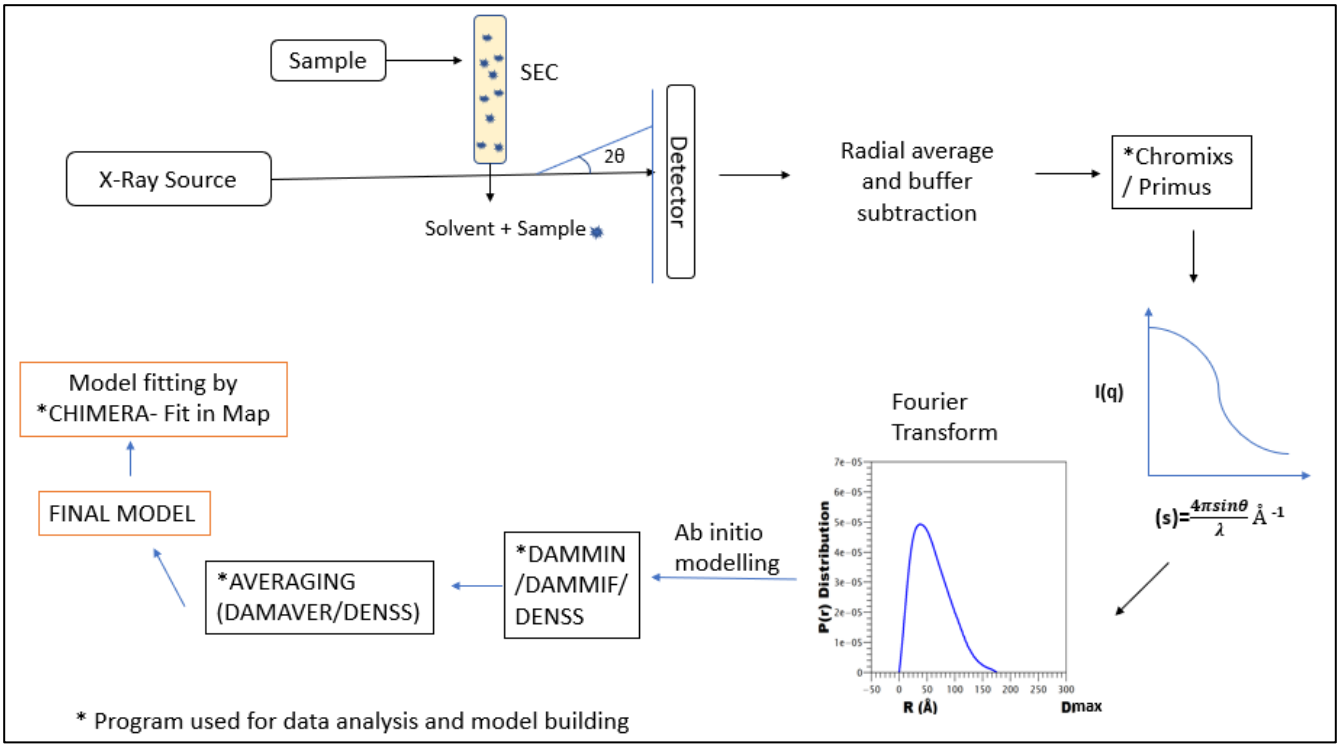

Figure 2.10 Workflow of small angle light scattering.

Proteins in solution cause scattering of x-ray beam at low angles as it elutes from the column and the scattered beam is recorded on the detector. Integration of radial intensity generates the SAXS scattering curve I(q) vs (s) (69,70). *The scattering curve is converted into a pairwise distribution to get knowledge about the maximum distance and radius of gyration in real space. Further ab initio models are builds with the help of various tools available* (71,72) *by rejecting all outlier models and averaging the other models to obtain the final averaged model. Finally Chimera* (44) *program is used to fit final model.*

The radius of gyration (R_g), the square root of the average squared distance of each scatterer from the particle center, gives the lowest resolution structural information. R_g is shape-dependent, similar to R_h and the Stroke's radius (Rs); therefore, it is a poor measure of the actual molecular weight of the macromolecule. A Guinier approximation can describe the solution scattering at low resolution:

$$I(q) = I(0)exp\left[-\frac{q^2R_g^2}{3}\right] \qquad \text{(Equation 2.14)}$$

where $I(0)$ is the intensity at zero scattering angle (q=0) and Rg is the radius of gyration (66). A Guinier plot of $\ln(I(q))$ against q^2 results in a straight line by which R_g and $I(0)$ can be determined. So, it is recommended to do a SAXS experiment over a range of concentrations in the same buffer, and as such, the R_g should not vary.

SAXS is a useful technique for identifying folded or unfolded states of proteins through the Kratky plot of $q^2I(q)$ as a function of q, calculated from the original scattering curve. For folded macromolecules, the scattering intensity at a higher q value falls off by Porod's law as $I(q) \alpha q^{-4}$ and appears roughly as a parabolic curve (66).

The P(r) function is an autocorrelation function that represents the histogram of the distance between all the pairs of electrons in the scattering particles (68). It can be directly calculated from an indirect Fourier transform of the scattering curve (68). D_{max} is also a very useful parameter to determine the maximum particle dimension and heavily relies on the P(r) function. The P(r) plot uses all the collected data to calculate the R_g and $I(0)$ (69). The P(r) function along with a Kratky plot can provide information for low-resolution modeling by indicating the overall shape of the macromolecule.

3D reconstruction of a 1D scattering curve is possible with many programs available even without the pre-defined structure input. The ab initio (lack of pre-defined structure input) modeling of the scattering data is done using the program DAMMMIF (72), a rapid ab-initio shape determination tool, and density from solution scattering (DENSS) (73) using pair distance distribution information about D_{max} and R_g. In bead modeling, a particle/solvent is represented as a collection of many dummy atoms packed densely inside a search volume. Sometimes limiting the search volume is very helpful in shape reconstruction except for very anisometric particles. To avoid any kind of artifact, the algorithm of DAMMIF allows searching in a variable volume. The program also uses energy minimization through a simulated annealing protocol. The comparison of the experimental and predicted scattering profiles of the sample gives the goodness of fit (χ). The program DAMAVER (33,72,74) rejects any outliers, filters, and superimposes all the low-resolution models to build a final average model.

Another program, DENsity from solution scattering (DENSS) (73), calculates the electron density map directly from the smooth fit to the scattering curve. The DENSS script "denss.all.py" calculates 20-100 electron density maps per data set (voxel size set to 5 Å and oversampling set to 3), which is aligned and averaged by the "denss.all.py" script. Refinement of average electron density maps against the original data uses the DENSS script "denss.refine.py" to ensure that the final maps are representative of the original scattering data.

SEC-SAXS Method

To gain information about solution structure, SEC-SAXS data on netrin-1 were collected at the B21 beamline at the Diamond Light Source (Didcot, UK) using an in-line Agilent 1200 (Agilent Technologies, Stockport, UK) HPLC system connected to a temperature-controlled quartz cell capillary. 50 µl of netrin-1ΔC sample in two buffers (50 mM tris pH 7.5, 200 mM NaCl and 50 mM MES pH 6.5, 150 mM NaCl) with a concentration of 9 mg/ml were injected into a respective buffer-equilibrated 4.6 ml Shodex KW402.5-4F size-exclusion column. For netrin-1ΔC and HS studies, tag-free netrin-1ΔC was shipped to the beamline at 1.0 mg/ml in 50 mM tris, pH 7.5, 1.0 M NaCl. Using a PD-10 desalting column

with Sephadex G-25 resin (Cytiva, Vancouver, Canada), the buffer was changed to 50 mM tris, pH 7.5, 0.2 M NaCl, and the protein was then concentrated to 9.2 mg/ml using an Amicon concentrator (MilliporeSigma, Etobicoke, Canada) with 30 kDa molecular weight cut-off. 20 µl of dp8 HS units in water was then added to 100 µl protein solution and then incubated for 40 - 80 min before injection. Each frame was exposed for 3 s at 1.0 Å wavelength. The frames in the sample peak region were integrated and buffer subtracted using the ScAtter software package (http://www.bioisis.net/scatter/). The software package Chromixs (70) was used to assess the separation of netrin-1ΔC species in SEC-SAXS experiments *via* elution profile and R_g and reduce SEC-SAXS data corresponding to each species to single scattering curves. Further processing utilized the GNOM program from the ATSAS software package (75) to obtain the radius of gyration (R_g) and maximum particle dimension (D_{max}) (76). The ab initio structures for netrin-1ΔC were calculated using the program DAMMIF (72), and each model was verified for quality by the goodness of fit parameter. Using identical parameters, sets of 20 models were generated with DAMMIF; however, a different random seed for each model was used. The ab initio models were then rotated and averaged using the program DAMAVER to obtain a representative shape for the final low-resolution model.

The software DENSS (71) was used to calculate electron density maps. Crystal structures of monomeric netrin-1 (4OVE) and an asymmetric unit from the dimeric netrin-1 SOS structure were fit into the electron density maps using the software packages UCSF-Chimera's the "Fit in Map" function (44). PyMOL was used to make the figures.

2.11 Microscale Thermophoresis Binding Assay

Microscale Thermophoresis (MST), as the name implies, is the movement of molecules under the application of a gradient of temperature on a microscopic level (77,78). It strongly depends on various properties such as size, charge, hydration shell, or conformation of the protein (77) and is very helpful to quantify biomolecular interactions (79). An IR laser of 1480 nm emission wavelength is used to generate the temperature gradient. One of the binding partners is fluorescently labeled in an MST experiment, therefore permitting the monitoring of the movement of fluorescent molecules through microscopic temperature gradient (77). Elevation of temperature in the glass capillary at a particular region leads to depletion of a molecule on the interface between solvent and molecule. MST offers advantages over most of the other techniques used for binding studies, such as isothermal titration calorimetry (ITC) or surface plasmon resonance (SPR), by avoiding surface immobilization and high sample requirement (77,78). New advancements allow a label-free approach (intrinsic fluorescence of tryptophan-containing proteins)

to use a variety of buffers or even cell lysate to study molecular interactions (80). The binding of small molecules to proteins, a substrate to enzymes, or liposomes are also detectable (78). An MST instrument gives different signals, starting with initial fluorescence (Laser OFF), followed by T-Jump (Laser ON, no thermophoresis), thermophoresis for 30 seconds, inverse T-jump (Laser OFF), and lastly, back diffusion of molecules by mass diffusion. Every step can give us information depending upon the type of interaction. If the interaction changes the binding state of the labeled protein, the T-jump would be affected, and if there is a change in size, hydration shell, or shape, it will show up in the thermophoresis (78). The T-jump **(Figure 2.11B, II)** corresponds to the change in fluorescence intensity of a dissolved fluorescent molecule with temperature, an inherent property of the fluorophore (81). The heating of the solution by an IR laser takes place on the order of less than a second (78). Intensity change with a change in temperature is due to changes in absorption, fluorescence lifetime, quantum yield, and a special shift of the emitted fluorescence (78,82). The temperature dependence of fluorophores is also sensitive to their local environment (79). Therefore, any change in the conformation of the protein after the binding event at a position close to the dye, will be detected by the MST T-jump (78).

In an MST equilibrium experiment, the concentration of fluorescently-labeled molecule is kept constant (low nM) whereas the concentration of binding partner is varied. As a rule of thumb,

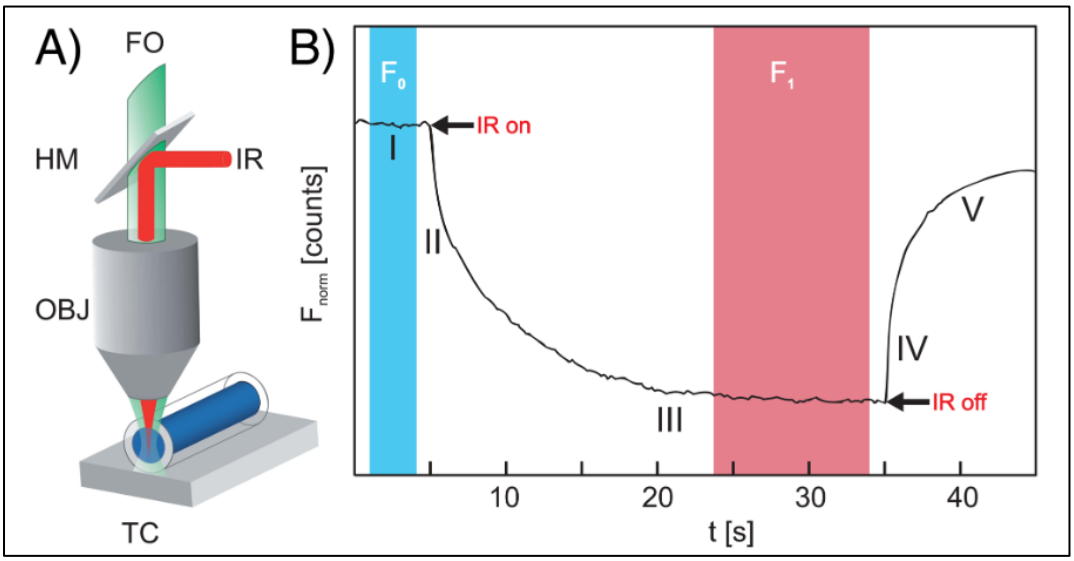

Figure 2.11 Microscale thermophoresis
A) *The capillary filled with sample placed on a temperature-controlled sample tray (TC) is heated with an IR-Laser (IR), coupled with fluorescence excitation and emission with an IR reflecting hot mirror (HM). FO: fluorescence observation; OBJ: objective.* ***B)*** *Schematic representation of the fluorescence time trace recorded by the MST instrumentation. I=initial fluorescence, II=T-Jump, III= thermophoresis, IV=inverse T-jump, and V= back diffusion. Figure with permission from "Microscale Thermophoresis quantifies biomolecular interactions under previously challenging conditions"* (85).

the concentration of the target is at least "10 times above the expected dissociation constant down to sub-stoichiometric concentration with respect to the labeled molecule" (78). The binding is detected from the MST signal that gives information about the change in fluorescence (78) (depends on target concentration):

$$F_{norm} = (1 - x)F_{norm}(unbound) + x\, F_{norm}(bound) \quad \text{(Equation 2.15)}$$

Where, F_{norm} (unbound) is the normalized fluorescence of unbound labeled molecules, and F_{norm}(bound) is the normalized fluorescence of the complexes. From this equation, the difference in normalized fluorescence will determine the fraction bound and thus the dissociation constant. An MST plot may contain F_{norm}, ΔF_{norm} (after subtraction of the baseline value), or ΔF_{norm} [‰] (values are multiplied by a factor of 1,000, relative fluorescence change in per thousand) (78).

MST Method

Netrin-1ΔC was labeled with Alexa 647 according to the manufacturer's protocol in 50 mM HEPES, 500 mM NaCl buffer at a concentration of 20 μM. This method exclusively labels primary amines. The binding check feature checks the binding before performing the full binding assay. This way, it also provides information about the highest concentration to start the dilution (a titration experiment). For a binding assay, the concentration of labeled netrin-1 was kept constant (10 nM) among all 16 capillaries, and ligand concentration was varied from 400 μM - 600 μM. The experiment was performed in MST buffer (50 mM tris-HCl pH 7.4, 150 mM NaCl, 10 mM $MgCl_2$, 0.05% Tween-20) supplemented with 1% BSA. Samples were incubated for 10 minutes before loading into NanoTemper standard capillaries. Microscale thermophoresis was carried out using 20% excitation power and 40% MST power on NanoTemper Monolith NT.115. K_d was calculated from three individual experiments using NanoTemper analysis software using K_d fit algorithm and plotted with Qtiplot using the Hill equation.

References

1. Serafini T, Kennedy TE, Galko MJ, Mirzayan C, Jessell TM, Tessler-Lavigne M. The Netrins Define a Family of Axon Outgrowth-Promoting Proteins Homologous to C. elegans UNC-6. Cell. 1994;79:409–24.

2. Keino-Masu K, Masu M, Hinck L, Leonardo ED, Chan SSY, Culotti JG, Tessier-Lavigne M. Deleted in Colorectal Cancer (DCC) Encodes a Netrin Receptor. Cell . 1996 May 23;87(2):175–85. Available from: http://dx.doi.org/10.1016/S0092-8674(00)81336-7

3. Leonardo E, Hinck L, Masu M, Keino-Masu K, Ackerman SL, Tessier-Lavigne M. Vertebrate homologues of C. e/egans UNC-5 are candidate netrin receptors. Nature. 1997;386:833–8.

4. Xu K, Wu Z, Renier N, Antipenko A, Tzvetkova- D, Xu Y, Minchenko M, Nardi-dei V, Kanagalaghatta R, Himanen J, Tessier-lavigne M, Nikolov DB. Structure of Netrin1 bound to two receptors provide insight into its Axon Guidance Mechanism. Science (80). 2014;344(6189):1275–9.

5. Geisbrecht B V., Dowd KA, Barfield RW, Longo PA, Leahy DJ. Netrin binds discrete subdomains of DCC and UNC5 and mediates interactions between DCC and heparin. J Biol Chem. 2003;278(35):32561–8.

6. Finci LI, Krüger N, Sun X, Zhang J, Chegkazi M, Wu Y, Schenk G, Mertens HDT, Svergun DI, Zhang Y, Wang J huai, Meijers R. The Crystal Structure of Netrin-1 in Complex with DCC Reveals the Bifunctionality of Netrin-1 As a Guidance Cue. Neuron. 2014;83(4):839–49.

7. Aronovich EL, McIvor RS, Hackett PB. The Sleeping Beauty transposon system: A non-viral vector for gene therapy. Hum Mol Genet. 2011;20(1):14–20.

8. Izsvák Z, Chuah MKL, VandenDriessche T, Ivics Z. Efficient stable gene transfer into human cells by the Sleeping Beauty transposon vectors. Methods . 2009;49(3):287–97. Available from: http://dx.doi.org/10.1016/j.ymeth.2009.07.001

9. Hackett PB, Ekker SC, Largaespada DA, McIvor RS. Sleeping Beauty Transposon-Mediated Gene Therapy for Prolonged Expression. Adv Genet. 2005;54(05):189–232.

10. Kowarz E, Löscher D, Marschalek R. Optimized Sleeping Beauty transposons rapidly generate stable transgenic cell lines. Biotechnol J. 2015 Apr 1;10(4):647–53.

11. Moya-Torres A, Gupta M, Heide F, Krahn N, Legare S, Nikodemus D, Imhof T, Meier M, Koch M, Stetefeld J. Homogenous overexpression of the extracellular matrix protein Netrin-1 in a hollow fiber bioreactor. Appl Microbiol Biotechnol. 2021;105(14–15):6047–57.

12. Das AT, Zhou X, Metz SW, Vink MA, Berkhout B. Selecting the optimal Tet-On system for doxycycline-inducible gene expression in transiently transfected and stably transduced mammalian cells. Biotechnol J . 2016 Jan 1;11(1):71–9.

13. Das AT, Tenenbaum L, Berkhout B. Tet-On Systems For Doxycycline-inducible Gene Expression. Curr Gene Ther . 2016 Jun 8;16(3):156.

14. Kearney BJ, Voorhees MA, Williams PL, Olschner SP, Rossi CA, Schoepp RJ. Corning HYPERFlask® for viral amplification and production of diagnostic reagents. J Virol Methods . 2017 Apr 1;242:9–13.

15. Corning® HYPERFlask® M Cell Culture Vessel. Available from: https://www.corning.com/catalog/cls/documents/protocols/CLS-CC-029.pdf

16. Moya-Torres A, Gupta M, Heide F, Krahn N, Legare S, Nikodemus D, Imhof T, Meier M, Koch M, Stetefeld J. Homogenous overexpression of the extracellular matrix protein Netrin-1 in a hollow fiber bioreactor. Appl Microbiol Biotechnol. 2021;105(14–15):6047–57.

17. Yang M, Butler M. Effects of ammonia on CHO cell growth, erythropoietin production, and glycosylation. Biotechnol Bioeng. 2000;68(4):370–80.

18. Ahler E, Sullivan WJ, Cass A, Braas D, York AG, Bensinger SJ, Graeber TG, Christofk HR. Doxycycline Alters Metabolism and Proliferation of Human Cell Lines. PLoS One . 2013 May 31;8(5). Available from: /pmc/articles/PMC3669316/

19. Gasteiger E, Gattiker A, Hoogland C, Ivanyi I, Appel RD, Bairoch A. ExPASy: the proteomics server for in-depth protein knowledge and analysis. Nucleic Acids Res . 2003 Jul 1;31(13):3784–8. Available from: http://www.ncbi.nlm.nih.gov/pmc/articles/PMC168970/

20. Fekete S, Beck A, Veuthey JL, Guillarme D. Theory and practice of size exclusion chromatography for the analysis of protein aggregates. J Pharm Biomed Anal . 2014;101:161–73. Available from: http://dx.doi.org/10.1016/j.jpba.2014.04.011

21. Hong P, Koza S, Bouvier ESP. Size-exclusion chromatography for the analysis of protein biotherapeutics and their aggregates. J Liq Chromatogr Relat Technol . 2012;35(20):2923–50.

22. Vander Heyden Y, Popovici ST, Schoenmakers PJ. Evaluation of size-exclusion chromatography and size-exclusion electrochromatography calibration curves. J Chromatogr A. 2002 May 31;957(2):127–37.

23. Arakawa T, Ejima D, Li T, Philo JS. The critical role of mobile phase composition in size exclusion chromatography of protein pharmaceuticals. J Pharm Sci . 2010 Apr 1;99(4):1674–92. Available from: https://onlinelibrary-wiley-com.uml.idm.oclc.org/doi/full/10.1002/jps.21974

24. Barth HG, Saunders GD. The State of the Art and the Sciences. LCGC North Am. 2012;30:544–63.

25. Lorber B, Bailly M, Kern D, Fischer F. Protein Analysis by Dynamic Light Scattering : Methods and Techniques for Students z. 2012;40(6):372–82.

26. Kwan TOC, Reis R, Siligardi G, Hussain R, Cheruvara H, Moraes I. Selection of Biophysical Methods for Characterisation of Membrane Proteins. Int J Mol Sci. 2019;20(10).

27. Stetefeld J, Mckenna SA, Patel TR. Dynamic light scattering : a practical guide and applications in biomedical sciences. Biophys Rev . 2016;409–27. Available from: http://dx.doi.org/10.1007/s12551-016-0218-6

28. Harding SE, Jumel K. Light scattering. Curr Protoc protein Sci. 2001 May;Chapter 7:Unit 7.8.

29. Pecora R. Dynamic Light Scattering-Applications of Photon Correlation Spectroscopy. In: Pecora R, editor. Phenum press, New York . Boston, MA: Springer US; 1985. Available from: http://link.springer.com/10.1007/978-1-4613-2389-1

30. Smith CA. Estimation of sedimentation coefficients and frictional ratios of globular proteins. Biochem Educ. 1988;16(2):104–6.

31. Malvern Panalytical Ltd. Intensity - Volume - Number: Which Size is Correct? Tech Note . 2016;i(1):1–3. Available from: http://www.malvern.com/en/support/resource-center/technical-notes/TN101104IntensityVolumeNumber.aspx

32. Niskanen I, Forsberg V, Zakrisson D, Reza S, Hummelgård M, Andres B, Fedorov I, Suopajärvi T, Liimatainen H, Thungström G. Determination of nanoparticle size using Rayleigh approximation and Mie theory. Chem Eng Sci. 2019 Jun 29;201:222–9.

33. Meier M, Moya-Torres A, Krahn NJ, McDougall MD, Orriss GL, McRae EKS, Booy EP, McEleney K, Patel TR, McKenna SA, Stetefeld J. Structure and hydrodynamics of a DNA G-

quadruplex with a cytosine bulge. Nucleic Acids Res. 2018 Jun;46(10):5319–31.

34. Wyatt PJ. Light scattering and the absolute characterization of macromolecules. Anal Chtmrca Acta. 1993;272.

35. Some D, Amartely H, Tsadok A, Lebendiker M. Characterization of Proteins by Size-Exclusion Chromatography Coupled to Multi-Angle Light Scattering (SEC-MALS). J Vis Exp . 2019 Jun 1;2019(148). Available from: https://pubmed.ncbi.nlm.nih.gov/31282880/

36. Hayashi Y, Matsui H, Takagi T. MEMBRANE ANALYSIS AND CHARACTERIZATION [28] Membrane Protein Molecular Weight Determined by Low-Angle Laser Light-Scattering Photometry Coupled with High-Performance Gel Chromatography. Methods of Enzymology, 1989; 172: 514-528.

37. Patel TR, Chojnowski G, Koul A, McKenna SA, Bujnicki JM. Structural studies of RNA-protein complexes: A hybrid approach involving hydrodynamics, scattering, and computational methods. Methods 118-119; 2016; 146-162. Available from:http://dx.doi.org/10.1016/j.ymeth.2016.12.002

38. Kwan TOC, Reis R, Siligardi G, Hussain R, Cheruvara H, Moraes I. Selection of Biophysical Methods for Characterisation of Membrane Proteins. Int J Mol Sci . 2019 May 27;20(10). Available from: /pmc/articles/PMC6566885/

39. Wen J, Arakawa T, Philo JS. Size-Exclusion Chromatography with On-Line Light-Scattering, Absorbance, and Refractive Index Detectors for Studying Proteins and Their Interactions. Anal Biochem. 1996;240:155–66.

40. Nachiappan M, Guru Raj Rao R, Richard M, Prabhu D, Rajamanikandan S, Chitra JP, Jeyakanthan J. 3D Structural Determination of Macromolecules Using X-ray Crystallography Methods. Mol Docking Comput Drug Des. 2021 Jan 1;119–40.

41. Kabsch W. Biological Crystallography. Res Pap Acta Cryst. 2010;66:125–32.

42. The CCP4 suite: programs for protein crystallography. Acta Crystallogr D Biol Crystallogr . 1994;50(Pt 5):760–3. Available from: https://pubmed.ncbi.nlm.nih.gov/15299374/

43. Mccoy AJ, Grosse-kunstleve RW, Adams PD, Winn MD, Storoni LC, Read RJ. Phaser crystallographic software. 2007;658–74.

44. Pettersen EF, Goddard TD, Huang CC, Couch GS, Greenblatt DM, Meng EC, Ferrin TE. UCSF Chimera--a visualization system for exploratory research and analysis. J Comput Chem. 2004 Oct;25(13):1605–12.

45. Terwilliger TC, Grosse-Kunstleve RW, Afonine P V., Moriarty NW, Zwart PH, Hung LW, Read RJ, Adams PD. Iterative model building, structure refinement and density modification with the PHENIX AutoBuild wizard. In: Acta Crystallographica Section D: Biological Crystallography. 2007. p. 61–9.

46. Adams PD, Pavel V, Chen VB, Ian W, Echols N, Moriarty NW, Read RJ, Richardson DC, Jane S, Thomas C. PHENIX : a comprehensive Python-based system for macromolecular structure solution research papers. 2010;213–21.

47. Emsley P, Lohkamp B, Scott WG, Cowtan K. Features and development of Coot. Acta Crystallogr Sect D Biol Crystallogr. 2010;66(4):486–501.

48. Chaton CT, Herr AB. Elucidating complicated assembling systems in biology using size-and-shape analysis of sedimentation velocity data Catherine. Method Enzym. 2015;562:187–204.

49. Cole JL, Lary JW, P. Moody T, Laue TM. Analytical Ultracentrifugation: Sedimentation Velocity and Sedimentation Equilibrium. Vol. 84, Methods in Cell Biology. 2008. p. 143–79.

50. Berkowitz SA. Role of Analytical Ultracentrifugation in Assessing the Aggregation of Protein Biopharmaceuticals. AAPS J . 2006;8(3):590–605. Available from: http://www.aapsj.org

51. Patel TR, Winzor DJ, Scott DJ. Analytical ultracentrifugation: A versatile tool for the characterisation of macromolecular complexes in solution. Vol. 95, Methods. Academic Press Inc.; 2016. p. 55–61.

52. Laue TM, Stafford WF. Modern applications of analytical ultracentrifugation. Annu Rev Biophys Biomol Struct . 1999;28:75–100. Available from: www.annualreviews.org

53. Lamm O. Die Differentialgleichung der Ultrazentrifugierung . Almqvist & Wiksell; 1929. (Arkiv för Matematik, Astronomi och Fysik). Available from: https://books.google.ca/books?id=2P4JHAAACAAJ

54. Brown PH, Schuck P. A new adaptive grid-size algorithm for the simulation of sedimentation velocity profiles in analytical ultracentrifugation. Comput Phys Commun . 2008 Jan 15;178(2):105. Available from: /pmc/articles/PMC2267755/

55. Zhao H, Brown PH, Schuck P. On the Distribution of Protein Refractive Index Increments. Biophysj. 2011;100:2309–17.

56. Salvay AG, Santamaria M, Le Maire M, Ebel C, Salvay AG, Ebel C, Santamaria M. Analytical Ultracentrifugation Sedimentation Velocity for the Characterization of Detergent-Solubilized Membrane Proteins Ca ++-ATPase and ExbB. J Biol Phys . 2007;33:399–419. Available from: http://blanco.biomol.uci.edu/Membrane_Proteins_xtal.html

57. Dam J, Schuck P. Calculating Sedimentation Coefficient Distributions by Direct Modeling of Sedimentation Velocity Concentration Profiles. Methods Enzymol. 2004 Jan 1;384:185–212.

58. Demeler B. UltraScan - A Comprehensive Data Analysis Software Package for Analytical Ultracentrifugation Experiments. Anal Ultracentrifugation. 2007;210–30.

59. Demeler B, Gorbet GE. Analytical Ultracentrifugation Data Analysis with UltraScan-III. Anal Ultracentrifugation Instrumentation, Software, Appl . 2016 Jan 1;119–43. Available from: https://link-springer-com.uml.idm.oclc.org/chapter/10.1007/978-4-431-55985-6_8

60. Claverie J -M, Dreux H, Cohen R. Sedimentation of generalized systems of interacting particles. I. Solution of systems of complete Lamm equations. Biopolymers. 1975;14(8):1685–700.

61. Demeler B, Saber H. Determination of Molecular Parameters by Fitting Sedimentation Data to Finite-Element Solutions of the Lamm Equation. Biophys J . 1998 Jan 1;74(1):444–54. Available from: http://www.cell.com/article/S0006349598778026/fulltext

62. Brookes E, Cao W, Demeler B. A two-dimensional spectrum analysis for sedimentation velocity experiments of mixtures with heterogeneity in molecular weight and shape. Eur Biophys J . 2010 Feb 27;39(3):405–14. Available from: https://link-springer-com.uml.idm.oclc.org/article/10.1007/s00249-009-0413-5

63. Demeler B, Brookes E. Monte Carlo analysis of sedimentation experiments. Colloid Polym Sci. 2008;129–37.

64. Brookes EH, Demeler B. Parsimonious Regularization using Genetic Algorithms Applied to the Analysis of Analytical Ultracentrifugation Experiments. Proc 9th Annu Conf Genet Evol Comput - GECCO ’07. 2007;

65. Edwards GB, Muthurajan UM, Bowerman S, Luger K. Analytical Ultracentrifugation (AUC): An Overview of the Application of Fluorescence and Absorbance AUC to the Study of

Biological Macromolecules. Curr Protoc Mol Biol . 2020 Dec 1;133(1):e131. Available from: https://onlinelibrary.wiley.com/doi/full/10.1002/cpmb.131

66. Putnam CD, Hammel M, Hura GL, Tainer JA. X-ray solution scattering (SAXS) combined with crystallography and computation: defining accurate macromolecular structures, conformations and assemblies in solution. Q Rev Biophys . 2007 Aug;40(3):191–285.

67. Boldon L, Laliberte F, Liu L. Review of the fundamental theories behind small angle X-ray scattering, molecular dynamics simulations, and relevant integrated application. Nano Rev. 2015;6(1):25661.

68. Putnam CD, Hammel M, Hura GL, Tainer JA. X-ray solution scattering (SAXS) combined with crystallography and computation: Defining accurate macromolecular structures, conformations and assemblies in solution. Q Rev Biophys. 2007;40(3):191–285.

69. Konarev PV, Volkov VV, Sokolova AV, Koch MHJ, Svergun DI, IUCr. PRIMUS: a Windows PC-based system for small-angle scattering data analysis. J Appl Cryst . 2003 Sep 8;36(5):1277–82. Available from: http://scripts.iucr.org/cgi-bin/paper?ks5004

70. Panjkovich A, Svergun DI. CHROMIXS: automatic and interactive analysis of chromatography-coupled small-angle X-ray scattering data. Bioinfomatics . 2018;34(11):1944–6. Available from: www.embl-hamburg.de/biosaxs/download.html

71. Grant TD. Ab initio electron density determination directly from solution scattering data. Nat Methods 2018 153 . 2018 Jan 29;15(3):191–3. Available from: https://www-nature-com.uml.idm.oclc.org/articles/nmeth.4581

72. Franke D, Svergun DI. DAMMIF, a program for rapid ab-initio shape determination in small-angle scattering. J Appl Crystallogr. 2009 Apr;42(Pt 2):342–6.

73. Grant TD. Ab initio electron density determination directly from solution scattering data. Nat Methods. 2018 Mar;15(3):191–3.

74. Volkov V V., Svergun DI. Uniqueness of ab initio shape determination in small-angle scattering. J Appl Crystallogr. 2003;36(3 I):860–4.

75. Petoukhov M V, Franke D, Shkumatov A V, Tria G, Kikhney AG, Gajda M, Gorba C, Mertens HDT, Konarev P V, Svergun DI. New developments in the ATSAS program package for small-angle scattering data analysis. J Appl Crystallogr. 2012 Apr;45(Pt 2):342–50.

76. Konarev P V., Volkov V V., Sokolova A V., Koch MHJ, Svergun DI. PRIMUS: A Windows PC-based system for small-angle scattering data analysis. J Appl Crystallogr. 2003;36(5):1277–82.

77. Jerabek-Willemsen M, André T, Wanner R, Roth HM, Duhr S, Baaske P, Breitsprecher D. MicroScale Thermophoresis: Interaction analysis and beyond. J Mol Struct . 2014;1077:101–13. Available from: http://dx.doi.org/10.1016/j.molstruc.2014.03.009

78. Jerabek-Willemsen M, Wienken CJ, Braun D, Baaske P, Duhr S. Molecular Interaction Studies Using Microscale Thermophoresis. Assay Drug Dev Technol . 2011;9(4):342–53.

79. Dijkman PM, Lea W a, Gmbh NT, Lazic A, Gmbh NT. Interactions under Previously Challenging Conditions. 2014;59(3):301–15.

80. Seidel SAI, Wienken CJ, Geissler S, Jerabek-Willemsen M, Duhr S, Reiter A, Trauner D, Braun D, Baaske P. Label-Free Microscale Thermophoresis Discriminates Sites and Affinity of Protein–Ligand Binding. Angew Chem Int Ed Engl . 2012 Oct 15;51(42):10656. Available from: /pmc/articles/PMC3588113/

81. Ross D, Gaitan M, Locascio LE. Temperature Measurement in Microfluidic Systems Using a Temperature-Dependent Fluorescent Dye. Anal Chem . 2001 Sep 1;73(17):4117–23.

82. Zelent B, Troxler T, Vanderkooi JM. Temperature Dependence for Fluorescence of β-NADH in Glycerol/Water Solution and in Trehalose/Sucrose Glass. J Fluoresc 2006 171 . 2006 Dec 14;17(1):37–42.

83. Some D. WP1615 : SEC-MALS for absolute biophysical characterization [White paper]. Wyatt Technol.

84. Creative Biostructure. Comparison of Crystallography, NMR and EM . Creative Biostructure. 2019. Available from: https://www.creative-biostructure.com/comparison-of-crystallography-nmr-and-em_6.htm

85. Seidel SAI, Dijkman PM, Lea WA, van den Bogaart G, Jerabek-Willemsen M, Lazic A, Joseph JS, Srinivasan P, Baaske P, Simeonov A, Katritch I, Melo FA, Ladbury JE, Schreiber G, Watts A, Braun D, Duhr S. Microscale Thermophoresis Quantifies Biomolecular Interactions under Previously Challenging Conditions. Methods . 2013 Mar 24;59(3):301–15.

CHAPTER 3: New Developments - Biophysical Analysis

3.1 Introduction-Biomolecular Interactions

Biomolecular interaction studies help understand the biological system, from metabolism and signal transduction to cell migration. The detailed characterization of these interactions is essential to understand biological systems better and apply the knowledge to the development of new drugs to target those interactions. Furthermore, determining the stability and other biophysical properties of proteins, nucleic acids, and small molecules is the key to understanding the biochemical processes to improve the quality of life. There are many attractive ways to study biomolecules and their interactions, including fluorescence-based assays, surface-based methods, and label-free methods. Here, I present two new biophysical technologies, mass photometry and Panta that helped me determine protein quality, homogeneity, and stability of an individual protein and complexes with interacting partners, all together in one step. Mass photometry is very useful in the case of complex and multivalent protein interactions. This chapter will start with a brief introduction to biophysical techniques that most labs use to analyze protein quality, stability, and interactions.

Firstly, interaction studies start from the cellular environment using a method named yeast two-hybrid system (1). Attaching an affinity tag to the protein of interest and passing it through the affinity column with the cell lysate to identify the binding partners is very common. Pulldown assays also work using the same approach (2). Combining affinity purification with mass spectrometry helps identify binding partners (3). BioID (proximity-dependent Biotin Identification) is a newly developed technique for proximity-based labelling (4). Again, the cell-based method allows the expression of a Protein of Interest (POI) as a fusion protein (POI + biotin ligase) that biotinylates proximal endogenous protein within a range of ~10-15 nm. These proteins can be isolated with affinity purification using Streptavidin conjugated beads and identified by MS (3).

Another way is to separate the interacting biomolecules based on their size. Size exclusion chromatography is one of them. Combining SEC with multiangle light scattering gives us more accurate results as it provides additional data like apparent molecular mass and heterogeneity. DLS is another a light scattering-based method. It can be used to study the interaction of two proteins if size changes more than double the individual binding partners (5). Native Mass spectrometry (Native MS) is another way to check the complexes. The main feature is mass precision, which allows the measuring of any change in mass with the binding of small molecules or even any change in glycosylation pattern (5). In the case of analytical ultra-centrifugation, macromolecules are separated in a centrifugal field depending upon their molecular mass. Thus, they give us different information about binding or even the individual proteins involved in the interaction (6).

The most used approaches for assessing the binding are Isothermal Titration Calorimetry (ITC), Biolayer Interferometry (BLI), Surface Plasmon Resonance (SPR), and MST. Every approach has its pros and cons. ITC is a label-free technique that measures heat evolution associated with the interaction (7). A concentrated solution of one binding partner is titrated into a dilute solution of another partner. This approach requires a large amount of protein.

SPR and BLI allow the immobilization of one binding partner on a biosensor surface via covalent binding or an affinity tag. Any physical changes on the immobilized surface are used to monitor the binding. SPR is based on the change in the local refractive index upon analyte binding that alters the momentum of the surface plasmon, while BLI measures the change in path length

between the ligand-bound and unbound surface (8,9). The main drawback of these approaches is the immobilization of protein that sometimes changes its properties and the relative sizes of the interacting molecules.

Another solution-based method is MST which allows the movement of the biomolecules under the application of temperature in a tiny area. One of the binding partners is fluorescently labeled and kept at constant concentration, and another one is titrated with it. An infrared laser is used to generate a micro heated area by 2-6 K. Any change in the fluorescently labeled protein that results from the binding (shape, size, or hydrodynamic radius) is monitored in real time (10). There are many fluorescence-based methods like intrinsic tryptophan fluorescence, fluorescence anisotropy, and fluorescence resonance energy transfer (FRET). All these techniques require fluorescently labeled proteins and a large amount of protein to study the interactions and are time-consuming.

3.2 Mass Photometry

Newly developed, the mass photometer introduced by Young *et al*. 2018, is a single molecule method based on interferometric scattering microscopy (11,12). Mass Photometry (MP) is a label-free, immobilization-free, solution-based method to quantify the molecular mass of biomolecules or interactions at a physiological concentration at the single-molecule level. A typical MP experiment requires 10-20 µl of sample with an approximate concentration of 100 nM or lower.

It can also measure sample purity, heterogeneity, aggregation, stoichiometry, binding affinity, and kinetics of biomolecules and their complexes (11–14). MP detects single molecules by light scattering as they bind non-specifically to a microscopic glass/solution interface **(Figure 3.1)**. The instrument is equipped with a green laser (520 nm). With the help of optimized interference between scattered and reflected light, any change in refractive index upon each binding event that alters the local reflectivity at the interface can be detected by a camera. Images captured by the camera during the measurement are further processed to obtain the contrast value of the signal from the landing molecules compared to the surrounding static background. Contrast values are proportional to the intensity of light scattered by a single particle. Thus, the single

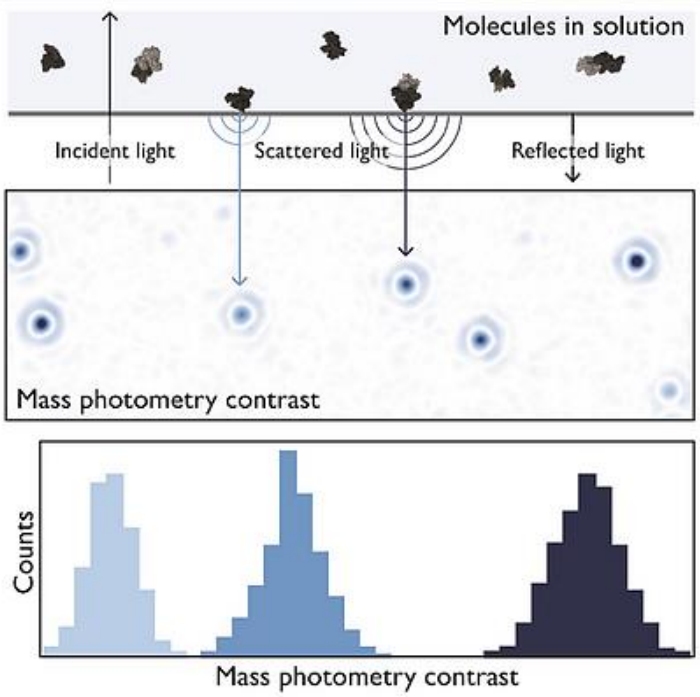

Figure 3.1 Principle of Mass photometry.

Label-free detection of single-molecules by imaging the interference of scattered and reflected light. (Figure from https://www.refeyn.com/about-mass-photometry).

molecular level based molecular mass determination is based on this relationship: the change in reflectivity generates a light scattering signal proportional to molecular mass. MP can give mass resolution up to 20 kDa and mass accuracy up to 2% by calibration with biomolecules of known mass (11).

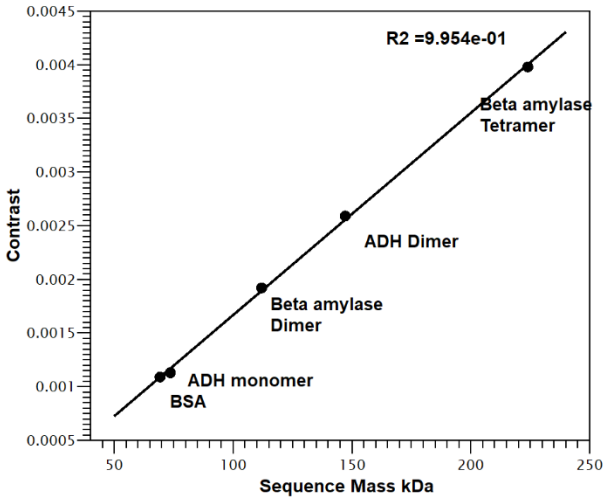

Figure 3.2 Contrast-mass calibration curve of mass photometry measurement. *Standard proteins used for calibration: BSA, beta-amylase, and ADH.*

Many methods can find the 1:1 binding event, but analysis becomes complicated in the case of multiple binding sites. MP is beneficial in such kinds of interaction studies. It can distinguish different binding events if the complex is sufficiently populated in the reaction mixture and shows a well-defined contrast distribution. Standard proteins, BSA, beta amylase, and alcohol dehydrogenase (ADH) are used to make the calibration curve for mass photometry measurement. These three standard

proteins give us a range of molecular mass from 60 to 230 kDa **(Figure 3.2).** All experimental conditions such as treatment of slides, buffer *etc*. should be the same for the standard and reference to calculate the molecular mass from the calibration curve. The sample should be centrifuged and filtered to remove any aggregates before the experiment.

Mass Photometry Method

Microscope slides (No. 1.5, 24 × 50, VMR) were plasma cleaned under oxygen. Prior to the measurements, the slides were treated with polyethylene glycol (PEG) silane and 3-aminopropyl triethoxysilane (APTES) (15) to produce an amino silane functionalized slide. For Polyethylene glycol (PEG)-silane treatment, the solution was prepared in 1% acetic acid in ethanol, and plasma cleaned slides were coated with PEG-silane solution. The coating was followed by baking at 70 °C for 45 minutes and further cleaned with Milli-Q water. For APTES functionalization, the slides were dipped in 2% APTES solution in acetone and then baked for 1-2 hours in a 110 °C preheated oven. After this, the slides were cleaned with isopropanol and Milli-Q water. Flow chambers (as described by Young *et al.* 2018), and silicone gasket slides (Culture well, reusable gasket, 3 mm diameter X 1 mm depth, GRACE BIO-LAB) were used for the sample application with netrin-1 alone and netrin-1 with oligosaccharides (dp8 and dp10), respectively.

Netrin-1 and netrin-1 with equimolar oligosaccharide concentration were dialyzed in 50 mM tris pH 7.5, 200 mM NaCl filtered buffer. BSA, ADH, and beta-amylase, were the three standard proteins used for calibration. The samples were diluted in the filtered assay buffer immediately before the experiment to the desired concentration to enable detection of enough particles landing and well separated. 15 µl of a sample (50 nM concentration) was loaded on the flow chamber (for netrin-1 alone studies), by replacing all the buffer without dilution. However, in a gasket (for netrin-1 interaction studies with oligosaccharides), the sample was diluted directly in the well, containing buffer to an approximate concentration of 100 nM. Interferometric videos were taken on a mass photometric system and processed as described (12). Each protein sample was measured in a new flow chamber and gasket. The objective was focused on the surface of the glass-solvent interface to a maximize the value of the sharpness parameter by adjusting the stage.

The collected data/movie was processed with software Discover MP (Refeyn Ltd.). The fitting parameters used for analysis were: number of binned frames (n) 10, threshold 1 = 1.5

(related to a given particle contrast amplitude relative to the background), and Threshold 2 = 0.2 (related to the radial symmetry of the detected point spread function of the same particle) (14).

3.3 Prometheus PANTA

The study of biomolecules, their interactions, and nanoparticles, usually requires analysis of the sample for its stability and size as well as optimization of buffer conditions. There are many ways to do this including DLS, thermal shift assay (TSA), and a nano-format of differential scanning fluorimetry (nanoDSF).

A DLS instrument measures the diffusion coefficient R_h. The Brownian motion of molecules in the sample causes the laser light to be scattered at different intensities depending upon the size of the biomolecules. Smaller molecules moving faster and changing location more frequently leads to faster intensity fluctuations than for larger particles. Thus, analyzing the intensity fluctuations from the Brownian motion of the particle via the autocorrelation function makes it helpful in analyzing the size, heterogeneity, and stability of proteins in solution. It requires the knowledge of the temperature and solvent viscosity as scattering changes with these parameters' changes. For DLS there is a possibility of using only one sample, so it is not optimal for screening.

TSA is a high-throughput method to study the stability of biomolecules as a function of temperature (16,17). There is a need to study the best buffer or ligand that maximizes the stability of a protein during the purification process and ultimately to get good quality protein for crystallization, any further biophysical analysis, and for functional studies. In addition, the thermal stability of individual proteins after complex formation can be measured. This requires small sample quantities and identifying good buffer conditions, ligands, small molecules, and modifications that increase their Tm and relative stability. A ThermoFluor assay mainly quantifies the changes in denaturation temperature of proteins in a range of buffers with different salts/ionic strength, pH, and additives with a Real Time-Polymerase Chain Reaction (RT-PCR) instrument (16–18). A fluorescent dye (SYPRO Orange) binds to the hydrophobic regions of the protein, and dye molecules are quenched in an aqueous solution while incubated with protein. An increase in temperature results in the unfolding of proteins and binding of the dye to the exposed hydrophobic surfaces, resulting in an increase in fluorescence by excluding water. The stability curve with

melting temperature T_m (50% of the maximum fluorescence intensity corresponding to 50% of the protein being unfolded) is obtained by measuring the changes in fluorescence with a gradual increase in the temperature and is very helpful in calculating the stability of proteins and protein complexes (17).

Many commercially available kits have a different variety of combinations of buffer and small molecules. They can be used to screen the relative thermal stability of a protein, the effects of different molecules, optimal buffers for proteins, protein-ligand interactions, storage conditions, and stability after any modification to the protein (16,17,19).

Prometheus nanoDSF, measures several different parameters of a protein like stability, folding-unfolding, aggregation, and ligand binding under different thermal and chemical conditions (20,21). It is a label-free, low sample consumption and high throughput technique (21). So, it is possible to do buffer optimization, ligand screening, and protein stabilization with this method. Protein aggregation at room temperature and thermally induced aggregation can also be studied. NanoDSF monitors the intrinsic tryptophan fluorescence changes with high time-resolution as a protein unfolds during the thermal treatment. An increase in temperature causes unfolding of the protein, and the extent of tryptophan exposure is determined by measuring fluorescence at 330 nm and 350 nm wavelength. Detection of protein aggregation is based on back reflection-optics. Reflection from the sample as the light passes through the capillary is quantified by the detector. Aggregation of the protein sample leads to the scattering of the incident light, and thus the intensity of reflected light is lost. The temperature range is 15 to 95˚C and the protein concentration range is broad. For back reflection, the size resolution is larger than 12.5 nm radius. It is a dye-free method and any buffer with any additives works.

Prometheus PANTA (Nanotemper) is a multi-parameter characterizing technique that characterizes the stability of biomolecules by combining nanoDSF, back reflection, and dynamic light scattering. Simultaneous measurement of size distribution, polydispersity, scattering intensity, self-interaction studies, thermal unfolding, and aggregation make this technique very powerful and attractive for biomolecule studies. The blue laser wavelength and a photomultiplier tube (PMT) detector are used for DLS to allow rapid measurement of DLS data and thermal unfolding measurements without any compromise. It is highly precise, reproducible, and easy to use.

3.4 Panta Applications:

Starting from protein purification to scale up, to keep protein stable and free from aggregates while maintaining the right size (conformational and colloidal stability), Panta measure protein thermal stability under different buffer conditions along with size analysis by DLS and measures turbidity by back reflection measurements (22). Sometimes thermal stability experiments show that two or three buffers have approximately the same Tm value. In that case, simultaneous DLS measurements help decide the best buffer that gives protein with the right size and low polydispersity. Self-interactions can also be studied using Panta (23). It has an option to study only the diffusion coefficient D that is related to the hydrodynamic radius R_h (24) by the Stokes-Einstein equation

$$D = \frac{k_b T}{6\pi\eta R_h} \qquad \text{Equation 3.1}$$

Where k_b is the Boltzmann constant, T is the Temperature in Kelvin and η is the viscosity. Equation 3.1 shows that D is inversely proportional to the R_h value. The particle with a smaller size shows faster diffusion than a particle with a larger size (24). If there is an interaction between the biomolecules, the diffusion value would be negative or smaller as there is an increase in size. A concentration series is the best way to study self-interaction by plotting diffusion vs. concentration (23). A negative slope indicates no aggregation with the increase in concentration.

Drug discovery, conjugate-based drug delivery (mAb + conjugates), and drug storage require information about aggregation with time or concentration (25). Some drugs need to be stored and delivered at high concentrations without aggregation. Panta can provide fast checking of such effects. In the case of conjugate-based drug delivery to a specific location, it is crucial to have all conjugate-bound mAb without any leftover conjugates. DLS helps to measure the increase in the size of mAb after the addition of conjugates and can check the polydispersity in the event that any extra conjugate is unbound or any aggregate forms after the reaction between the conjugate and mAb (26).

Structural studies require high-quality protein with excellent stability. In particular, protein crystallography requires more than 95% monodisperse sample along with high stability. Thus, Panta is very useful to study protein before starting any crystallizing trials. With the use of a combination of DLS and nanoDSF, we can get enough knowledge about the protein stability

quickly starting with buffer optimization to the presence of any additive on the stability and ultimately choosing the best conditions that yield with monodispersed protein and low PDI (27,28).

Panta allows the study of protein stability after ligand or small molecule interaction or any change in the structure after binding along with aggregation, polydispersity index, and heterogeneity (22). As mentioned before, screening ligand or small molecules in different buffer conditions can be used to discover the best binding partner and can also be useful for other biophysical analyses and crystallography. It can study 48 samples and provide analyzed results within two hours. The concentration range for the instrument is 200 mg/ml to 5 μg/ml (Nanotemper Prometheus Panta), so it is beneficial for membrane protein-containing detergent (25,29) and even for highly concentrated antibodies for aggregation prediction (30,31).

Panta Method

The dialyzed netrin-1ΔC samples in different buffers were centrifuged before filling the capillaries to remove dust and aggregates. Firstly, the fluorescence was checked to decide which excitation power (%) would be suitable for all the samples with PR Panta control software. There is an option to do another discovery scan too. In the case of samples with different concentrations, the software can pick the best excitation power that will work with each sample. Different measurements were done such as thermal unfolding, and size analysis (thermal unfolding with DLS). Parameters used for the measurements were 40% excitation power (selected from the initial scan), temperature slope (0.5 ˚C/min), high sensitivity mode of scattering, Temperature range:15-95 ˚C, Refolding Ramp (OFF), Dynamic Light Scattering (ON), and DLS Laser Power (100%).

References

1. Brückner A, Polge C, Lentze N, Auerbach D, Schlattner U. Yeast two-hybrid, a powerful tool for systems biology. Int J Mol Sci. 2009;10(6):2763–88.

2. Louche A, Salcedo PS, Bigot S. Bacterial Protein Secretion Systems: Methods and Protocols. Methods Mol Biol . 2017;1615:257–75. Available from: http://link.springer.com/10.1007/978-1-4939-7033-9

3. Morris JH, Knudsen GM, Verschueren E, Johnson JR, Cimermancic P, Greninger AL, Pico AR. Affinity purification-mass spectrometry and network analysis to understand protein-protein interactions. Nat Protoc. 2014;9(11):2539–54.

4. Sears RM, May DG, Roux KJ. BioID as a tool for protein-proximity labeling in living cells. Methods Mol Biol. 2019;2012:299–313.

5. Stetefeld J, Mckenna SA, Patel TR. Dynamic light scattering : a practical guide and applications in biomedical sciences. Biophys Rev . 2016;409–27. Available from: http://dx.doi.org/10.1007/s12551-016-0218-6

6. Cole JL, Lary JW, P. Moody T, Laue TM. Analytical Ultracentrifugation: Sedimentation Velocity and Sedimentation Equilibrium. Vol. 84, Methods in Cell Biology. 2008. p. 143–79.

7. Duff MR, Grubbs J, Howell EE. Isothermal titration calorimetry for measuring macromolecule-ligand affinity. J Vis Exp. 2011;(55):2–5.

8. Drescher DG, Drescher MJ, Ramakrishnan NA. Surface plasmon resonance (SPR) analysis of binding interactions of proteins in inner-ear sensory epithelia. Methods Mol Biol. 2009;493:323–43.

9. Müller-Esparza H, Osorio-Valeriano M, Steube N, Thanbichler M, Randau L. Bio-Layer Interferometry Analysis of the Target Binding Activity of CRISPR-Cas Effector Complexes. Front Mol Biosci. 2020;7(May):1–10.

10. Jerabek-Willemsen M, André T, Wanner R, Roth HM, Duhr S, Baaske P, Breitsprecher

D. MicroScale Thermophoresis: Interaction analysis and beyond. J Mol Struct . 2014;1077:101–13. Available from: http://dx.doi.org/10.1016/j.molstruc.2014.03.009

11. Soltermann F, Foley EDB, Pagnoni V, Galpin M, Benesch JLP, Kukura P, Struwe WB. Quantifying Protein–Protein Interactions by Molecular Counting with Mass Photometry. Angew Chemie - Int Ed. 2020;59(27):10774–9.

12. Young G, Hundt N, Cole D, Fineberg A, Andrecka J, Tyler A, Olerinyova A, Ansari A, Marklund EG, Collier MP, Chandler SA, Tkachenko O, Allen J, Crispin M, Billington N, Takagi Y, Sellers JR, Eichmann C, Selenko P, Frey L, Riek R, Galpin MR, Struwe WB, Benesch JLP, Kukura P. Quantitative mass imaging of single biological macromolecules. Science. 2018;360(6387):423–427.

13. Wu D, Piszczek G. Measuring the affinity of protein-protein interactions on a single-molecule level by mass photometry. Anal Biochem. 2020;592(January).

14. Li Y, Struwe WB, Kukura P. Single molecule mass photometry of nucleic acids. Nucleic Acids Res. 2020;48(17):E97.

15. Nicholas MP, Rao L, Gennerich A. Covalent Immobilization of Microtubules on Glass Surfaces for Molecular Motor Force Measurements and Other Single- Molecule Assays. Bone. 2014;(1136):137–69.

16. Ericsson UB, Hallberg BM, DeTitta GT, Dekker N, Nordlund P. Thermofluor-based high-throughput stability optimization of proteins for structural studies. Anal Biochem . 2006 Oct 15;357(2):289–98. Available from: https://pubmed.ncbi.nlm.nih.gov/16962548/

17. Huynh K, Partch CL. Analysis of protein stability and ligand interactions by thermal shift assay. Curr Protoc protein Sci . 2015 Feb 2;79:28.9.1-28.9.14. Available from: https://pubmed.ncbi.nlm.nih.gov/25640896/

18. Phillips K, de la Peña AH. The combined use of the Thermofluor assay and ThermoQ analytical software for the determination of protein stability and buffer optimization as an aid in protein crystallization. Curr Protoc Mol Biol . 2011;Chapter 10(SUPPL.94). Available from: https://pubmed.ncbi.nlm.nih.gov/21472694/

19. Boivin S, Kozak S, Meijers R. Optimization of protein purification and characterization using Thermofluor screens. Protein Expr Purif . 2013;91(2):192–206. Available from: https://pubmed.ncbi.nlm.nih.gov/23948764/

20. Wen J, Lord H, Knutson N, Wikström M. Nano differential scanning fluorimetry for comparability studies of therapeutic proteins. Anal Biochem . 2020 Mar 15;593. Available from: https://pubmed.ncbi.nlm.nih.gov/31935356/

21. Real-Hohn A, Groznica M, Löffler N, Blaas D, Kowalski H. nanoDSF: In vitro Label-Free Method to Monitor Picornavirus Uncoating and Test Compounds Affecting Particle Stability. Front Microbiol . 2020 Jun 26;11. Available from: https://pubmed.ncbi.nlm.nih.gov/32676065/

22. Lobo SA, Wyss B, Widmer JC, Jesus LP, Gomes J, Batista AP, Hartmann S, Wassmann P. Stability liabilities of biotherapeutic proteins: Early assessment as mitigation strategy. J Pharm Biomed Anal . 2021;192:113650. Available from: https://doi.org/10.1016/j.jpba.2020.113650

23. Valldorf B, Fricke A, Kall S. Use of self-interaction parameters derived from light scattering experiments for better developability assessment of biologic therapeutics. NanoTemper Technologies application note. 2021.

24. Stetefeld J, McKenna SA, Patel TR. Dynamic light scattering: a practical guide and applications in biomedical sciences . Vol. 8, Biophysical Reviews. Biophysical Reviews; 2016. p. 409–27. Available from: http://dx.doi.org/10.1007/s12551-016-0218-6

25. Khongorzul P, Ling CJ, Khan FU, Ihsan AU, Zhang J. Antibody-drug conjugates: A comprehensive review. Mol Cancer Res . 2020 Jan 1;18(1):3–19. Available from: https://aacrjournals.org/mcr/article/18/1/3/90017/Antibody-Drug-Conjugates-A-Comprehensive

26. Bailly M, Mieczkowski C, Juan V, Metwally E, Tomazela D, Baker J, Uchida M, Kofman E, Raoufi F, Motlagh S, Yu Y, Park J, Raghava S, Welsh J, Rauscher M, Raghunathan G, Hsieh M, Chen YL, Nguyen HT, Nguyen N, Cipriano D, Fayadat-Dilman L. Predicting Antibody Developability Profiles Through Early Stage Discovery

Screening. MAbs . 2020 Jan 1;12(1). Available from: /pmc/articles/PMC7153844/

27. Haffke M, Rummel G, Boivineau J, Münch A, Jaakola V pekka. Thermal Unfolding of GPCRs nanoDSF : Label-free Thermal Unfolding Assay of G Protein- Coupled Receptors for Compound Screening and Buffer Composition Optimization. Appl Note. 2016;NT-PR-008:1–8.

28. Rucktooa P, Cheng RKY, Segala E, Geng T, Errey JC, Brown GA, Cooke RM, Marshall FH, Doré AS. Towards high throughput GPCR crystallography: In Meso soaking of Adenosine A2A Receptor crystals. Sci Reports 2017 81 . 2018 Jan 8;8(1):1–7. Available from: https://www.nature.com/articles/s41598-017-18570-w

29. Maschberger M, Hüttl S, Mueller TD, Breitsprecher D. Thermal Unfolding of Membrane Proteins Detergent Screen for solubilized membrane proteins – Case study on the SLAC-protein HiTehA from Haemophilus influenzae. Appl Note. 2015;NT-PR-002:1–8.

30. Breitsprecher D, Linke P, Schulze A, Söltl F, Garidel P, Blech M. Getting the Full Picture: Predicting the Aggregation Propensity of mAbs Using Chemical and Thermal Denaturation on a Single , Fully Automated Platform. Chem Therm Denaturation Appl Note. 2015;1–10.

31. Schramm P, Würtenberger S, Kleusch C, Kall S. Analyze self-interaction to predict viscosity and aggregation propensity at higher concentrations. NanoTemper Technologies application note. 2021.

CHAPTER 4: Results

4.1 Expression of the extracellular protein Netrin-1 in a Hyper-flask and Hollow fiber Bioreactor

The C-terminal domain of netrin-1, a positively charged domain, has been suggested to bind to heparan sulfate and forms higher order aggregates (1,2). The C domain is attached *via* a flexible linker to the V-3 domain and is not required for receptor binding (2–4); therefore, for this study, a construct containing netrin-1 domain V and VI was used and named as netrin-1ΔC (without C terminal domain) from chicken. The stable expression of netrin-1ΔC was based on the sleeping beauty transposons system, a transposase-mediated DNA genome integration technique. Puromycin-resistant selected clone, containing multiple copies of the gene of interest in the chromosome, V311, was gifted by Dr. Manuel Koch, University of Cologne, Center for Molecular Medicine, Köln, Germany.

A further selection of the highest producing clone was based on the Tet-On inducible system (5), which controls the activation of downstream genes only in the presence of doxycycline that induces the reverse tTA (rtTA) to bind the promoter PTigh (a modified Tet-Responsive Element (TREmod)) and switches on the expression of the regulated gene (5). In our construct, the netrin-1ΔC gene is controlled by the Tet-On doxycycline-inducible system. The netrin-1 V311 clone was successfully grown to confluency in T75 flasks and moved to 96 well plates, ensuring one cell per well for proper clonal selection. A dot-blot system was used to select high protein secreting clones. The highest producing clone induced by the TRE promoter was detected by western blot using a monoclonal antibody (anti-strep) for visualization. Purified proteins with and without strep tag were used as a positive and negative controls respectively.

The highest producing clone of netrin-1ΔC was further used to inoculate HYPERFlask® multilayer vessels. The yield of expressed protein increased from 1 mg to 15 mg/550 ml of conditioned medium from the earlier transient expression system used in the lab. HYPERFlask® is a ten-layer flask that allows ten times higher surface area than another traditional flask and is easy to handle. The main limitation is the loss of cell viability over time as cells become confluent, resulting in reduced protein expression yields. The initial four media collections containing expressed netrin-1ΔC were done without compromising the expression yield, making it slow and interrupted. At collection 6, the level of lactose increased in the media **(Figure 4.1)**, which may change the cell growth, cell viability, and ultimately yield poor protein stability. Netrin-1ΔC

requires multiple downstream steps to get the final purified protein, and in every step, there is a loss of protein. Therefore, there was a need to get the constant protein yield with continuous production.

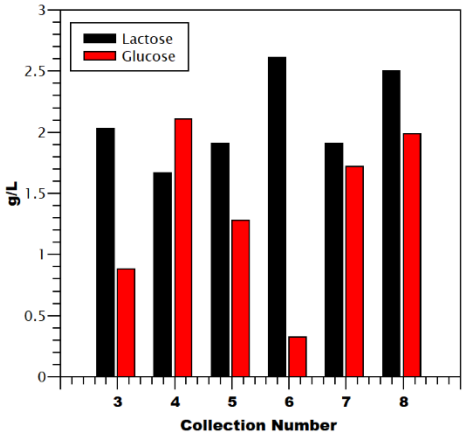

Figure 4.1 *Levels of Glucose and Lactose collected at different collections of media from HYPERflask containing netrin-1ΔC protein. Figure with permission from* (6)**.**

The Hollowfiber Bioreactor (HFBR) allowed continuous protein production with a constant protein yield for each collection. The HFBR was operated with a continuous media flow with daily removal of protein and dead cells. As glucose levels decreased to 50% of the initial glucose level, media was replaced with fresh media to ensure the continuous delivery of all the nutrients to the cells and stable protein production. The volume of media collected from the cartridge was 20 ml, allowing further downstream processing to achieve the same protein quantity as in the HYPERFlask® (~8 mg). The high-density cell growth in the HFBR reduced the serum requirement which was the primary contaminant in the earlier protein production trials.

To optimize the growth conditions and protein expression in the presence of the inducer, we studied the expression of netrin-1ΔC at increasing concentrations of doxycycline over time starting from 0.062 µg/ml to 2.0 µg/ml. Glucose and lactate levels were measured in the media at different concentrations of doxycycline **(Figure 4.2)**. The expressed netrin-1ΔC with streptag at different concentrations was analyzed *via* SDS-PAGE and showed an enhancement of the tagged protein band as the concentration of doxycycline increased **(Figure 4.3).** Protein quantity in media was determined using Biolayer Interferometry (BLI), combining

it with an antibody fragment (Fab) specific for netrin-1ΔC (data not shown) (6). Maximum protein production was associated with 1 µg/ml of doxycycline with good cell viability, and this concentration was used in the HFBR.

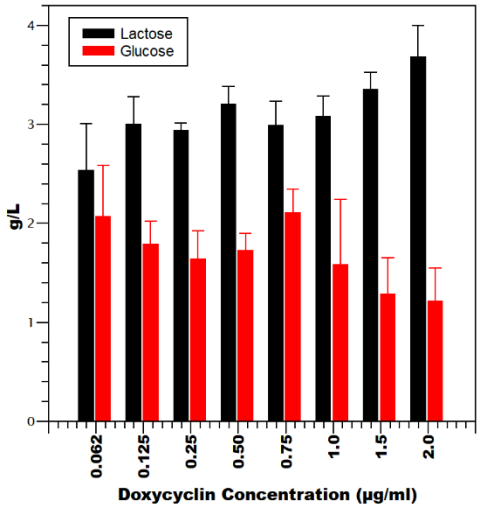

Figure 4.2 Levels of Glucose (Red) and Lactose (Black) collected at different concentrations of doxycycline in the ECS media. *Data shown is the average of three measurement with error bars that represent the standard deviations. Small increases were observed in the lactose level as the doxycycline level increases as it boosted the cell growth and protein production. Figure with permission from* (6).

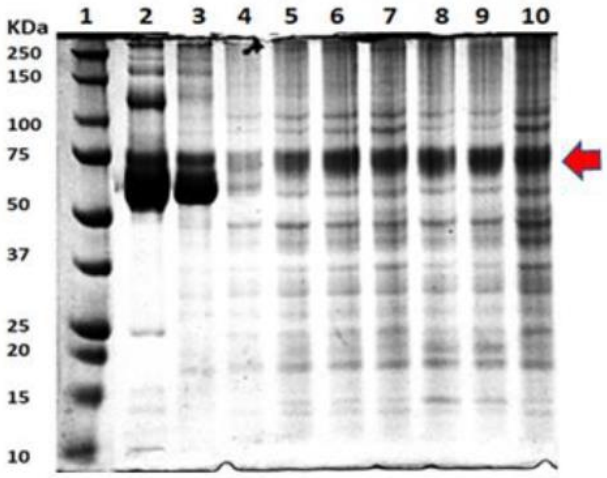

Figure 4.3 8% SDS-PAGE shows bands corresponding to selected individual ECS collection at different concentrations of doxycycline. *Red arrow indicates the region corresponding to the netrin-1 relative migration band. Lane 1) Molecular weight ladder, 2) No Doxycycline, 3) 0.062 µg/ml Doxycycline, 4) 0.125 µg/ml Doxycycline, 5) 0.25 µg/ml Doxycycline, 6) 0.5 µg/ml Doxycycline, 7) 0.75 µg/ml Doxycycline, 8) 1.0 µg/ml Doxycycline, 9) 1.5 µg/ml Doxycycline, and 10) 2 µg/ml Doxycycline. Figure with permission from* (6)

As mentioned before, the HFBR was maintained at >50% of the initial glucose level for optimal growth conditions and optimal protein production for an extended period. Failure to maintain the optimal level of nutrients will disturb cell growth, induce cell death, and ultimately the reduce stability of the protein (7). Stable protein production was maintained by replacing the nutrient-depleted media with new media to recirculate nutrients again through the system. Accumulation of expression by-products, such as lactate and ammonia, inhibit cell growth and protein expression and modify protein glycosylation patterns (8). Replacing the media in the reservoir once initial glucose level reached 50%, reduced the accumulation of by-products thus, maintaining the optimal cell metabolism.

4.2 Biophysical characterization of Netrin-1

Netrin-1 is composed of an N-terminal domain VI, followed by Laminin-type epidermal growth factor (V-1, V-2, V-3) repeats (LE domains) and a C terminal domain (1,9). Since only domain VI and V are involved in interaction with its dependence receptors (1), therefore netrin-1 without the C domain (netrin-1ΔC) was used for all the studies and characterization reported here. For structural and biophysical studies, the stability of a protein is essential. This chapter will include the purification process, biophysical analysis, and solution structure information. This initial analysis is fundamental to permit study of protein-protein interactions as well as protein-small molecules and ligand-receptor interactions.

4.2.1 Purification process

The protein expression and production were explained in this chapter's first section. The further purification started with the streptactin affinity purified protein. The eluted sample from the streptactin column and untagged protein sample after thrombin cleavage were run on SDS-PAGE. The SDS-PAGE analysis of the thrombin cleaved protein showed two bands corresponding to the tagged and untagged protein **(Figure 4.4A),** indicating incomplete cleavage. Thrombin cleavage was performed again to increase the yield of untagged protein. The initial attempt was not successful in achieving 100% untagged protein. Since netrin-1 forms aggregates (data not shown), it is vital to separate tagged and untagged proteins at a certain point to avoid a mixture of tagged and untagged netrin-1 for further biophysical analysis. Therefore, thrombin cleavage was done for 24 hours for the next batch of eluted proteins and was immediately followed by a second round of Streptactin purification. The SDS-PAGE analysis finally showed the cleaved protein **(Figure 4.4B).**

Further purification on an analytical Superdex 200 gel filtration column in 50 mM tris pH 7.5, 500 mM NaCl showed some aggregates (data not shown). The first peak that eluted after the void volume contained only high molecular weight proteins or aggregates; however, other peaks eluted after 10.5 ml. According to the gel analysis, peaks 2 and 3 correspond to netrin-1ΔC.

Since 95% pure protein is essential for the crystallization process, netrin-1ΔC was dialyzed in 50 mM tris pH 7.5, 1 M NaCl overnight. The sample was loaded on a size-exclusion column equilibrated with the same buffer. The first peak eluted at 11.68 ml shortly after the void

volume (10.5 ml) and another peak eluted at 13.25 ml **(Figure 4.5)**. In this attempt there was a very less aggregated product (*) than the first attempt **(Figure 4.5)**.

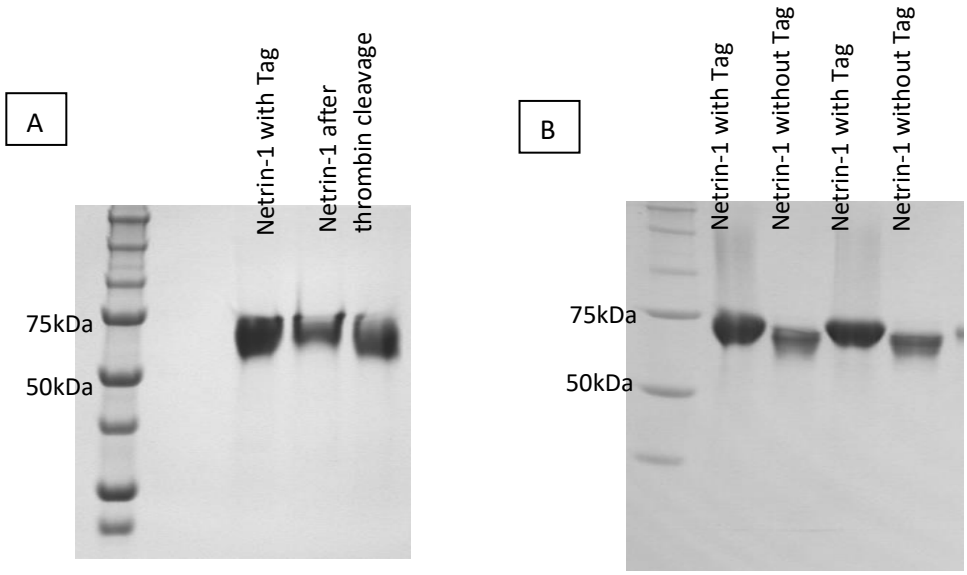

Figure 4.4 Coomassie SDS PAGE of netrin-1ΔC with and without tag. *Affinity chromatography (Streptactin) of purified netrin-1 with and without tag. A) Gel with all bands at the same position. First trial of thrombin cleavage did not work. B) incubation with enzyme for 24 hours followed by a second round of streptactin column purification showed untagged netrin-1. Run on 8% Tricine SDS PAGE.*

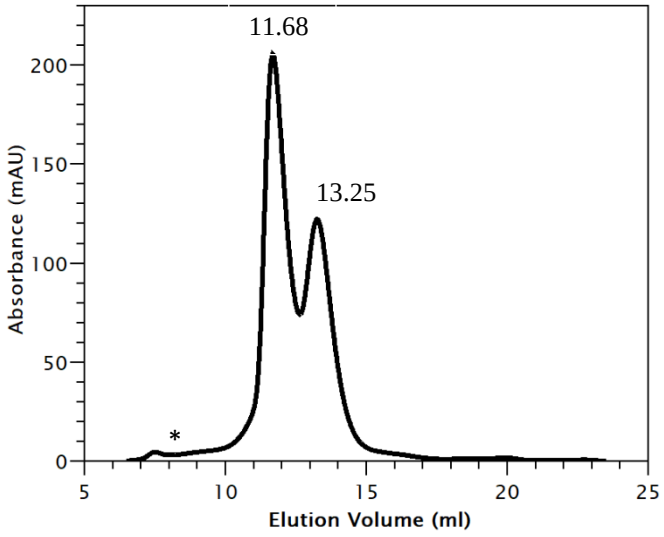

Figure 4.5 Size exclusion chromatography of netrin-1ΔC without tag*. Elution profile of netrin-1 without strep-tag acquired from Superdex200 6 10/300GL column in 50 mM tris pH 7.5, 1 M NaCl buffer.*

4.2.2 Improving protein purification

To further purify the protein, the untagged netrin-1ΔC was dialyzed overnight in buffer 50 mM tris pH 7.5, 500 mM NaCl and containing an additional 500 mM $(NH_4)_2\ SO_4$ and loaded on the column equilibrated with the same buffer. The gel filtration profile showed a smaller first peak compared to the first profile (Figure not shown). Since netrin-1 binds with HSPG, leading to higher molecular weight aggregates (10,11), a subsequent dialysis in ammonium sulfate buffer was performed in 25 kDa cutoff dialysis membrane to get rid of most of the bound GAGs and was followed by size exclusion chromatography purification on a Superose 6 10/300GL column in the same buffer. The gel filtration profile showed a small first peak (marked as *) **(Figure 4.6)**. As discussed before, netrin-1 forms aggregates, so sulfates might help to replace any bound HS and prevent aggregation. The peak that eluted at 11.75 ml had a shoulder and SDS PAGE analysis showed that all the fractions in the peak correspond to netrin-1ΔC without strep tag (data not shown).

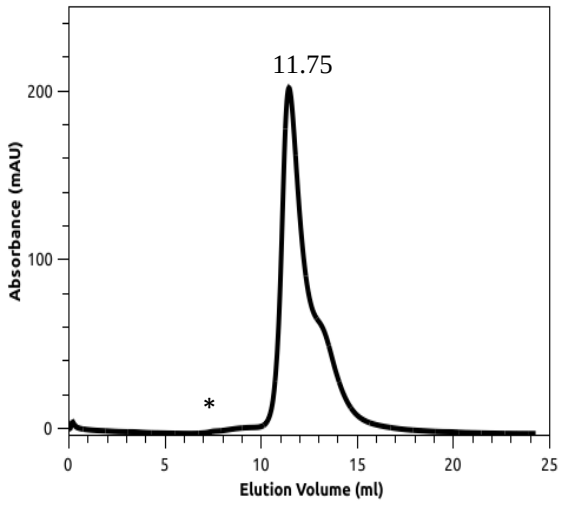

Figure 4.6 Size exclusion chromatography of netrin-1ΔC treated with ammonium sulfate*. Elution profile of netrin-1 without strep-tag acquired from Superose 6 10/300GL column in 50 mM tris pH 7.5, 500 mM NaCl and 500 mM* $(NH_4)_2\ SO_4$.

Another trial to purify netrin-1ΔC included $(NH_4)_2\ SO_4$ in the buffer during the initial purification process. After passing the media collected from a HFBR, the column was washed with high salt to remove any non-specifically bound proteins from the Streptactin column. The high salt washing step was replaced with another buffer with ammonium sulfate (50 mM tris pH 8.0, 500

mM NaCl, and 500 mM $(NH_4)_2$ SO_4 (results in section 4.2.3). The main objective was to remove any GAGs and get less aggregated proteins from the first step.

We also characterized the ammonium sulfate-treated and untreated netrin-1ΔC in 50 mM tris pH 7.5, 200 mM NaCl buffer (low ionic strength buffer) using DLS. DLS measurements to check the sample's homogeneity are essential for the further crystallization of the protein. DLS data analysis at multiple concentrations for untreated netrin-1ΔC showed a reduction in the R_h values with an increase in concentration **(Figure 4.7A)**, which means the sample is not stable. Extrapolation to infinite dilution gave an R_h value of more than 7.41 ± 0.24 nm **(Figure 4.7A)**. However, ammonium sulfate-treated netrin-1ΔC could be concentrated to 9 mg/ml without any change in the R_h and the protein was highly monodisperse **(Figure 4.7B)**. Extrapolation of the ammonium sulfate-treated netrin-1ΔC R_h measurements to infinite dilution provided an R_h value of 6.42 ± 0.14 nm **(Figure 4.7B)**. DLS volume distribution plots showed a single peak

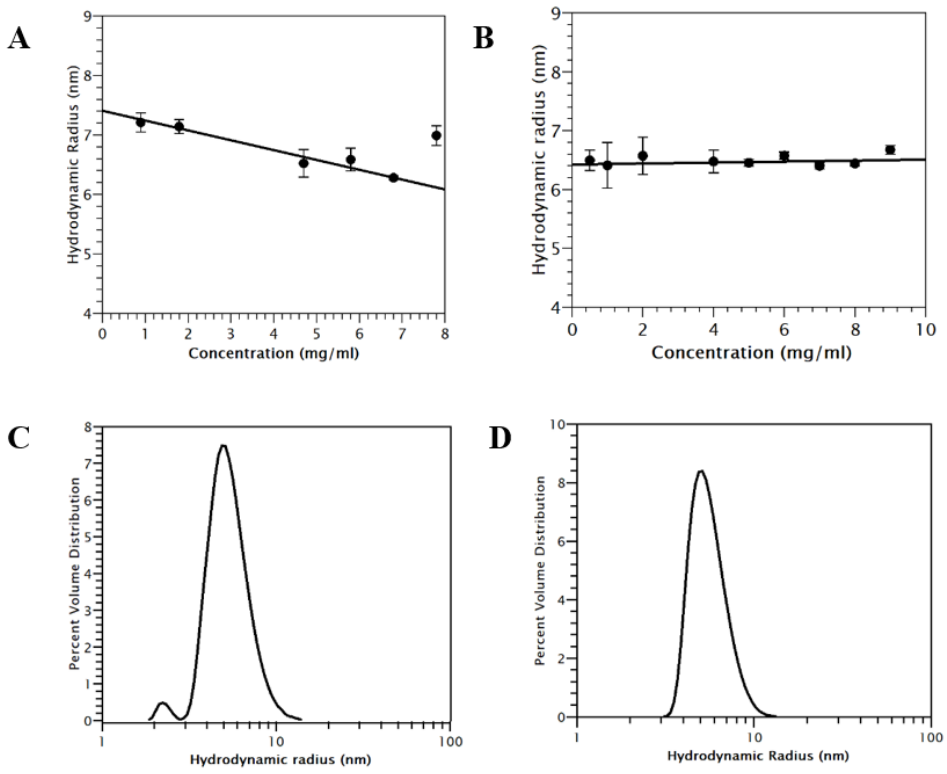

Figure 4.7 DLS Hydrodynamic radius distribution of netrin-1ΔC without and with ammonium sulfate in the SEC purification. *The R_h of both samples were plotted at different protein concentrations with vertical error bars indicating the standard deviation from five measurements. All measurements were done in 50 mM tris pH 7.5, 200 mM NaCl at 20˚C. A) SEC purified sample with 50 mM tris pH 7.5 1 M NaCl (protein A) B) SEC purified sample with 50 mM tris pH 7.5, 500 mM NaCl, 500 mM $(NH_4)_2$ SO_4 (protein B) C) Volume distribution at 7.8 mg/ml concentration for protein A. D) Volume distribution at 9 mg/ml for protein B.*

(homogeneous sample) at the highest concentrations in both netrin-1ΔC preparations with a little degraded product in the untreated netrin-1, <2 nm **(Figure 4.7C).** No change in R_h **(Figure 4.7B)** and the monodisperse nature of the protein with increases in concentration **(Figure 4.7D)** show the stability of the ammonium sulfate-treated netrin-1 protein. The decreasing R_h values with increasing concentration **(Figure 4.7A)** along with the polydispersity show that untreated netrin-1 protein is unstable as concentration is increased except at the highest concentration suggesting aggregation there.

4.2.3 SEC-MALS and Native Mass Spectrometry

The purified netrin-1ΔC was also checked by SEC-MALS to gain information about the apparent molecular mass and state of homogeneity among the peaks. BSA was used as a control at a 9 mg/ml concentration. It gave distinguishable monomer, dimer, and negligible trimer peaks **(Figure 4.8A)**. The netrin-1ΔC samples were 1) SEC purified netrin-1 in the buffer containing ammonium sulfate (AS treated netrin-1ΔC) **(Figure 4.8B)** 2) only dialysis in ammonium sulfate buffer. No further SEC purification **(Figure 4.8C)** 3) Addition of a washing step in the streptactin column purification step **(Figure 4.8D)**, that involved washing the column with ammonium sulfate buffer before eluting the netrin-1ΔC with tag. In each case, the netrin-1ΔC sample was run at a concentration of 7 mg/ml, and the analysis gave information about the relative molecular mass, polydispersity, and oligomerization of the protein. Treatment on the Streptactin column yielded lots of aggregates **(Figure 4.8D)** in comparison to the other samples in which repeated dialysis was performed in buffer with ammonium sulfate **(Figure 4.8C)**. The sample purified with size exclusion chromatography after dialysis in the buffer containing ammonium sulfate **(Figure 4.8B)** yielded negligible aggregates therefore this was the best to use for further studies.

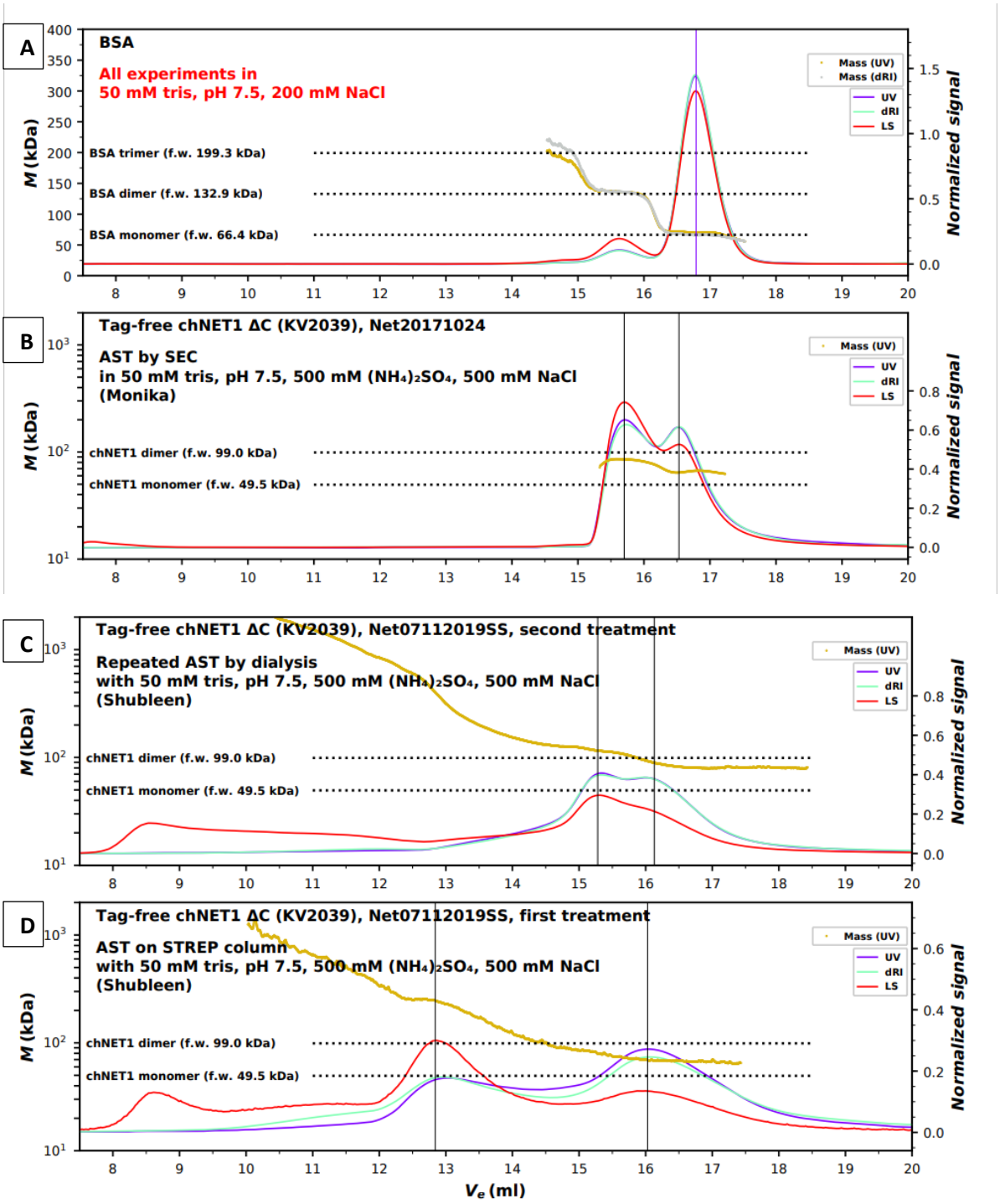

Figure 4.8 SEC-MALS analysis of netrin-1 on Superose 6 10/300GL column A) *BSA as a control,* ***B)*** *SEC purified netrin-1ΔC after dialysis in ammonium sulfate buffer shows monomeric and dimeric netrin-1.* ***C)*** *Ammonium sulfate dialysis with ammonium sulfate buffer shows the presence of aggregates.* ***D)*** *Streptactin column netrin-1 purification with ammonium sulfate buffer washing step also shows lots of aggregates. Mass distributions across the peaks which were traced by UV (A280) show heterogeneity. All the samples were run in 50 mM tris pH 7.5 200 mM NaCl. Dotted calculated formula mass lines for netrin-1 do not go with measured lines because netrin-1 has four glycosylation sites. Dimer netrin-1 measured lines do not go with calculated mass because first peak is a result of monomer dimer equilibrium (correspond to average mass).*

Netrin-1ΔC shows interaction with its dependence receptor at lower salt and pH conditions (data not shown). To check and compare the purified netrin-1ΔC in two different buffer and pH conditions, we again performed SEC-MALS. The netrin-1ΔC showed two peaks at pH 7.5 with 200 mM NaCl: a monomer (55 kDa), and a dimer (90 kDa) **(Figure 4.9A)**. In the case of pH 6.5 with 150 mM NaCl, it showed only one broad peak with relative molecular mass with a distribution of masses ranging from 55 to 80 kDa **(Figure 4.9B)**. A 52.4 kDa molecular weight species is consistent with the amino acid sequences with glycosylation consideration. The netrin-1ΔC has four glycosylation sites, a possible reason for the broader peaks and heterogeneity among the peaks. This heterogeneity was also seen when we performed native mass spectrometry on peptide N-glycosidase F (PNGase) treated netrin-1 with Prof. John S. Klassen, University of Alberta, Department of Chemistry, Edmonton, Canada. It gave different relative molecular masses of netrin-1ΔC from 53-54 kDa / 58- 59 kDa **(Figure 4.10)**. MS did not show any dimer peak.

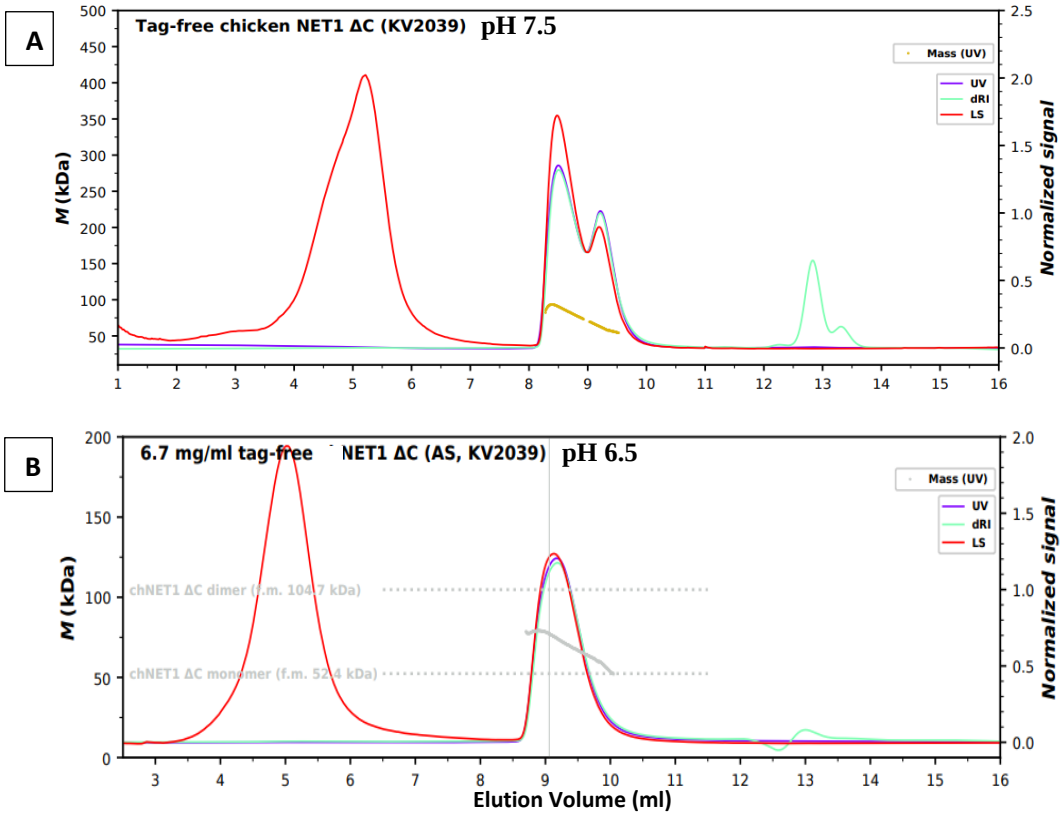

Figure 4.9 SEC-MALS analysis of netrin-1ΔC on Superose 6 10/300GL column *in* ***A****) 50 mM tris pH 7.5 and 200 mM NaCl buffer which shows monomeric and dimeric netrin-1.* ***B****) 50 mM MES pH 6.5 and 150 mM NaCl buffer which shows mostly monomeric netrin-1. Mass distributions across the peaks which were traced by UV (A280) show heterogeneity.*

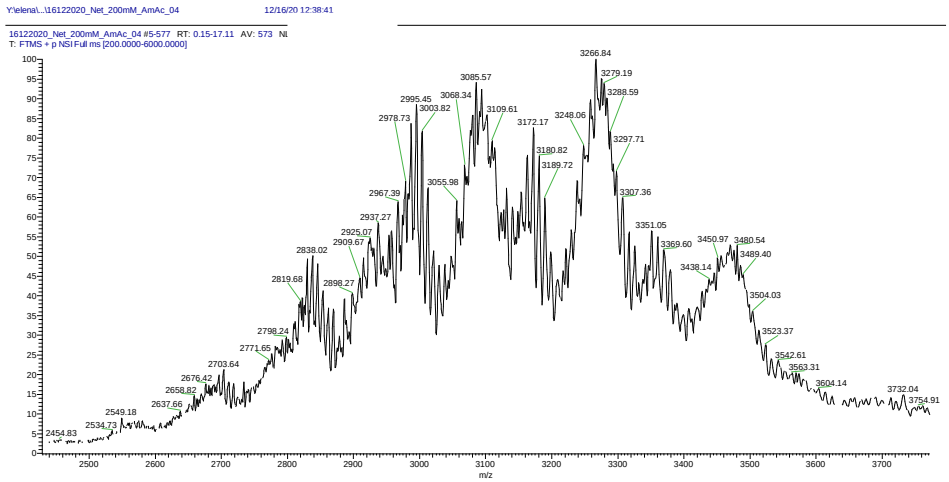

Figure 4.10 Electrospray Ionization-Mass Spectrometry (ESI-MS) profile of netrin-1ΔC without tag*. Peptide N-glycosidase F (PNGase) treated netrin-1ΔC after buffer exchange into 200 mM Ammonium Acetate pH 6.8 shows many proteoforms and glycoforms. Used with permission from Prof. John S. Klassen, University of Alberta, Department of Chemistry, Edmonton, Canada.*

4.2.4 Stability of Netrin-1

To further check the stability of the protein, some experiments were performed using the newly developed techniques Prometheus and Panta. They check the melting temperature (T_m) and the polydispersity with temperature change without fluorescent labeling.

The melting curve obtained for netrin-1ΔC under different buffer conditions 50 mM MES pH 6.5 150 mM NaCl, 50 mM HEPES pH 7.0 200 mM NaCl and 50 mM tris pH 7.5 200 mM NaCl gave Tm of ~ 45.6 ˚C **(Figure 4.11)**. Different buffer conditions and pH values did not show much difference in the T_m values. Since netrin-1 has a Ca^{2+} sensor loop (1), therefore the addition of Ca^{2+} to the buffer was also tested for its effect on stability. $CaCl_2$ was added in the concentrations 2.5 mM and 5 mM. The buffer containing Ca^{2+} had a Tm slightly higher (~51.6 ˚C) than the buffer without Ca^{2+} (~45.6 ˚C) **(Figure 4.11)**. A temperature shift of 6 ˚C shows that netrin-1ΔC is thermally more stable after the addition of Ca^{2+}. Buffer with 2.5 mM $CaCl_2$ was enough to make this change. Further studies to get information about the hydrodynamic radius and its polydispersity, and some other experiments were performed with Panta Nanotemper. Analysis showed that 2.5 mM $CaCl_2$ in the MES buffer lowers the polydispersity index (PDI), which is potentially beneficial for structural studies **(Figure 4.12, Table 4.1)**.

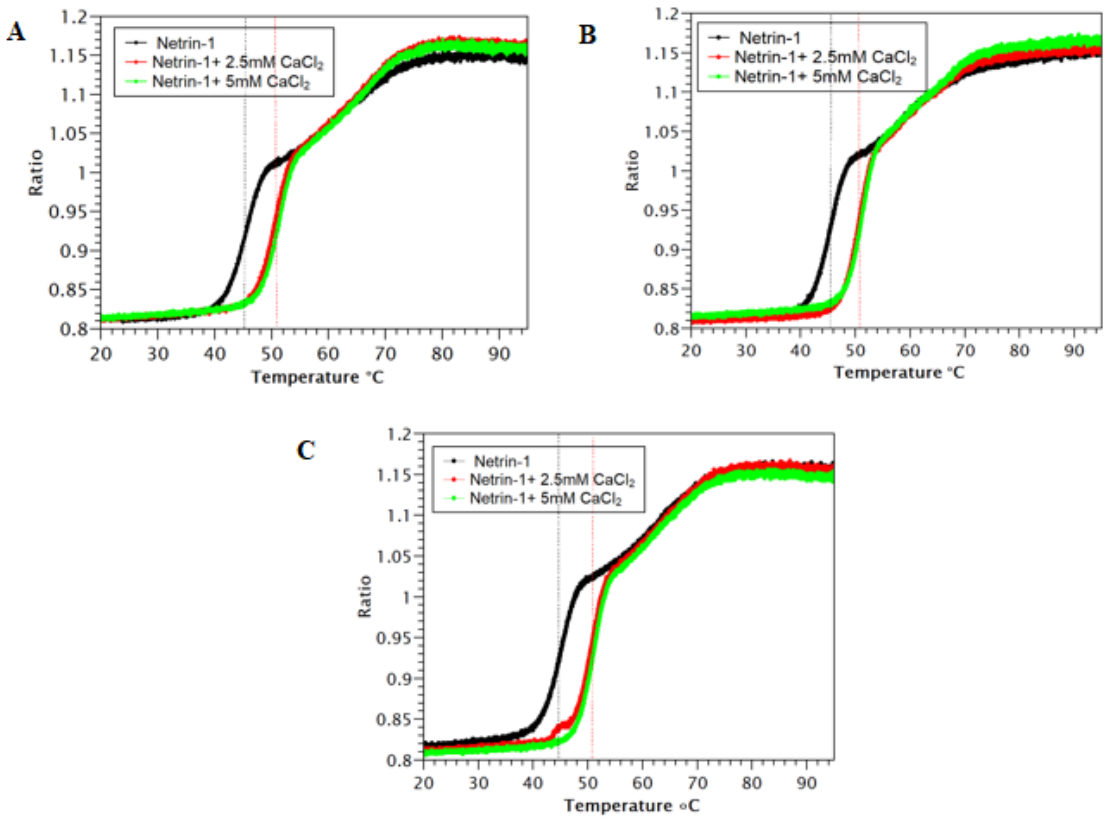

Figure 4.11 Ratio of fluorescence at 350 nm and 330 nm (Em_{350nm}/Em_{330nm}) with respect to temperature in three different buffers in the presence and absence of $CaCl_2$.

All buffers show the same trend. Without $CaCl_2$, the Tm value is approximately the same in every buffer. Addition of $CaCl_2$ changed the Tm value from 45.6 to ~51.6 with the same change in all the buffers. A) 50 mM MES pH 6.5, 150 mM NaCl B) 50 mM HEPES pH 7.0 200 mM NaCl C) 50 mM tris pH 7.5 200 mM NaCl.

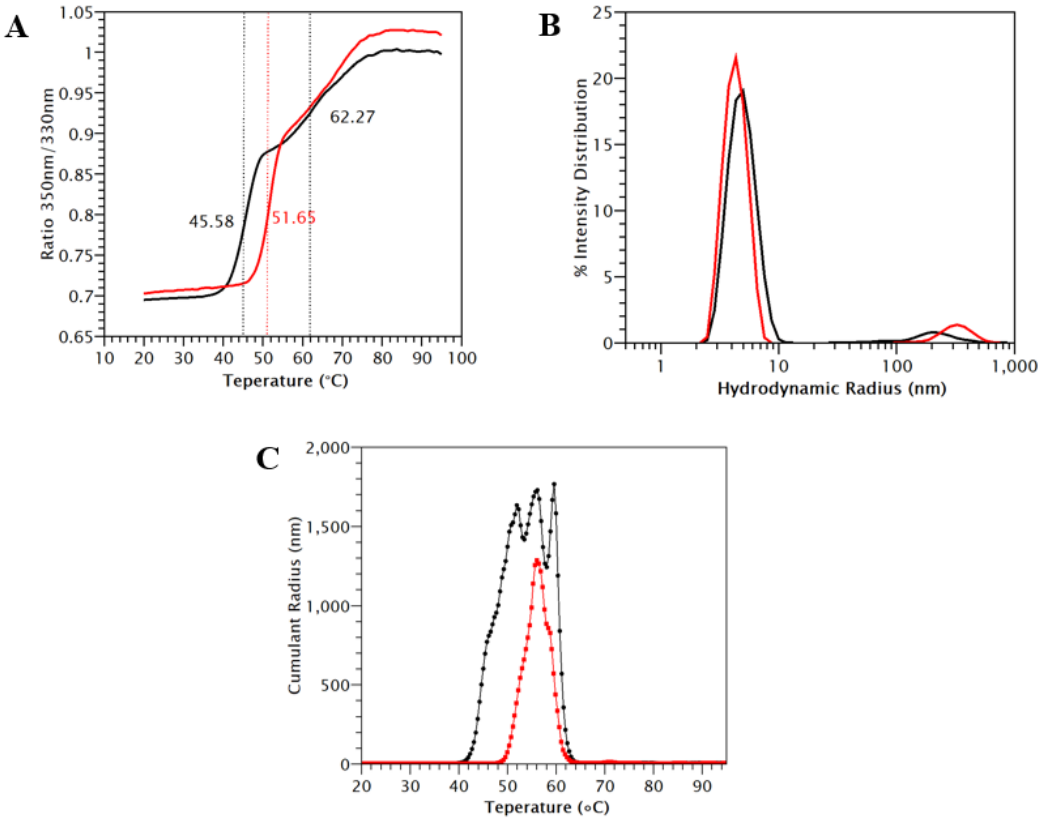

Figure 4.12 Panta analysis of netrin-1ΔC in 50 mM MES pH 6.5 150 mM NaCl (MES Buffer).

A) Ratio of Em_{350nm}/Em_{330nm} with respect to temperature from 20˚C to 95˚C in MES Buffer (black line) and MES buffer with 2.5 mM $CaCl_2$ (red line). B) Percent intensity distribution profile of netrin-1. Some bigger size molecules (aggregates) at 200-300 nm scatter more and can be detected with intensity. C) Cumulant radius of netrin-1 with respect to temperature shows netrin-1 in MES buffer with $CaCl_2$ (red line) is more stable over the range of temperatures as shown in graph A too (Tm value 51.65).

Table 4.1 Properties of 20 µM netrin-1ΔC-T_m with poly dispersity index (more than 0.25 is polydisperse sample).

Buffer	**Tm**	**R_h (nm)**	**PDI**
50 mM MES pH 6.5, 150 mM NaCl	45.5 (Tm1) 62.2 (Tm2)	4.98±0.77	0.40
50 mM MES pH 6.5, 150 mM NaCl, 2.5 mM CaCl2	51.6	4.98±0.35	0.03

4.2.4 Solution Behavior of Netrin-1

In addition to SEC-MALS **(Figure 4.8)**, sedimentation velocity experiments revealed that netrin-1 exists in a monomer-dimer equilibrium in solution with lots of aggregates in the case of netrin-1ΔC that was not treated with ammonium sulfate (data not shown). These higher molecular aggregates made the SV analysis a little complicated. Purification of netrin-1 in buffer containing 500 mM of ammonium sulfate resolved this problem, and two resolved populations were observed. Analysis showed one peak equivalent to monomer (50 ± 13 kDa Molecular mass) with a sedimentation (s) value of 3.5 S and another with a molecular mass of 109 ± 23 kDa and s value of 4.2 S, dimer **(Figure 4.13).** AS treated netrin-1ΔC was dialyzed in 50 mM tris pH 7.5 200 mM NaCl buffer for the sedimentation velocity experiment. Solvent properties of the buffer used for the data analysis are mentioned in Table 4.2.

Table 4.2 Solvent properties of buffer for sedimentation velocity experiments.

Solvent properties of Buffers	**Buffer density (20˚C) g/cm^3**	**Buffer Viscosity (20˚C) (P)**
50 mM tris pH 7.5 200 mM NaCl	1.0079	0.0103173

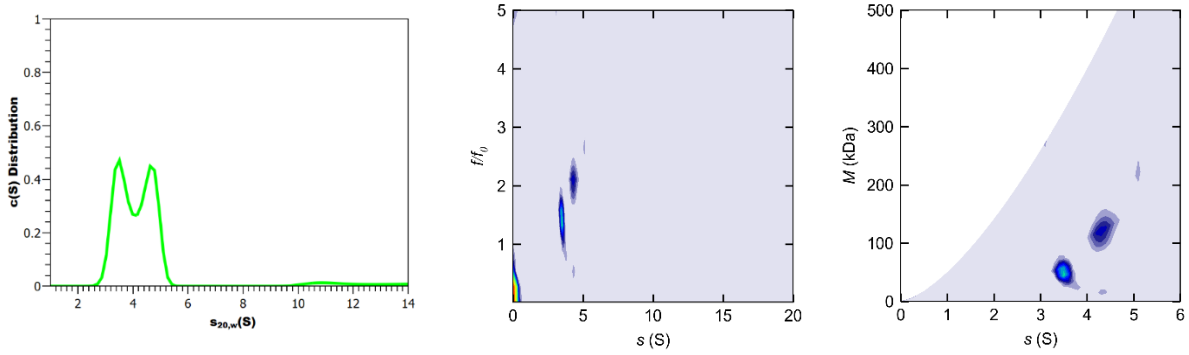

Figure 4.13 Sedimentation coefficient distribution of netrin-1ΔC*. (A) The one-dimensional c(s) distribution. (B) The 2-dimensional distribution converted to frictional ratio, yielding the c (s, f/f$_0$) distribution. (C) The 2-dimensional distribution converted to mass, c (s, M) distribution. Values were converted to standard conditions (pure water at 20˚C. AS treated netrin-1ΔC in 50 mM tris pH 7.5, 200 mM NaCl.*

Finally, single-molecule mass photometry measurements were performed at a physiological concentration <150 nM (12). Low concentration is preferred to obtain a suitable particle density for single-molecule measurements (13). The calibration curve to calculate the molecular weight could be made with any standard proteins to get enough points. I used BSA, Beta Amylase (BA), and ADH in two different buffers and these proteins also form oligomers such as BSA forms monomer and dimer. These standard proteins gave a range of molecular mass from 60 to 230 kDa. To get reliable data, the protein of interest should be run at the same conditions as the standard proteins such as treatment of slides and buffer. PEG silane treated slides with flow channels were used for the sample application. Raw MP data was processed in Refeyn DiscoverMP software. The analysis showed a broad peak with a mean mass of 63±11 kDa in 50 mM MES pH 6.5, 150 mM NaCl and 69±9 kDa in 50 mM tris pH 7.5, 200 mM NaCl **(Figure 4.14).** Since netrin-1 has four glycosylation sites and expression could be heterogeneous, peak broadening is expected and likely leads to more error in the molecular weight calculation. Another minor peak or tailing of the first peak presumably corresponds to the dimer with MW ~109 kDa (not well resolved).

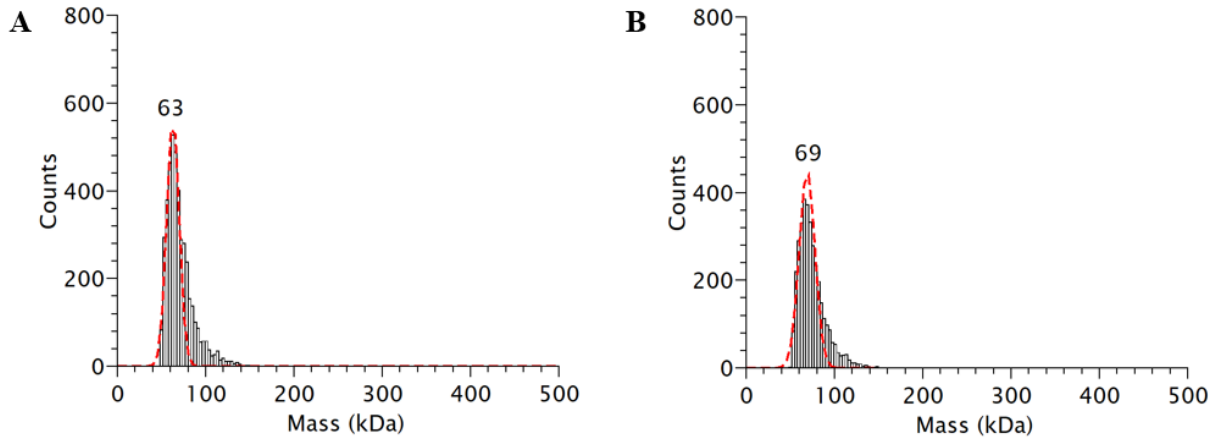

Figure 4.14 Mass Photometry of netrin-1ΔC in two different buffers.

A) 30 nM of netrin-1 in 50 mM MES pH 6.5, 150 mM NaCl shows a peak at 63±11 kDa B) 15 nM netrin-1 in 50 mM tris pH 7.5, 200 mM NaCl shows a peak at 69±9 kDa. Red dashed lines represent the gaussian fit to a histogram.

Other techniques like AUC, SEC-MALS also showed slight variation in the mass from different batches of expressed proteins.

SEC-SAXS experiments helped provide information about the shape and size of netrin-1 in solution. AS treated netrin-1ΔC was dialyzed in two different buffers followed by synchrotron data collection. HPLC-SAXS was necessary to obtain accurate solution information as scattering from X-rays occurs as soon as the sample elutes from the column. SAXS data were collected at the Diamond Light Source Limited (Chilton, Didcot, Oxfordshire) for netrin-1ΔC at ~7-9 mg/ml concentration. The elution profile of netrin-1ΔC in MES buffer at pH 6.5 showed a single peak, and in tris buffer at pH 7.5 showed a peak with a long tail and that eluted at approximately frame number 290 corresponding to two species (monomer and dimer) **(Figure 4.15)**. The initial analysis involves sample peak integration, buffer subtraction, and merging to generate SAXS plots. Netrin-1ΔC exists as a monomer and dimer in solution, according to the AUC data above. The P(r) distribution function, which measures the paired set of distances between all the electrons in the macromolecular structure, differed in these buffers.

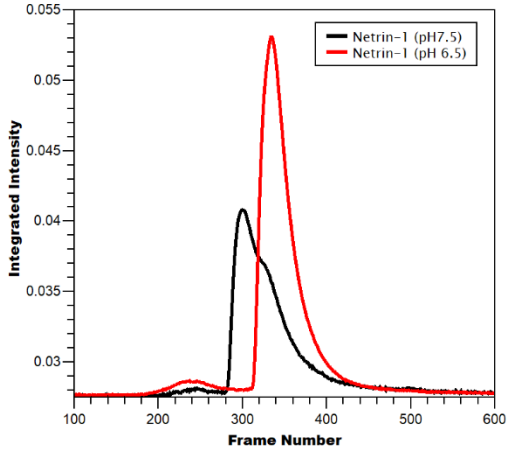

Figure 4.15 SEC-SAXS X-ray scattering profile of netrin-1ΔC while eluting from the SEC column. *Netrin-1ΔC elution profile shows the presence of a single species corresponding to a monomer in 50 mM MES pH 6.5 150 mM NaCl* ***(Red)*** *and two species corresponding to monomer and dimer in 50 mM tris pH 7.5 200 mM NaCl* ***(Black).***

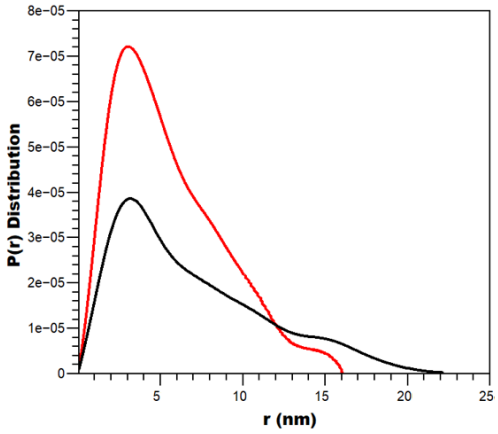

Figure 4.16 P(r) distributions of netrin-1ΔC *in 50 mM MES pH 6.5 150 mM NaCl* ***(Red)*** *and in 50 mM tris pH 7.5 200 mM NaCl* ***(Black).***

The P(r) distributions of netrin-1ΔC in both buffers depict a single peak with a longer tail, characteristic of an elongated molecule **(Figure 4.16)**. The D_{max} values were ~2.18 nm and ~1.79 nm in pH 7.5 and 6.5, respectively **(Table 4.3)**.

Ab initio electron density maps were generated using DENSS and DAMMIN from ten averaged adjacent frames from the centers of the elution peaks. DAMMIN analysis generated twenty models for each peak. 30/40 models for the first peak and 20 models for the second elution peak were generated to obtain low-resolution structures using DENSS. Rigid body fitting of the netrin-1ΔC (4OVE) crystal structure into the second peak and a non-crystallographic dimer to the first peak confirmed our monomer and dimer, respectively.

Together, the low-resolution models from DENSS **(Figure 4.17)**, suggest that netrin-1ΔC is an elongated molecule in solution and exists as monomer and dimer in the buffer at pH 7.5, 200 mM NaCl and is mainly monomeric in the buffer at pH 6.5, 150 mM NaCl. This was also shown

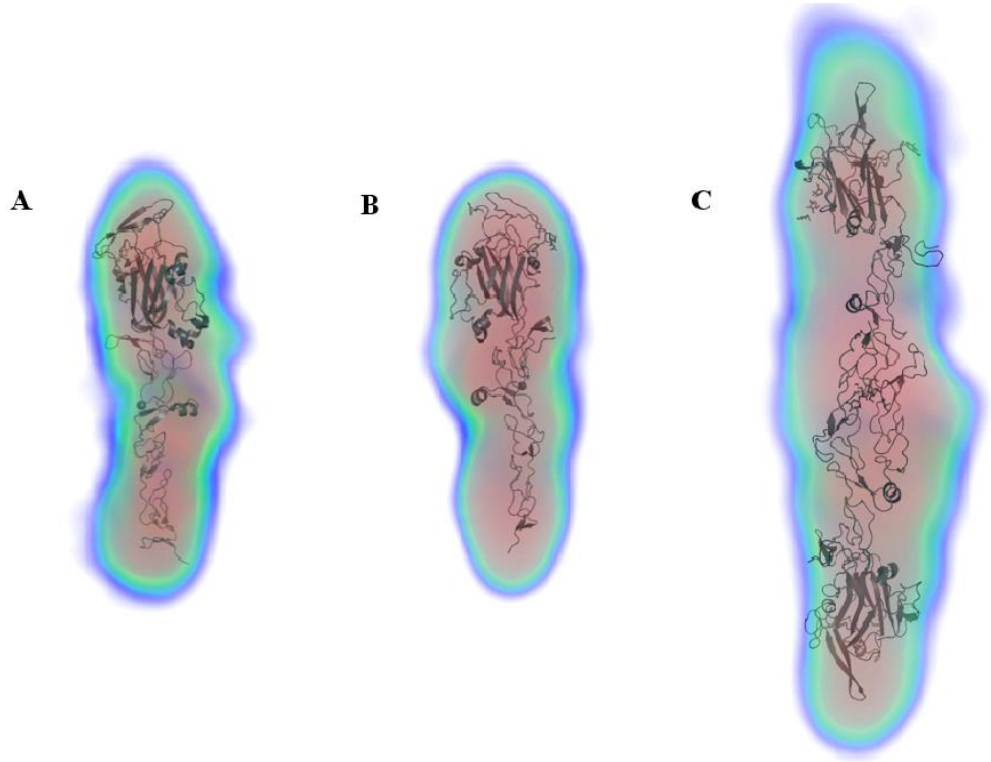

Figure 4.17 Low-resolution models of netrin-1ΔC (DENSS ENVELOP). *A) Low resolution DENSS model of netrin-1ΔC in MES buffer at pH 6.5 superimposed with a high-resolution crystal structure (PDB code: 4OVE). B) low-resolution monomer DENSS model of netrin-1ΔC in tris buffer at pH 7.5 superimposed with a high-resolution crystal structure (PDB code: 4OVE) and C) low-resolution DENSS dimer model in tris buffer at pH 7.5 superimposed with non-crystallographic dimer of 4OVE.*

by SEC-MALS **(Figure 4.9)**. The hydrodynamic properties of netrin-1 were calculated for each model using the program HYDROPRO (14) **(Table 4.3).**

Table 4.3 Summary of Hydrodynamic properties for netrin-1ΔC based on SEC-SAXS.

	50 mM tris pH 7.5 200 mM NaCl		50 mM MES pH 6.5 150 mM NaCl
Parameters	Monomer	Dimer	
Concentration (mg/ml)	9		6.7
Longest Dimension Dmax (nm)	1.59 (datclass) 1.79 (DAMMIN)	1.74 (datclass) 2.18 (DAMMIN)	1.50 (datclass) 1.79 (DENSS)
Radius of Gyration Rg (nm)	4.51 ±0.5 (AUTORG) 4.91 (DAMMIN) 4.44 (DENSS)	5.15±0.31(AUTORG) 5.82 (DAMMIN) 52.5 (DENSS)	42.6 ±3.9 (AUTORG) 4.22 (DENSS)
Support Volume (nm^3)	179.594 (DAMMIN)	268.083 (DAMMIN)	181.1 (DENSS)
Formula Mass (kDa)	52.4	104.7	52.4
Chi square of fit	0.792	0.631	0.418
Resolution of averaged map (Å)	38.2 (20 maps)	33.8 (30 maps)	40 (39 maps)

4.2.9 Crystallization of Netrin-1

The SEC purified protein was concentrated to 9 mg/ml for the crystallization experiments. Crystallization trials were performed with different commercially available screens from Jenna Biosciences and Hampton research that cover different combinations (pH, precipitates, salts, or additives). Only two conditions gave us a single crystal, and only one diffracted well. Since a netrin-1ΔC structure has already been solved by our group (1), therefore, after checking the space group and phasing it using phaser, a crystal was used for soaking experiments with peptides and small length oligosaccharides for further studies. Soaking of netrin-1ΔC crystals with 10 mM sucrose octa sulfate (SOS) or HS-decasaccharide dp10 for a week gave crystals with a physical resolution of 3.21 Å. Trials to optimize the conditions were performed with 20% w/v polyethylene glycol (PEG) 8,000 and 100 mM CHES pH 9.5 but did not yield good crystals. Only one well came back with a crystal and it was used for other soaking experiments.

4.3 NETRIN-1 IN COMPLEX WITH HEPARAN SULFATE PROTEOGLYCANS

Heparan sulfate proteoglycans are glycoproteins, with covalently attached highly acidic extended GAG chains that act as an attachment factor for many protein-protein interactions (10). Glypican is a well-known HSPG that modulates netrin-1 signaling (15). Netrin-1 shows attraction and repulsion of growth cone depending upon which receptor is present on the cell surface, netrin-1 extracellular concentration, or other molecules on the extracellular surface like HSPG. Very little is known about netrin-1 interactions with HSPG and its involvement in netrin-1 signaling. This section will present the primary amino acid residues involved in netrin-1ΔC GAG binding (crystal structure), the interaction of netrin-1ΔC with its receptors in the presence of HSPG (mainly short-chain HS oligosaccharides), and how the interaction between netrin-1 with HSPG changes its solution behavior.

4.3.1 Netrin-1 binding with Heparan sulfate proteoglycans

The binding of short-length heparin oligosaccharides was observed as a change in a thermophoretic property of labeled netrin-1 upon complex formation. MST experiments were performed to check the binding of these medium-chain oligosaccharides. 10 nM Alexa647 fluorescently labeled netrin-1ΔC was used. The highest concentration for oligosaccharide (ligand) used in the experiment was measured by a binding check tool in the NanoTemper Affinity software that gives information about the concentration where we would see enough difference between bound and unbound proteins. Once we have this information, serial dilution manually can be performed according to the experiment requirement. For netrin-1ΔC oligosaccharide interaction studies, netrin-1ΔC concentration was kept constant, and serial dilution of the ligand was done starting from the highest concentration of 400 µM dodecasaccharide (dp12) and 600 µM tetradecasaccharide (dp14). The dissociation constant (K_d) was calculated from three individual experiments using the Nano temper analysis software K_d fit algorithm and plotted with Qtiplot. The calculated K_d was 2.55±1.04 µM for netrin-1ΔC+dp12 and 3.39±0.42 µM for netrin-1ΔC+dp14 **(Figure 4.18)**. The change in normalized fluorescence amplitude depends on the binding site, conformation, size, and hydration shell upon binding (16,17). Here, a change in conformation/size upon oligosaccharide binding leads to the change in thermophoretic behavior.

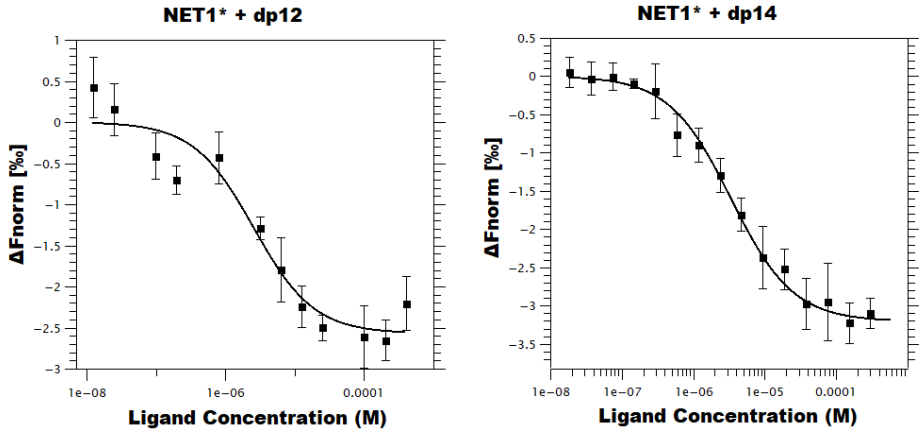

Figure 4.18 Protein-Ligand Interaction study using Microscale Thermophoresis

The interaction study of labelled netrin-1ΔC(NET1) with dp12 and dp14. The netrin-1ΔC concentration was kept constant at 10 nM and the ligand concentrations were varied (dp12 - 400 to 0.0976 µM and dp14 - 600 to 0.0183 µM). The difference in normalized fluorescence is plotted for analysis of thermophoresis. Error bars represent standard deviations of three individual measurements. K_d calculated = 2.55±1.04 µM (netrin-1ΔC+dp12) and 3.39±0.42 µM (netrin-1ΔC+dp14).*

4.3.2 Heparan sulfate proteoglycans do not act like a coreceptor for netrin-1 receptor binding

To determine the binding of netrin-1 with glypican and any change in the interaction between netrin-1ΔC and its receptors when glypican is bound, ELISA binding studies were performed. For this experiment, 96-well plates were coated with netrin-1ΔC and netrin-1ΔC bound to its dependence receptors. Strep-tagged glypican-3 in different concentrations were incubated in the liquid phase. Binding was detected using strep-HRP antibody. The results show the binding of netrin-1ΔC with glypican-3 (absorbance at 450 nm), and the receptors do not affect the binding of glypican (500 nM) **(Figure 4.19)**. In addition to glypicans, netrin-1 also showed binding to smocs, testicans and syndecans (data not shown). Glypican-3 binding to receptors was also measured and did not show any binding (data not shown). This suggests that the binding sites for GAG chains of proteoglycan and receptor are different and non-overlapping on netrin-1.

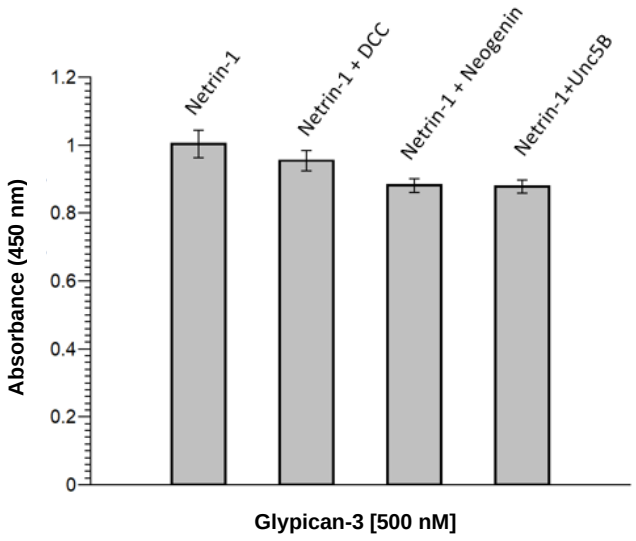

Figure 4.19 *ELISA Binding studies show protein-proteoglycan interactions of immobilized netrin-1 and netrin-1+receptor to glypican-3. Error bars indicate the standard deviation of n=3 technical repeats.*

The binding of netrin-1ΔC with its receptors was also measured in the absence and presence of dp12 short length and dp20 medium length HS oligosaccharides. 96-well plates were coated with his-tagged netrin-1ΔC followed by overnight incubation at 4˚C. After blocking the non-specific binding sites with BSA in assay buffer, a competition assay was performed for HS-dp12 and dp20. After incubation with 1 µM HS for 1 hour, the plate was washed for any non-specific binding. Strep-tagged netrin-1 receptors were added in a serial dilution and incubated for 90 minutes before washing and fixing with 1% glutaraldehyde. The bound receptor was detected with a strep-HRP conjugate. Results suggest that binding epitopes on netrin-1 for heparan sulfate oligosaccharides or GAG chains and receptors are distinct **(Figure 4.20)**.

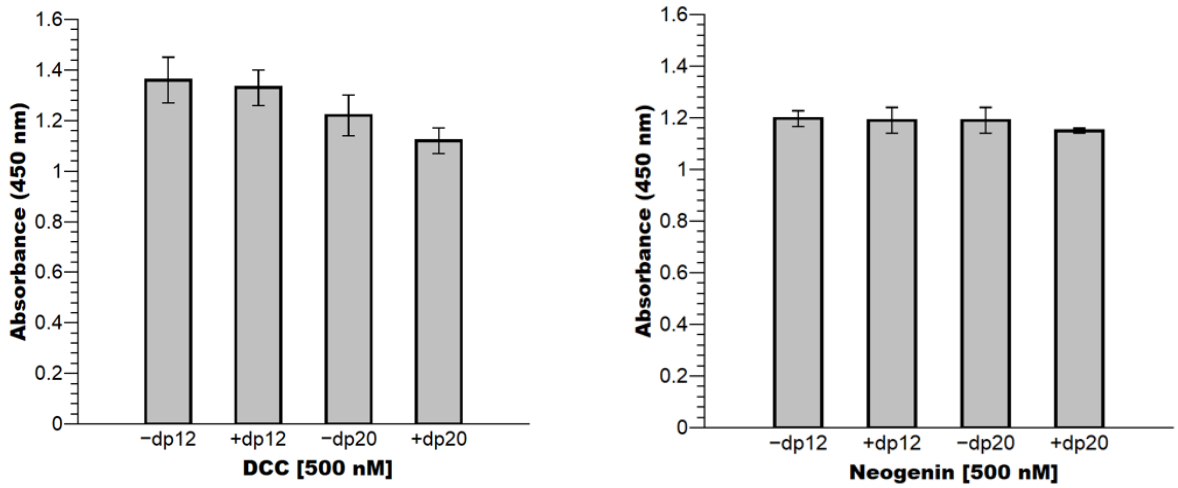

Figure 4.20 *ELISA binding studies show protein-protein interaction of immobilized netrin-1ΔC to netrin-1ΔC receptor in the absence and presence of HS oligosaccharides (short chain dp12 and medium length dp20) Error bars indicate the standard deviation of n=3 technical repeats. Negative signs show the absence of oligosaccharide and positive signs show the presence of oligosaccharide.*

To further study the effect of different heparan oligosaccharides on the size of the netrin-1ΔC, DLS experiments were performed. Different length oligosaccharides were added in 8 times excess to probe for any change in the size of netrin-1 and incubated for 1 hour. There is an apparent change in hydrodynamic radius after the addition of oligosaccharides as shown in **Figure 4.21** below. Intensity distribution analysis of netrin-1 with heparan oligosaccharides shows the presence of some higher molecular weight species or aggregates >100 nm as bigger molecules scatter more strongly and can be detected by intensity **(Figure 4.21A)**. Volume distribution analysis shows a clear change in R_h value after adding oligosaccharides **(Figure 4.21B)**. Comparison of dp8 and dp20 oligosaccharide peaks shows that the peak is less broad in dp20 (black line) than in dp8 (blue line) **(Figure 4.21 A and B)**, showing greater homogeneity of the sample in dp20.

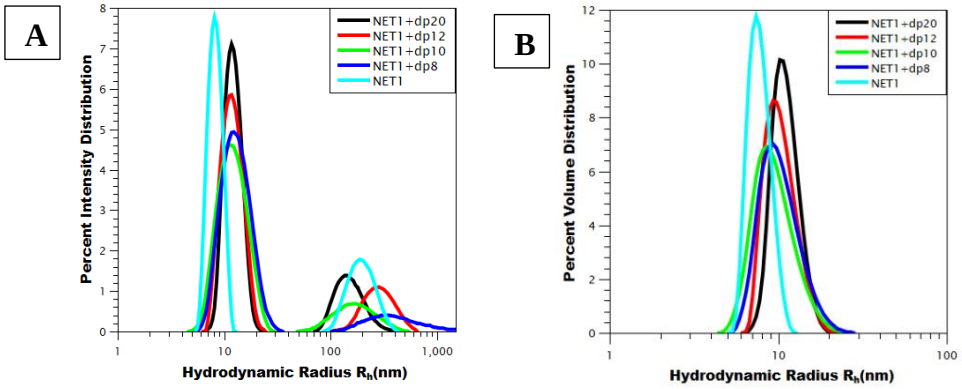

Figure 4.21 Netrin-1 and HS oligosaccharide interaction studies with DLS. *A) Percent Intensity distribution profile of netrin-1 with heparin oligosaccharides shows some bigger molecules or aggregates above 100 nm but they are present in every sample. Since larger molecules scatter more strongly, even a trace amount can be detected with intensity distribution analysis B) R_h distribution by volume derived from intensity profile shows only a single peak.*

4.3.3 Molecular details of the Netrin-1 and SOS interaction

Further, crystallographic studies were performed with the smallest unit of heparin, SOS, sucrose octasulfate that mimics HS, to gain molecular insight into the structure of the netrin-1 with GAG chain of proteoglycans bound. A netrin-1ΔC crystal was soaked with SOS for one week. The crystal structure revealed an antiparallel netrin-1 dimer in the asymmetric unit with one SOS per monomer **(Figure 4.22)**. Details of the data collection and refinement statistics can be found in **(Table 4.4)**. The antiparallel arrangement spans a maximum dimension of ~200 Å and this arrangement is the same as already published for netrin-1 structures pdb 4OVE and 4PLM (1,3). There is a clear electron density for glycan additions at four asparagine-glycosylation sites, Asn97, Asn118, Asn133, and Asn419. The crystal structure of netrin-1 by Xu *et. al*, 2014 and Meier *et. al*, 2016, both did not find any electron density for glycans at Asn419. The calcium binding site is in the globular LN domain at the sugar binding edge of the β sandwich encompassing Asn97 and Asn118 and is also reported in a previously reported crystal structure of netrin-1 (1). The V-2 subdomain is highly electropositive and characterized by a cluster of arginine and lysine sidechains (1). The detected SOS binding epitope is also located on the V-2 subdomain. The CW motif RRXR and the R374-H375, H399-R400 tandem form the loop ab and loop cd, respectively, that are involved in GAG binding, **(Figure 4.23)** and it can form an extended linear structure over loop ab

and cd. The primary interacting residues on both sites are basic and interact with negatively charged sulfate groups of the SOS. In addition to this, there are many contributions by hydrogen bonding and van der Waal's contacts *via* Y325, N355, H375, and H399.

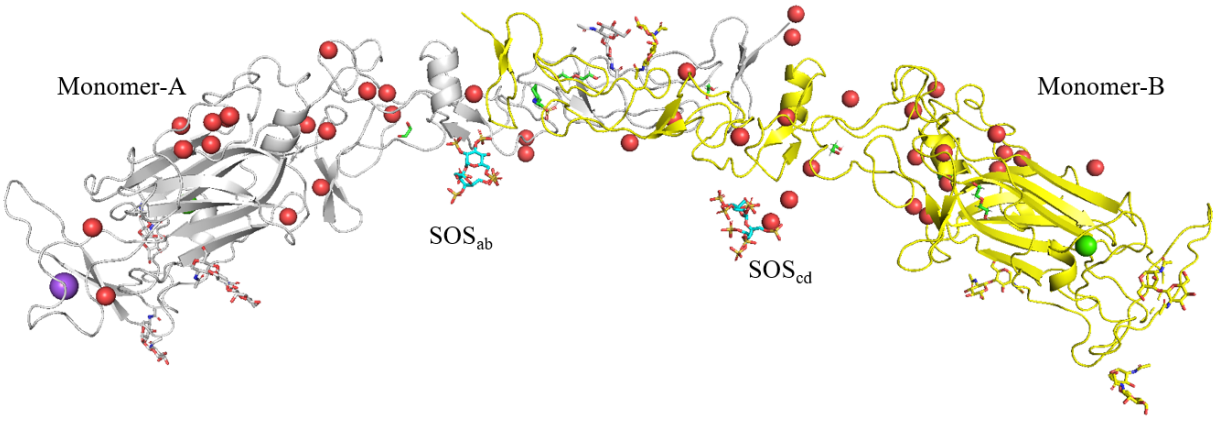

Figure 4.22 Crystal structure of netrin-1ΔC with SOS an HS mimic. *The antiparallel netrin-1ΔC dimer spans a maximum dimension of ~200 Å. Cartoon of monomer A (silver) and monomer B (yellow) with one sucrose octasulfate (SOS) per monomer (presented as sticks and balls, SOS$_{ab}$ and SOS $_{cd}$). Calcium ions are shown as green spheres, the sodium ion is magenta, and water molecules as red balls.*

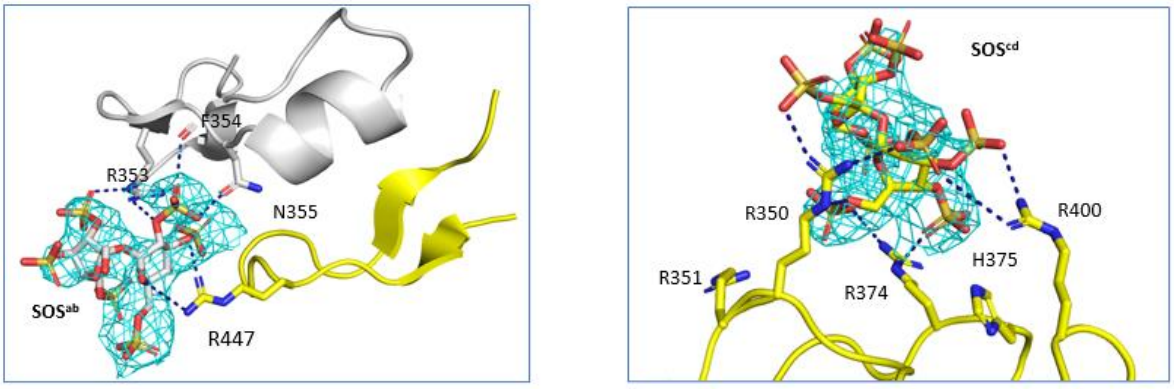

Figure 4.23 SOS binding motifs from X-ray crystal structure. *SOS^{ab} and SOS^{cd} both show binding via V-2 domain. A) SOS^{ab} mainly involves CW motif (RRXR)-loop ab and B) SOS^{cd} involves R374-H375 and H399-R400 tandems - loopcd.*

Table 4.4 Data collection and refinement statistics

	Netrin-1 with SOS pdb:7LRF
Data collection	
Space group	P 21 21 21
Cell dimensions	
a, b, c (Å)	75.105, 80.152, 241.702
α β γ (°)	90, 90, 90
Resolution (Å)	47.08-3.21 (3.325-3.21) *
R_{sym} or R_{merge}	0.188 (1.061)
I /σI	9.8 (2.0)
Completeness (%)	99.47 (98.67)
Redundancy	8.3 (8.4)
$CC_{1/2}$	0.994 (0.634)
Refinement	
No. reflections	24519 (2375)
R_{value} / R_{free}	0.2273/0.2799
No. atoms	6727
Protein	6301
Ligand/ion	422
B-factors	
Protein	88.84
Ligand/ion	154.22
R.m.s. deviations	
Bond lengths (Å)	0.011
Bond angles (°)	1.10
Ramachandran Statistics	
Favoured (%)	85.42
Disallowed (%)	1.94

*Values in parentheses are for highest-resolution shell.

4.3.4 Mutation of the loop ab and the loop cd

Binding assays were performed using different netrin-1 mutants to validate the structural observations. Sequence alignment of netrin-1 from mouse, chicken, and human showed that both loop ab and cd are highly conserved **(Figure 4.24A).** Amino acid residues involved in SOS binding from loop ab and cd **(Figure 4.24B)** were mutated for the binding assay. A series of netrin-1 modifications were produced by changing the amino acid residues with alanine that contribute to the binding motifs **(Figure 4.24)** and that include 1) Double RR mutant (R350A and R351A), 2) loop ab (RRXRFN) mutant (R350A, R351A, R353A, and N355A), 3) Loop cd mutant (RH-HR) (R374A, H375A, H399A, R400A, and K401A), and 4) combined loop ab and cd mutant.

A

NET1_MOUSE
CNCNLHARRCRFNMELYKLSGRKSGGVCLNCRHNTAGRHCHYCKEGFYRDMGKPITHRKACKA
NET1_HUMAN
CNCNLHARRCRFNMELYKLSGRKSGGVCLNCRHNTAGRHCHYCKEGYYRDMGKPITHRKACKA
NET1_CHICK
CNCNLHARRCRFNMELYKLSGRKSGGVCLNCRHNTAGRHCHYCKEGFYRDLSKPISHRKACKA

B

Netrin-1_Chicken

```
          **  *                 * *       * *                  * * *
343CNCNLHARRCRFNMELYKLSGRKSGGVCLNCRHNTAGRHCHYCKEGFYRDLSKPISHRKACKE405
```

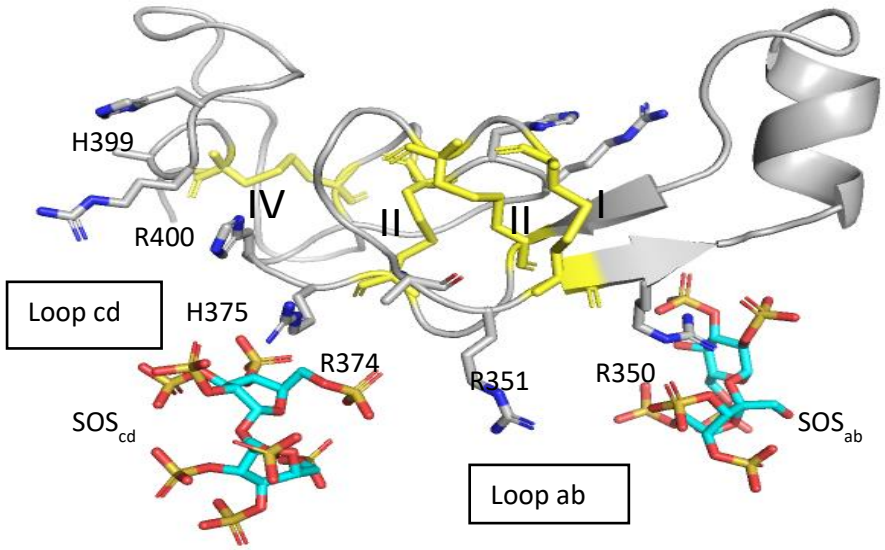

Figure 4.24 *A) Sequence alignment of V-2 subdomain of mouse netrin-1 (NP_008744), human netrin-1 (NP_004813) and chicken netrin-1 (NP_990750). Sequence of V-2 subdomain (amino acid 343-405) of different netrin-1. B) The eight cysteine residues, yellow (I-IV) (netrin-1 chicken) show disulfide linkages to create the four loops a-d. Both SOS are shown on the monomer-A.*

Strep-tag netrin-1ΔC and mutants were coated onto 96-well plates. After overnight incubation at 4 ˚C, washing was done, followed by blocking to remove any non-specific binding. Biotinylated HS was then added in serial dilution starting from 1 pM concentration. Detection was performed with a biotin-HRP antibody. The binding assay showed that wild-type netrin-1ΔC was bound to porcine HS firmly, whereas the double RR mutant, and the loop ab and loop cd mutants showed reduced binding **(Figure 4.25)**. The combined loop abcd mutation showed no binding **(Figure 4.25)**. The observation of no binding with the combined mutants validates the observed netrin-1 GAG interface.

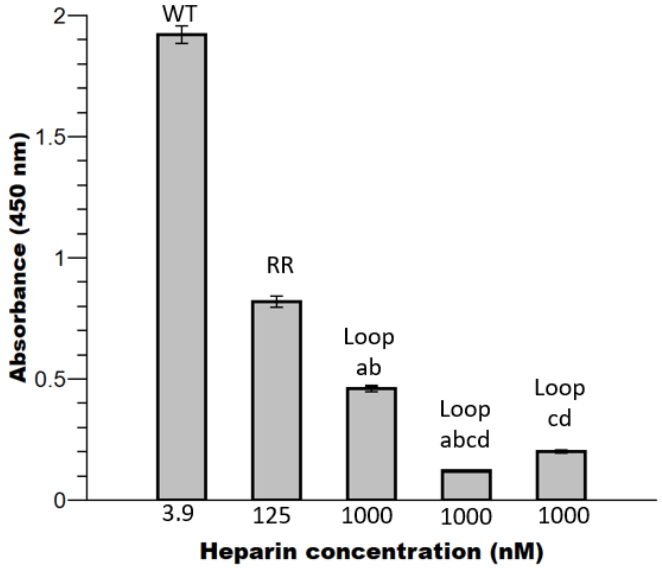

Figure 4.25 ELISA-based GAG binding study of netrin-1 and netrin-1 mutants. *Wild type (WT), double RR Mutant (RR), loop ab-RRXR (loop ab), loop cd-RH-HR (loop cd) and loop abcd mutant. Mutation of only RR from RRXR, loops ab and cd show decreased binding to heparin, and combined loop abcd mutant shows reduced binding.*

4.3.5 Effect of HS oligosaccharide on the oligomerization of Netrin-1

To study the effect of GAG on oligomerization of netrin-1 different experiments were performed on SEC-MALS, AUC, SEC-SAXS, and mass photometry.

SEC-MALS showed the first sign of oligomerization after the addition of heparan-oligosaccharides. Incubation of netrin-1 (~48 µM) with dp8, dp10, dp12, and dp20 HS oligosaccharides (10 times netrin-1 concentration) for an hour led to the formation of different species larger than monomer and dimer **(Figure 4.26)**. The addition of dp20 resulted in the disappearance of the monomer-dimer peak and the appearance of a homogeneous higher-order oligomer with a calculated molecular mass of 358.3 ± 0.5 kDa **(Figure 4.27)**.

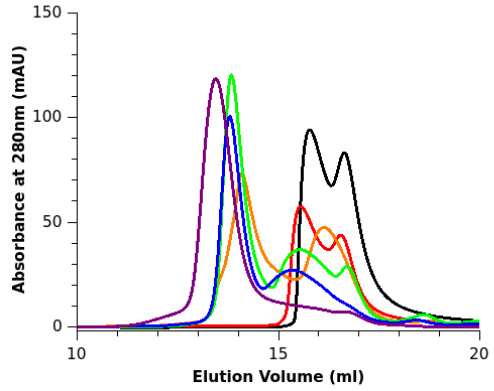

Figure 4.26 Effect of adding different sizes of heparan oligosaccharide (dp6-dp20) to netrin-1ΔC using SEC-MALS.

In the absence of heparin, netrin-1ΔC (black line) runs as a mixture of monomer and dimer on a Superose 6 10/300GL column in 50 mM tris pH 7.5, 200 mM NaCl buffer. Incubation of netrin-1ΔC with oligosaccharide dp 6 (red), dp8 (orange), dp10 (green), dp12 (blue) and dp20 (purple) for an hour shows the gradual interconversion between the monomer/dimer mixture to a single higher order oligomeric species in the presence of heparin (dp20).

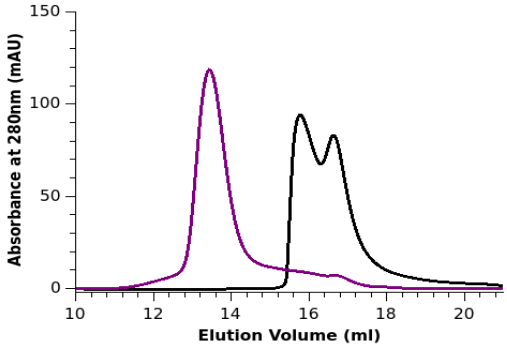

Figure 4.27 Size exclusion chromatography coupled with MALS-netrin-1ΔC in the presence and absence of oligosaccharide dp20.

In the absence of dp20 oligosaccharides, netrin-1ΔC (black line) runs as a mixture of monomer and dimer on a Superose 6 10/300GL column. In the presence of a defined heparin species (dp20), netrin-1ΔC (purple line) runs as a single higher order oligomer on the Superose 6 column. Experiment was performed in 50 mM tris pH 7.5, 200 mM NaCl buffer. (These are the same results as in the figure 4.26 above).

To further prove the oligomerization, AUC sedimentation velocity experiments were performed. HS oligosaccharide dp8 and protein were dialyzed separately in a Float-A-Lyzer G2 dialysis device overnight with MWCO 0.5 kDa membrane in 50 mM tris pH 7.5, 200 mM NaCl buffer. After buffer and components reached equilibrium, both were mixed to various ratios with netrin-1ΔC at a concentration of 13 µM. After a temperature equilibration, the sedimenting samples were measured at rotor speeds of first 30,000 rpm and in the second experiment at 42,000 rpm for 24 h. Both absorbance and interference data were collected. As discussed in section 4.2.4, netrin-1ΔC exists in a monomer-dimer equilibrium in solution **(Figure 4.28A),** and the addition of an equimolar amount of dp8 HS oligosaccharide resulted in an increase in the sedimentation coefficient from 7.9 S to 10.2 S **(Figure 4.28 B).** Resolved species have associated molecular masses of 163 ± 26 kDa (Trimers), 273 ± 48 kDa (Pentamers), and larger species. Solvent properties used for data analysis are mentioned in **Table 4.5**.

Table 4.5 Solvent properties of Netrin-1ΔC, HS-Octasaccharide dp8 and buffer

Netrin-1ΔC at 20 °C (Sednterp)		
Property	**Value**	
Partial specific volume ν	0.70998 cm³/g	
Molecular mass*	52367.5 Da	
Hydration	0.390089 g/g	
Octasaccharide dp8 (Iduron # HO08) at 20 °C		
Property	**Value**	**Source**
Partial specific volume ν	0.467 cm³/g	Pavlov *et al*., 2003
Mean molecular mass	~2400 Da	Iduron

*Chicken netrin-1ΔC without tag has four common core pentasaccharides (6x β-D-N-Acetyl glucosamine (GlcNAc), 9x β-D-Mannose (Man), 3x glycosidic linkage) based on the netrin-1ΔC sequence. By assuming that the sugars are present, molecular mass was calculated according to the core sugars (14).

50 mM tris, pH 7.5, 200 mM NaCl at 20 °C (Sednterp)	
Density ρ	1.007900 g/cm³
Viscosity η	0.0103573 P

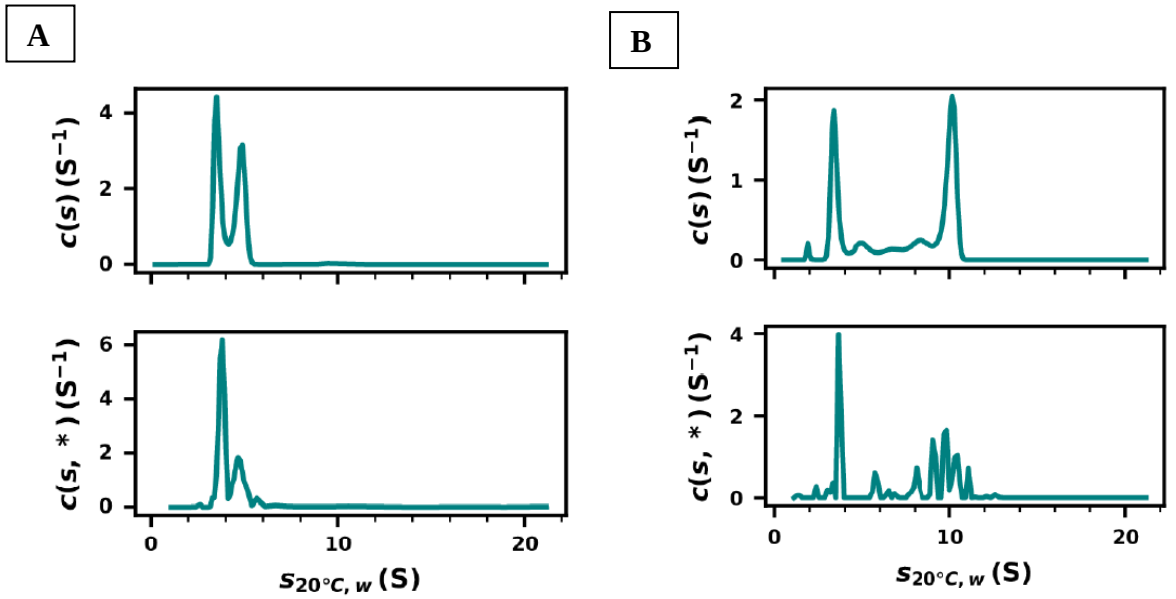

Figure 4.28 Sedimentation velocity experiments with netrin-1ΔC in the absence (A) and presence (B) of octasaccharide dp8 in 50 mM tris pH 7.5, 200 mM NaCl. *In the 1-dimensional sedimentation coefficient c(s) distribution A) the plots show two peaks whereas in B) the plots show a series of different populations in the presence of short chain oligosaccharide. c(s,*) represents apparent sedimentation coefficient distribution (sedimentation profile of non-diffusing species).*

MASS photometry measurements were performed to validate the findings at physiological concentrations <150 nM that was measured by axonal outgrowth (12,18). The experiment was performed with filtered 50 mM tris pH 7.5, 200 mM NaCl buffer. Since netrin-1ΔC carries lots of charged residues on its surface leading to more binding events, APTES functionalized glass slides were used for the experiment. Standard proteins for calibration were also studied on the same functionalized glass slides. Netrin-1ΔC was incubated with an equimolar concentration of HS-oligosaccharide overnight in the assay buffer. Commercially available deep culture well gaskets were used, and the sample was diluted directly in the well, containing buffer just before the measurements. 50-100 nM concentration of netrin-1ΔC was used to see highly separated and enough particles to do the further analysis. Netrin-1ΔC was treated with PNGase before adding the oligosaccharide. Netrin-1ΔC is primarily monomer at lower concentration, nM range **(Figure 4.29A)** (discussed earlier in section 4.2.4, **Figure 4.14**, netrin-1 was not treated with PNGase), and the addition of octasaccharides dp8 leads to the appearance of the dimer **(Figure 4.29B)**. A higher-order netrin-1ΔC hexamer appears after adding decasaccharides dp10 at the same concentration **(Figure 4.29C)**.

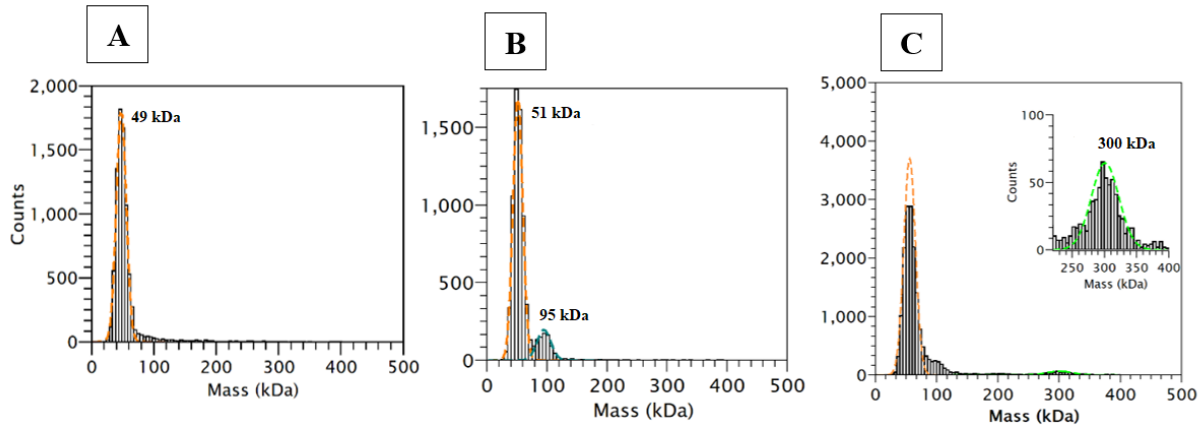

Figure 4.29 Mass photometry of netrin-1 in the presence of short chain oligosaccharides.

A) Netrin-1ΔC alone (49±1 kDa). *B) Netrin-1ΔC+ dp8, leads to the appearance of a dimer peak (94*±4 kDa) along with monomer peak (51±2 kDa). *B) Netrin-1ΔC + dp10, shows additional peak corresponding to molecular mass of six netrin-1ΔC (inset). Orange and green dashed lines represent the gaussian fit to a histogram. Netrin-1ΔC was PNGase treated and 50 mM tris pH 7.5, 200 mM NaCl buffer was used for the experiment.*

To measure the overall shape of the higher mass species and to obtain molecular structural information in solution, data were collected using an SEC-SAXS where data were collected every 3 seconds during elution from a size-exclusion column. It is a useful technique for separating aggregated or degraded products as SEC is attached to the SAXS setup. The predominant peak eluted at approximately frame number 290 after addition of HS-dp8 to the netrin-1ΔC while netrin-1ΔC eluted at frame number 350 (monomer) and 320 (dimer) **(Figure 4.30A)**. In general, the signal in the chromatogram is the integral of the ratio of the scattering intensity of the individual frames to the background intensity measured from the buffer. The individual scattering intensity profiles that provided uniform Rg distribution and homogeneity were merged using the program chromixs/PRIMUS (19,20), followed by Guinier analysis and demonstrated a monodisperse preparation. The P(r) analysis (which represents a histogram of the inter-electron distances within the structure) (21,22) was performed using the GNOM software (21). Based on the P(r) analysis, we obtained the Rg and Dmax of netrin-1ΔC with bound octasaccharide dp8 as 6.56±0.005 nm and 23.53±0.07 nm, respectively **(Figure 4.30B, Table 4.6)**. The number of DENSS models generated was 94. A low-resolution DENSS model of netrin-1 with dp8 was superimposed with the high-resolution X-ray diffraction structure (4OVE) (monomer) (1), netrin-1ΔC SOS dimer and

chimera (23) “fit in map” tools were used to fit netrin-1 into the DENSS envelope **(Figure 4.30C)**. After fitting the netrin dimer into the DENSS envelope, it clearly showed the space for another netrin-1ΔC monomer.

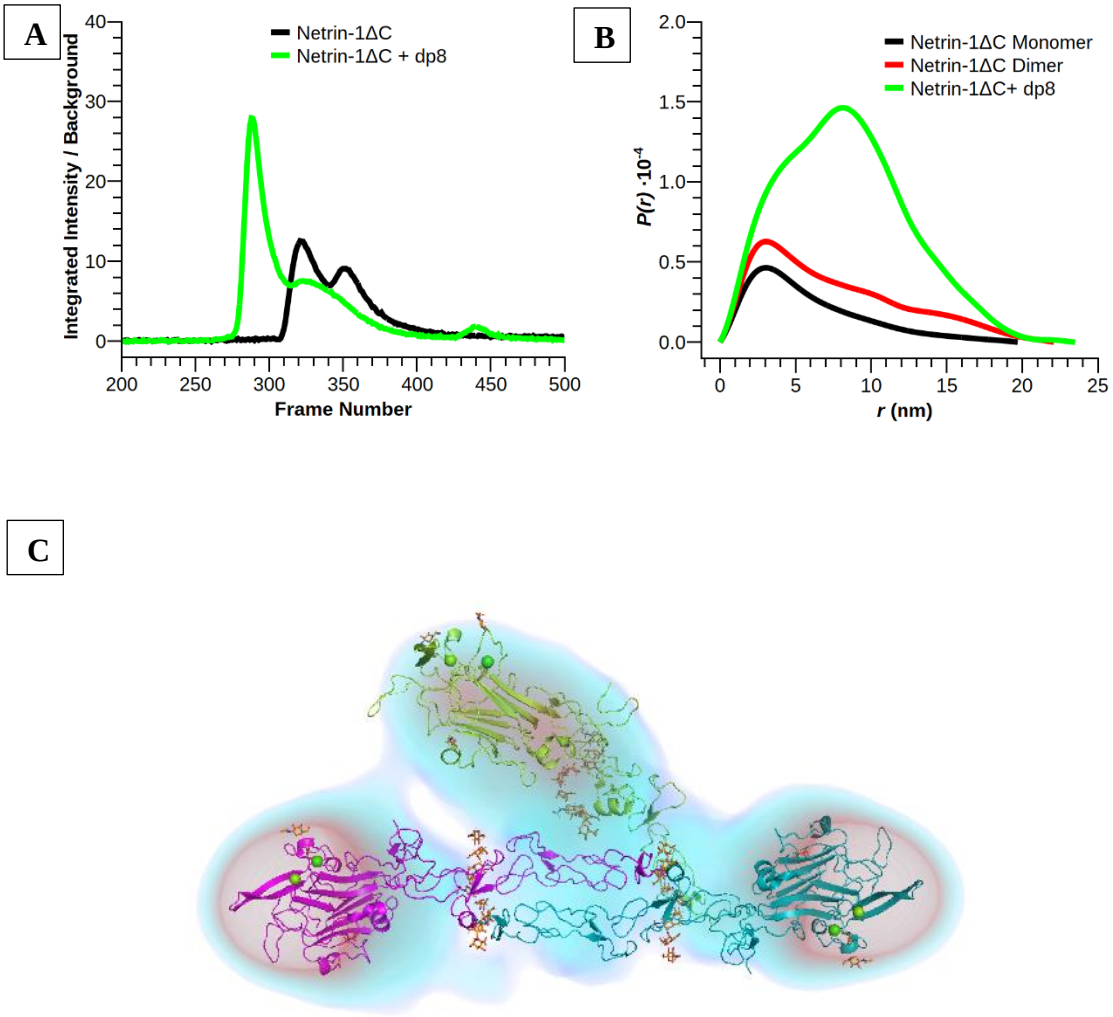

Figure 4.30 SEC-SAXS X-ray scattering of netrin-1ΔC with short chain HS. *A) X-ray scattering profile of netrin-1 and netrin-1 with dp8 while eluting from the Shodex column. B) Pair distance distribution calculated from selected frames from the elution peaks for netrin-1 monomer and dimer and netrin-1 bound to dp8. C) Low resolution DENSS models superimposed with netrin-1ΔC crystal structure bound to SOS.*

Table 4.6 Summary of hydrodynamic properties for netrin-1ΔC + octasaccharide dp8.

Parameters	**Netrin-1ΔC + octasaccharide Dp8**
Hydrodynamic radius Rh (nm)	7.16 ±0.02 (HYDROMIC DENSS)
Longest Dimension Dmax (nm)	20.7(DATCLASS) 23.53 ±0.07 (DENSS)
Radius of Gyration Rg (nm)	6.43±0.07 (AUTORG) 6.567±0.005 (DENSS)
Support Volume (nm^3)	618±5
Formula Mass (kDa)	261.8375 (Sednterp)
χ^2 square of fit	0.136±0.007
Resolution of averaged map (Å)	62.72

References

1. Grandin M, Meier M, Delcros JG, Nikodemus D, Reuten R, Patel TR, Goldschneider D, Orriss G, Krahn N, Boussouar A, Abes R, Dean Y, Neves D, Bernet A, Depil S, Schneiders F, Poole K, Dante R, Koch M, Mehlen P, Stetefeld J. Structural Decoding of the Netrin-1/UNC5 Interaction and its Therapeutical Implications in Cancers. Cancer Cell. 2016;29(2):173–85.

2. Geisbrecht B V., Dowd KA, Barfield RW, Longo PA, Leahy DJ. Netrin binds discrete subdomains of DCC and UNC5 and mediates interactions between DCC and heparin. J Biol Chem. 2003;278(35):32561–8.

3. Xu K, Wu Z, Renier N, Antipenko A, Tzvetkova- D, Xu Y, Minchenko M, Nardi-dei V, Kanagalaghatta R, Himanen J, Tessier-lavigne M, Nikolov DB. Structure of Netrin1 bound to two receptors provide insight into its Axon Guidance Mechanism. Science (80). 2014;344(6189):1275–9.

4. Finci L, Zhang Y, Meijers R, Wang JH. Signaling mechanism of the netrin-1 receptor DCC in axon guidance. Prog Biophys Mol Biol . 2015 Sep 14;118(3):153–60. Available from: http://www.ncbi.nlm.nih.gov/pmc/articles/PMC4537816/

5. Das AT, Tenenbaum L, Berkhout B. Tet-On Systems For Doxycycline-inducible Gene Expression. Curr Gene Ther . 2016 Jun 8;16(3):156. Available from: /pmc/articles/PMC5070417/

6. Moya-Torres A, Gupta M, Heide F, Krahn N, Legare S, Nikodemus D, Imhof T, Meier M, Koch M, Stetefeld J. Homogenous overexpression of the extracellular matrix protein Netrin-1 in a hollow fiber bioreactor. Appl Microbiol Biotechnol. 2021;105(14–15):6047–57.

7. Gregersen N, Bross P. Protein Misfolding and Cellular Stress: An Overview. Methods Mol Biol . 2010;648:3–23. Available from: https://link.springer.com/protocol/10.1007/978-1-60761-756-3_1

8. Yang M, Butler M. Effects of ammonia on CHO cell growth, erythropoietin production, and glycosylation. Biotechnol Bioeng. 2000;68(4):370–80.

9. Livesey FJ, Hunt SP. Netrin and netrin receptor expression in the embryonic mammalian nervous system suggests roles in retinal, striatal, nigral, and cerebellar development. Mol Cell Neurosci. 1997;8(6):417–29.

10. Shipp EL, Hsieh-Wilson LC. Profiling the Sulfation Specificities of Glycosaminoglycan Interactions with Growth Factors and Chemotactic Proteins Using Microarrays. Chem Biol. 2007;14(2):195–208.

11. Wang H, Copeland NG, Gilbert DJ, Jenkins NA, Tessier-Lavigne M. Netrin-3, a mouse homolog of human NTN2L, is highly expressed in sensory ganglia and shows differential binding to netrin receptors. J Neurosci . 1999 Jun 15;19(12):4938–47. Available from: https://pubmed.ncbi.nlm.nih.gov/10366627/

12. Castets M, Mehlen P. Netrin-1 role in angiogenesis: To be or not to be a pro-angiogenic factor? . Vol. 9, Cell Cycle. 2010. p. 1466–71. Available from: https://www.tandfonline.com/action/journalInformation?journalCode=kccy20www.landesbioscience.com/journals/cc/article/11197

13. Soltermann F, Foley EDB, Pagnoni V, Galpin M, Benesch JLP, Kukura P, Struwe WB. Quantifying Protein–Protein Interactions by Molecular Counting with Mass Photometry. Angew Chemie - Int Ed. 2020;59(27):10774–9.

14. García De La Torre J, Huertas ML, Carrasco B. Calculation of Hydrodynamic Properties of Globular Proteins from Their Atomic-Level Structure. Biophys J . 2000 Feb 1 ;78(2):719–30. Available from: http://www.cell.com/article/S0006349500766306/fulltext

15. Blanchette CR, Perrat PN, Thackeray A, Bénard CY. Glypican Is a Modulator of Netrin-Mediated Axon Guidance. PLoS Biol . 2015;13(7):e1002183. Available from: http://journals.plos.org/plosbiology/article?id=10.1371/journal.pbio.1002183

16. Jerabek-Willemsen M, Wienken CJ, Braun D, Baaske P, Duhr S. Molecular Interaction Studies Using Microscale Thermophoresis. Assay Drug Dev Technol . 2011;9(4):342–53. Available from: http://www.pubmedcentral.nih.gov/articlerender.fcgi?artid=3148787&tool=pmcentrez&rendertype=abstract%5Cnhttp://www.liebertonline.com/doi/abs/10.1089/adt.2011.0380

17. Dijkman PM, Lea W a, Gmbh NT, Lazic A, Gmbh NT. Interactions under Previously Challenging Conditions. 2014;59(3):301–15.

18. Serafini T, Kennedy TE, Galko MJ, Mirzayan C, Jessell TM, Tessler-Lavigne M. The Netrins Define a Family of Axon Outgrowth-Promoting Proteins Homologous to C. elegans UNC-6. Cell. 1994;79:409–24.

19. Konarev PV, Volkov VV, Sokolova AV, Koch MHJ, Svergun DI, IUCr. PRIMUS: a Windows PC-based system for small-angle scattering data analysis. J Appl Cryst . 2003 Sep 8;36(5):1277–82. Available from: http://scripts.iucr.org/cgi-bin/paper?ks5004

20. Panjkovich A, Svergun DI. CHROMIXS: automatic and interactive analysis of chromatography-coupled small-angle X-ray scattering data. Bioinfomatics . 2018;34(11):1944–6. Available from: www.embl-hamburg.de/biosaxs/download.html

21. Svergun DI. Determination of the regularization Parameter in indirect-Transform methods using perceptual criteria. J Appl Ichthyol. 1992;25:495-503.

22. Glatter O. A new method for the evaluation of small-angle scattering data. J Appl Crystallogr. 1977;10(5):415–21.

23. Pettersen EF, Goddard TD, Huang CC, Couch GS, Greenblatt DM, Meng EC, Ferrin TE. UCSF Chimera--a visualization system for exploratory research and analysis. J Comput Chem. 2004 Oct;25(13):1605–12.

CHAPTER 5: Discussion

This study presents the expression, purification, and biophysical characterization of a human netrin-1ΔC construct. Further, it provides new molecular binding and structural knowledge about the axon guidance cue netrin-1ΔC along with SOS, a heparan mimic. The crystal structure and effects of HSPG allowed us to understand the dynamic nature of this guidance cue.

One of the main challenges in the structural and biophysical studies of proteins is to produce proteins in milligram quantity (1). The expression of the protein in a high amount by maintaining its stability must consider many factors. Chapter 4.1 showed the establishment of a protocol for expressing netrin-1ΔC containing domains VI and V that was started with HYPERFlask protein production and followed by hollow fiber protein production. Netrin-1ΔC was expressed in mammalian cells for proper posttranslational modifications, as it contains four glycosylation sites and 17 disulfide bonds forming cysteine residues. Earlier studies in the lab by Dr. Markus Meier showed that transiently transfected cells produce less expressed protein netrin-1ΔC (not published). So, stably transfected cell lines using the sleeping beauty transfection method were used and proved to yield reliable expression. Netrin-1 full length (FL) forms higher molecular weight aggregates (2–4). Netrin-1 without the C-terminal domain (ΔC) used in this study binds with its receptors the same as netrin-1FL and enough was produced for structural and binding studies (4–6).

Stable transfection of HEK293T cells using the sleeping beauty transposon system and further selection allowed the higher netrin-1 DNA integrated cells. Clonal selection helped select a clone with high protein expression that also retained homogeneous glycosylation. Keeping all the necessary factors under control like pH, glucose, and any by-products helped reduce the batch-to-batch differences in the protein stability. Maintaining these factors also helped obtain a protein with proper posttranslational modifications, which is more stable and helpful in further biophysical studies.

After selecting the higher protein-producing clones, the expression of netrin-1ΔC started in a HYPERFlask. After four collections from the HYPERFlask, the cells began to detach and produced less protein in the media. Since cells keep on dividing as we provide nutrients to them, therefore, after 8-9 days, all the layers of the HYPERFlask were confluent. They started consuming more nutrients, and ultimately the yield and stability of expressed protein were not good. Media

with FBS also led to the BSA contamination which is problematic because netrin-1ΔC and BSA have approximately the same molecular weight.

Consequently, the cell culture work was migrated to HFBR for continuous production of netrin-1ΔC in large quantities. The main factors that maintain good protein yield and stability are nutrient availability, removal of byproducts, oxygenation, and optimized inducer concentrations (1). The *in vivo*-like high cell density in the HFBR allows maximizing the protein production. Inducer doxycycline affects cell metabolic rates and protein production by altering the glycolysis and oxidative phosphorylation pathways (6). A higher level of doxycycline produces changes in cell metabolism that could lead to overproduction of toxic molecules such as lactate that can hamper protein production. Therefore, to explore the optimal level, doxycycline concentration was increased gradually to a maximum of 2 µg/ml over one month. The protein concentration and lactate production measurements indicated that a higher concentration of doxycycline decreases the netrin-1ΔC expression and increases cellular lactate **(Figure 4.2 & 4.3)**. Further protein production then used an optimal doxycycline concentration of 1 µg/ml. The usage of CDM-HD also overcame the BSA contamination that was a problem with HYPERFlask-produced netrin-1 ΔC.

Chapter 4.2 showed the purification and assessment of the protein quality using different biophysical tools for further analysis and structural studies. The main challenge during the purification process was protein aggregation. The addition of the high salt wash step in the streptactin purification protocol helped to remove any nonspecifically bound protein to the netrin-1ΔC as it has a highly positively charged V2 subdomain with a net charge of +9.64 (3). The abundant side chains of arginine and lysine in V2 provide recognition sites for acidic ligands (3). It was challenging to remove the double strep tag as the protein formed aggregates; thus, there was a reduction in the yield of untagged protein to half. Aggregation of tagged and untagged proteins also showed partial cleavage by the enzyme thrombin and poor separation by the Streptactin column. Changing the duration of the thrombin cleavage reaction and adding $CaCl_2$ helped to get approximately 80% cleavage yield.

Further purification *via* size-exclusion chromatography showed higher molecular weight aggregates but using buffer containing higher salt reduced the aggregation **(Figure 4.6)**. The V2 domain of netrin-1ΔC is highly positively charged (3). The addition of ammonium sulfate

in the dialysis buffer and the use of a higher MWCO membrane may have allowed the exchange of any negatively charged molecules like HSPG with the sulfates from the buffer to make the protein less aggregated and suitable for further interaction studies of netrin-1 ΔC with HSPG.

Further stability measurements of purified netrin-1ΔC were performed using DLS, AUC, SEC-MALS, and Prometheus Panta. Producing high amounts of protein is often associated with higher metabolic stress, leading to lower protein stability by preventing proper folding (7). Improper folding leads to non-functional proteins, and in experimental conditions, they start aggregating and show different behavior. DLS is a non-destructive method and gave us information about the R_h and homogeneity of netrin-1ΔC as structural studies require >95% homogenous sample preparation **(Figure 4.7)**. AUC can provide information about the oligomerization, equilibrium in a protein, and a precise measurement of molecular mass. It clearly showed that netrin-1ΔC in solution exists in a monomer-dimer equilibrium **(Figure 4.13)**. SEC-MALS provided additional information about the protein's apparent molecular mass, oligomerization, and homogeneity among the netrin-1ΔC samples. Integration of all these biophysical methods made the stability assessment fast and easy.

A crystal structure of netrin-1ΔC solved by our group showed the presence of a Ca^{2+} binding site in the VI domain (3). The addition of 2.5 mM Ca^{2+} to the buffer increased the thermal stability (T_m) of the netrin-1 ΔC by 13% **(Figure 4.12)**. Different buffers with different pH and salt did not show much difference in the Tm value as Prometheus showed **(Figure 4.11)**. Another approach to assess protein stability over the temperature range used the newly developed technique Panta which also showed a lower PDI of the protein after adding $CaCl_2$ to the assay buffer **(Table 4.1)**, which was very useful for structural studies. Panta helped to check the thermal stability of the sample with different buffers along with its turbidity, hydrodynamic radii, and heterogeneity, leading to the conclusion of using 2.5 mM $CaCl_2$ in the buffers for further studies. The simultaneous measurement of all these properties made it a handy tool to assess stability before undergoing structural studies and crystallization trials.

Netrin-1ΔC in two different buffers with pH 6.5 and 7.5 and salt concentrations of 150 mM and 200 mM, respectively, showed different behavior. In pH 6.5, netrin-1 ΔC mainly behaved as a monomer as shown by SEC-MALS **(Figure 4.9B)** and BIO-SAXS **(Figure 4.17A)**. SEC-MALS showed that the protein displayed fast monomer-dimer equilibrium behavior. In pH

7.5, netrin-1ΔC exists as a monomer and dimer in equilibrium as shown by SEC-MALS **(Figure 4.9A)**. The protein concentration used in these methods was beyond the physiological range, but protein samples did not aggregate at a high concentration as netrin-1ΔC was purified by multiple steps using a buffer containing ammonium sulfate. Hofmeister discovered a series of salts that have an effect on the solubility and stability of the protein and anions appear to have a larger effect than cations (8,9). It has been shown that there is linear dependence of protein stability with the molar concentration of salt (means following the Hofmeister ion series $CO_3^{2-} > SO_4^{2-} > S_2O_3^{2-} > H_2PO_4^- > F^- > Cl^- > Br^- > NO_3^- > I^- > ClO_4^- > SCN^-$) and also the role of nonspecific interactions in stabilizing the protein by the Hofmeister effect (10). Therefore, netrin-1 stability could be the Hofmeister effect of the ions SO_4^{2-} and its direct interaction with the protein netrin-1. One can also speculate that sulfate might allow the replacement of bound heparin.

SEC-SAXS studies also confirmed that netrin-1ΔC in pH 7.5 exists in a monomer-dimer equilibrium **(Figure 4.15 & 4.17B&C)**, but in pH 6.5, only one peak was observed corresponding to monomer **(Figure 4.15 & 4.17A)** The Pr distribution function also gave a D_{max} value of ~218 nm for netrin-1ΔC in pH 7.5, 200 mM NaCl and ~180 nm for netrin-1ΔC in pH 6.5, 150 mM NaCl **(Figure 4.16)**. Low-resolution SAXS models showed clear monomer when netrin-1ΔC is present in low salt and pH 6.5 while both monomer and dimer when present in pH 7.5 with 200 mM NaCl buffer. Mass photometry allowed us to determine the behavior of netrin-1ΔC at the physiological concentration range. Regardless of their pH, both buffers showed mostly monomer of netrin-1ΔC in the solution at a concentration less than 50 nM **(Figure 4.14)**.

Crystallization trials of netrin-1ΔC came up with one condition that yielded good, diffracting crystals. Soaking experiments with SOS gave crystal with a resolution of 3.2 Å. Since netrin-1 ΔC is glycosylated, there could be chemical heterogeneity in the carbohydrate moieties among different batches of protein. This may explain why further refinement of the original crystal-forming conditions did not yield crystals. MS also showed a broad peak, indicating heterogeneity within the sample with a difference in sizes of netrin-1ΔC of 53-54 kDa and 58-59 kDa. Crystals soaked with a medium length decasaccharide, flexible GAG, did not provide much information. So, there is no supportive evidence of netrin-1 bound to bigger oligosaccharides using crystallography.

Chapter 4.3 presented the interaction of netrin-1ΔC with HSPG and how it changed the monomer-dimer equilibrium of netrin-1ΔC in solution. It is known that netrin-1ΔC has an electropositive V-2 domain that might allow binding of negatively charged molecules (3). Heparin-binding proteins contain a stretch of contiguous arginine and lysine residues like XRRXR motifs (11), along with ionic and non-ionic interacting amino acids for the specificity of GAGs. Measurements of netrin-1 interactions with SOS might help to explain the role of GAGs in netrin-1 activity, for example whether it acts as an activator, repressor, selector for receptors, or concentrator to localize netrin-1 near the cell surface (12). Here, based on our structural model, I propose the oligomerization of netrin-1 with the help of GAGs **(Figure 5.1)** on the cell surface and ECM. Furthermore, in the literature (5) researchers mentioned netrin-1ΔC switches between receptors to change its function in axon guidance from attraction to repulsion (5). The involvement of heparan sulfate in receptor switching or acting as a co-receptor is not well elucidated. Netrin-1 interaction studies with HSPG at the molecular level and further with receptors might help to understand the switching of receptor binding.

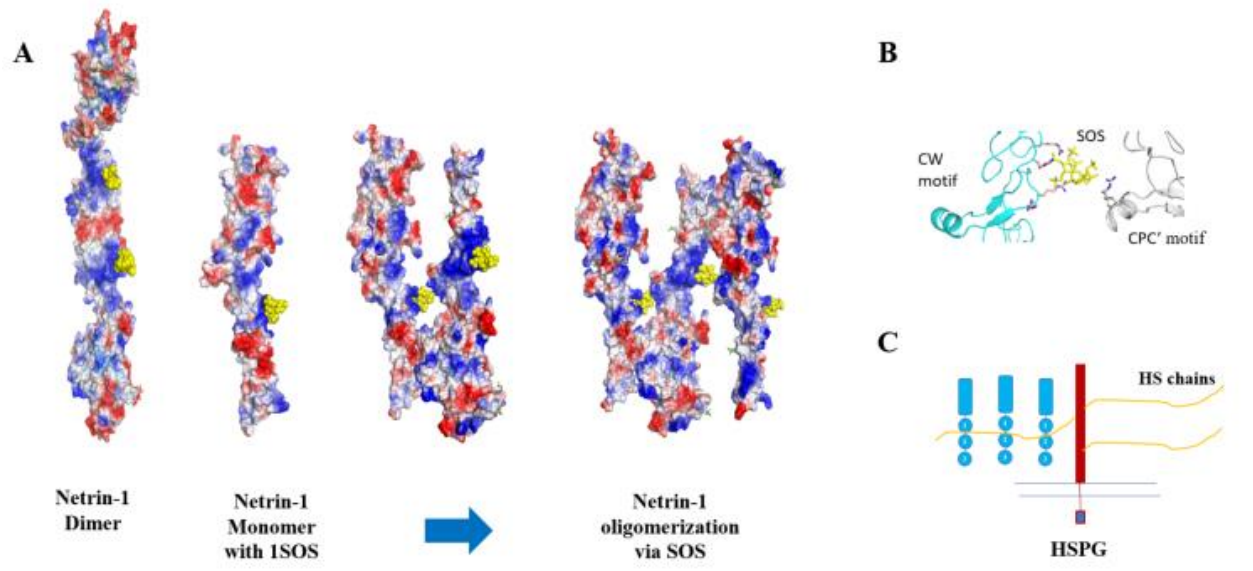

Figure 5.1 Netrin-1 oligomerization with GAGs/HS chains. *A) Netrin-1 dimer with one SOS each (yellow), considering these binding interactions, netrin-1 molecules form oligomers via SOS. Netrin-1 electrostatic potential (-71.49 red and +71.49 blue) B) Binding motifs on netrin-1(blue and silver) for SOS (yellow) that allow oligomerization. C) Proposed model: GAGs or HS chains (orange) on HSPG allow oligomerization of netrin-1 (blue) near the cell surface.*

Binding studies of netrin-1ΔC with medium-length oligosaccharides using MST showed fluorescent changes with increasing concentrations of oligosaccharides. MST can detect any change in shape, size, or hydrodynamic radius after ligand addition. Oligosaccharides might allow the binding of one netrin-1ΔC to another and make a chain of it *via* oligosaccharides connections. The changes in fluorescence measured by MST confirmed that the medium-length oligosaccharides bind with netrin-1ΔC **(Figure 4.18)**, and that binding induces the formation of bigger assemblies.

Using the same netrin-1 construct I used here, Finci *et al*. 2014, hypothesized that heparan sulfate might mediate receptor binding in netrin-1 and that distinct heparan sulfates may favor binding of a particular receptors (5). Here, my ELISA-like binding assay results showed the binding of netrin-1ΔC to its receptors. The addition of glypican and different lengths of heparan oligosaccharides to study the interaction did not show any change in the binding affinity of netrin-1 to its receptors **(Figure 4.19)**. This observation suggests that GAGs have no effect on the interaction between netrin-1ΔC with its dependence receptors. Both GAGs and receptors bind independently to netrin-1.

The asymmetric unit of netrin-1ΔC in the crystal structure showed an antiparallel arrangement of monomers in the netrin-1ΔC dimer with one SOS molecule bound per monomer **(Figure 4.22)**. Clusters of arginine and lysine are involved in the binding of GAG molecules (11), and our finding also observed the involvement of the V-2 subdomain of netrin-1ΔC. Meier *et al.* 2016, showed the electropositive nature of the laminin-type EGF-like fold of netrin-1 (same construct as in my study, without C-terminal domain) with a cluster of arginines and lysines. The GAG binding sites involved basic amino acids and other ionic and non-ionic amino acids interacting *via* hydrogen bonding and van der Wall's interactions for more specificity. The netrin-1 SOS structure also suggests the contribution of ionic and non-ionic amino acids near the SOS binding region to accommodate the flexible HS.

Deeper insight into identifying amino acids involved in the GAG binding came *via* netrin-1ΔC mutant studies that confirmed the role of the RRXR motif and the RH-HR tandem. RR double mutant, RRXR, and RH-HR mutants showed reduced binding. However, the complete loss of binding in the case of both mutants together indicated the involvement of both sites to make the binding region strong **(Figure 4.25)**.

Biophysical characterization showed that netrin-1ΔC exists in a monomer-dimer equilibrium in solution at low µM concentration range and mostly as a monomer at a physiological concentration that is nM concentration range (13). The addition of HS oligosaccharides showed the formation of another species apart from monomer and dimer **(Figure 4.26)**. The complete disappearance of monomer-dimer heterogeneous species and a new homogeneous peak emerged after adding oligosaccharide dp20 **(Figure 4.27)**. This oligomeric species may contain six to seven netrin-1ΔC molecules interacting *via* HS-oligosaccharide based on the molecular mass calculated from the SEC-MALS experiment. AUC also showed dp8-induced multimerization of netrin-1ΔC **(Figure 4.28)**.

Finci *et al*., 2014, Xu *et al*., 2014, and Ross *et al*., 2021, proposed the formation of an extended signaling cluster of netrin-1 and DCC and the involvement of multiple netrin-1 molecules for this clustering. SEC-MALS **(Figure 4.27)**, AUC **(Figure 4.28B)**, Mass Photometry **(Figure 4. 29)**, and BIOSAXS **(Figure 4.30A&C)** confirmed the formation of multimeric netrin-1ΔC assemblies *via* highly charged oligosaccharides that may lead to the receptor clustering. These results along with the netrin-1 SOS structure could contribute to the field to understand the role of HSPG in netrin-1 receptor interactions.

Furthermore, these findings could help explain multiple processes, including pathological conditions where participation of netrin-1 has been shown along with its receptors. GAG molecules might allow netrin-1 to colocalize near the cell surface (haptotaxis) and lead to multimeric netrin-1 assemblies that cause receptor clustering and ultimately cell signaling (14). Moreover, this study's results could lead to thinking about netrin-1ΔC chemotropic gradient generation along with netrin-1 mobility *via* different length short-chain GAGs. The different length HS oligosaccharides induced a gradual transition of netrin-1 from a monomer-dimer equilibrium to trimer, tetramer, and higher-order assembly formation **(Figure 4.26 & 4.28)** and might allow building of a concentration gradient. Additionally, the involvement of GAG chains in bringing netrin-1 near the cell surface and binding of these GAGs molecules might prevent netrin-1 from proteolysis as happens with Fibroblast Growth Factor (FGF)-HS complex (15). Therefore, targeting the GAG binding site with a small molecule could be a good strategy for treating cancer, neurodegenerative diseases, and developmental disorders.

References

1. Moya-Torres A, Gupta M, Heide F, Krahn N, Legare S, Nikodemus D, Imhof T, Meier M, Koch M, Stetefeld J. Homogenous overexpression of the extracellular matrix protein Netrin-1 in a hollow fiber bioreactor. Appl Microbiol Biotechnol. 2021;105(14–15):6047–57.

2. Wang H, Copeland NG, Gilbert DJ, Jenkins NA, Tessier-Lavigne M. Netrin-3, a mouse homolog of human NTN2L, is highly expressed in sensory ganglia and shows differential binding to netrin receptors. J Neurosci . 1999 Jun 15;19(12):4938–47. Available from: https://pubmed.ncbi.nlm.nih.gov/10366627/

3. Grandin M, Meier M, Delcros JG, Nikodemus D, Reuten R, Patel TR, Goldschneider D, Orriss G, Krahn N, Boussouar A, Abes R, Dean Y, Neves D, Bernet A, Depil S, Schneiders F, Poole K, Dante R, Koch M, Mehlen P, Stetefeld J. Structural Decoding of the Netrin-1/UNC5 Interaction and its Therapeutical Implications in Cancers. Cancer Cell. 2016;29(2):173–85.

4. Keino-Masu K, Masu M, Hinck L, Leonardo ED, Chan SSY, Culotti JG, Tessier-Lavigne M. Deleted in Colorectal Cancer (DCC) Encodes a Netrin Receptor. Cell . 1996 May 23;87(2):175–85. Available from: http://dx.doi.org/10.1016/S0092-8674(00)81336-7

5. Finci LI, Krüger N, Sun X, Zhang J, Chegkazi M, Wu Y, Schenk G, Mertens HDT, Svergun DI, Zhang Y, Wang J huai, Meijers R. The Crystal Structure of Netrin-1 in Complex with DCC Reveals the Bifunctionality of Netrin-1 As a Guidance Cue. Neuron. 2014;83(4):839–49.

6. Xu K, Wu Z, Renier N, Antipenko A, Tzvetkova- D, Xu Y, Minchenko M, Nardi-dei V, Kanagalaghatta R, Himanen J, Tessier-lavigne M, Nikolov DB. Structure of Netrin1 bound to two receptors provide insight into its Axon Guidance Mechanism. Science (80). 2014;344(6189):1275–9.

7. Gregersen N, Bross P. Protein Misfolding and Cellular Stress: An Overview. Methods Mol Biol . 2010;648:3–23. Available from: https://link.springer.com/protocol/10.1007/978-1-60761-756-3_1

8. Sedlák E, Stagg L, Wittung-Stafshede P. Effect of Hofmeister ions on protein thermal stability: Roles of ion hydration and peptide groups? Arch Biochem Biophys. 2008 Nov 1;479(1):69–73.

9. Boström M, Parsons DF, Salis A, Ninham BW, Monduzzi M. Possible origin of the inverse and direct hofmeister series for lysozyme at low and high salt concentrations. Langmuir . 2011 Aug 2;27(15):9504–11. Available from: https://pubs.acs.org/doi/pdf/10.1021/la202023r

10. Tadeo X, Ló Pez-Mé Ndez B, Castañ D, Trigueros T, Millet O. Protein Stabilization and the Hofmeister Effect: The Role of Hydrophobic Solvation. Biophysj. 97:2595–603.

11. Vallet SD, Clerc O, Ricard-Blum S. Glycosaminoglycan–Protein Interactions: The First Draft of the Glycosaminoglycan Interactome. J Histochem Cytochem. 2021;69(2):93–104.

12. Meijers R, Smock RG. Roles of glycosaminoglycans as regulators of ligand/receptor complexes. Open Biol . 2018;8. Available from: http://dx.doi.org/10.1098/rsob.180026

13. Castets M, Mehlen P. Netrin-1 role in angiogenesis: To be or not to be a pro-angiogenic factor? . Vol. 9, Cell Cycle. 2010. p. 1466–71. Available from: https://www.tandfonline.com/action/journalInformation?journalCode=kccy20www.landesbioscience.com/journals/cc/article/11197

14. Hong K, Hinck L, Nishiyama M, Poo M ming, Tessier-Lavigne M, Stein E. A Ligand-Gated Association between Cytoplasmic Domains of UNC5 and DCC Family Receptors Converts Netrin-Induced Growth Cone Attraction to Repulsion. Cell . 1999 Apr 10;97(7):927–41. Available from: http://dx.doi.org/10.1016/S0092-8674(00)80804-1

15. Ornitz DM. FGFs, heparan sulfate and FGFRs: Complex interactions essential for development. BioEssays. 2000;22(2):108–12.

CHAPTER 6: Conclusion & Future Perspective

In my research, I characterized the dynamic behavior of netrin-1 containing domain VI and V (netrin-1ΔC) in solution. I also solved the structure of netrin-1ΔC with the HS mimic, SOS by X-ray crystallography. HSPGs interactions with netrin-1 have been known for a long time (1,2), and here I showed how it binds with netrin-1ΔC and changes its behavior. The structure of netrin-1ΔC with SOS revealed two distinct binding sites for SOS which suggested that GAG chains of different length could associate with netrin-1. Addition of short chain oligosaccharide shifts the monomer-dimer equilibrium to higher order assemblies. The biological relevance of these bigger assemblies should be examined. Moreover, *in vivo* studies *via* electron microscopy (EM) would be great to show the localization of netrin-1 on the cell surface along with short chain oligosaccharide. Heparanase-1 is expressed by cancerous cells and is involved in tumor metastasis (3). Heparanase-1 the only known mammalian endoglycosidase, degrades HS chains in the extracellular matrix (4) and short chain HS molecules are formed. One might also consider studying the effect of Heparanase treatment on the distribution of netrin-1ΔC and FL protein on the cell surface and on cell survival. I speculate that netrin-1 release with short chain HS molecules from the cell surface and form oligomers. These netrin-1 oligomers might diffuse from its location and induce the cell signaling *via* interacting with its receptors and might cause cell survival, migration of cells and angiogenesis resulting in metastasis. It is well known that domains VI and V of netrin-1 are involved in interactions with dependence receptors (5–7) but still there is a need to study the distribution of netrin-1 with HS oligosaccharide on the cell surface and ECS and its effects on receptor binding.

Through biophysical techniques I was able to show oligomerization of netrin-1ΔC with short chain oligosaccharides as well as identify a binding region for netrin-1 with HS with a high-resolution crystal structure with SOS. I hypothesize that these oligomerizations act as a seed for bigger assemblies. A cryo-EM structure of netrin-1 with short chain oligosaccharide should be employed to provide structural knowledge of these bigger assemblies. Still there is a lot to uncover about these interactions and any effect on netrin-1 receptors complex formation. In this study, ELISA-like binding experiments showed that short length oligosaccharides and receptors bind netrin-1 independent to each other. In the previous studies (6), a proposed model suggested that different HS recruit different receptors on a netrin-1 binding site at domain V2 and thus switch the attraction of the growth cone to repulsion or vice versa. Further structural studies with cryo-EM

should be a good method to see whether netrin-1 can bind to its receptors after forming big assemblies or if there is any effect of different length oligosaccharides on binding of receptor to the netrin-1 assemblies like the receptor protein tyrosine phosphatase (RPTP) and FGF (8,9).

References

1. Geisbrecht B V., Dowd KA, Barfield RW, Longo PA, Leahy DJ. Netrin binds discrete subdomains of DCC and UNC5 and mediates interactions between DCC and heparin. J Biol Chem. 2003;278(35):32561–8.

2. Blanchette CR, Perrat PN, Thackeray A, Bénard CY. Glypican Is a Modulator of Netrin-Mediated Axon Guidance. PLoS Biol. 2015;13(7):e1002183. Available from: http://journals.plos.org/plosbiology/article?id=10.1371/journal.pbio.1002183

3. Arvatz G, Shafat I, Levy-Adam F, Ilan N, Vlodavsky I. The heparanase system and tumor metastasis: Is heparanase the seed and soil? Cancer Metastasis Rev. 2011;30(2):253–68.

4. Hermano E, Goldberg R, Rubinstein AM, Sonnenblick A, Maly B, Nahmias D, Li JP, Bakker MAH, Van Der Vlag J, Vlodavsky I, Peretz T, Elkin M. Heparanase accelerates obesity-associated breast cancer progression. Cancer Res. 2019;79(20):5342–54.

5. Xu K, Wu Z, Renier N, Antipenko A, Tzvetkova- D, Xu Y, Minchenko M, Nardi-dei V, Kanagalaghatta R, Himanen J, Tessier-lavigne M, Nikolov DB. Structure of Netrin1 bound to two receptors provide insight into its Axon Guidance Mechanism. Science (80). 2014;344(6189):1275–9.

6. Finci LI, Krüger N, Sun X, Zhang J, Chegkazi M, Wu Y, Schenk G, Mertens HDT, Svergun DI, Zhang Y, Wang J huai, Meijers R. The Crystal Structure of Netrin-1 in Complex with DCC Reveals the Bifunctionality of Netrin-1 As a Guidance Cue. Neuron. 2014;83(4):839–49.

7. Grandin M, Meier M, Delcros JG, Nikodemus D, Reuten R, Patel TR, Goldschneider D, Orriss G, Krahn N, Boussouar A, Abes R, Dean Y, Neves D, Bernet A, Depil S, Schneiders F, Poole K, Dante R, Koch M, Mehlen P, Stetefeld J. Structural Decoding of the Netrin-1/UNC5 Interaction and its Therapeutical Implications in Cancers. Cancer Cell. 2016;29(2):173–85.

8. Coles CH, Shen Y, Tenney AP, Siebold C, Sutton GC, Lu W, Gallagher JT, Jones EY, Flanagan JG, Aricescu AR. Proteoglycan-specific molecular switch for RPTPσ clustering and neuronal extension. Science (80). 2011 Apr 22;332(6028):484–8.

9. Harada M, Murakami H, Okawa A, Okimoto N, Hiraoka S, Nakahara T, Akasaka R, Shiraishi YI, Futatsugi N, Mizutani-Koseki Y, Kuroiwa A, Shirouzu M, Yokoyama S, Taiji M, Iseki S, Ornitz DM, Koseki H. FGF9 monomer-dimer equilibrium regulates extracellular matrix affinity and tissue diffusion. Nat Genet. 2009;41(3):289–98.